ALUMINIZING OF ALLOY 690 AND ALLOY 800, THEIR MICROSTRUCTURAL CHARACTERIZATION AND PROPERTY EVALUATION

By

RABI SANKAR DUTTA

(Enrolment Number: ENGG01200904024)

Bhabha Atomic Research Centre,
Mumbai-400 085, India.

A thesis submitted to the
Board of Studies in Engineering Sciences
In partial fulfillment of requirements
For the Degree of

DOCTOR OF PHILOSOPHY
of
HOMI BHABHA NATIONAL INSTITUTE

August, 2015

Homi Bhabha National Institute

Recommendations of the Viva Voce Board

As members of the Viva Voce Board, we certify that we have read the dissertation prepared by Rabi Sankar Dutta entitled "Aluminizing of Alloy 690 and Alloy 800, their microstructural characterization and property evaluation" and recommend that it may be accepted as fulfilling the dissertation requirement for the Degree of Doctor of Philosophy.

Date: 21/08/15
Chairman: Prof. V. Kain

Date: 21/08/15
Guide/Convener: Prof. R. Tewari

Date: 21/08/15
Co-guide/Member: Prof. A. K. Arya

Gautam Kumar Dey
Date: 21/8/15
Technical Adviser: Prof. G.K. Dey

Date: 21/8/15
Member: Prof. J. B. Singh

Alok Awasthi
Date: 21/8/2015
Member: Prof. A. Awasthi

A. S. Gandhi
Date: 21/8/15
External Examiner: Prof. Ashutosh S. Gandhi

Final approval and acceptance of this dissertation is contingent upon the candidate's submission of the final copies of the dissertation to HBNI.

I hereby certify that I have read this dissertation prepared under my direction and recommend that it may be accepted as fulfilling the dissertation requirement.

Date: 21st August 2015

Place: Mumbai
Co-guide
Guide:

STATEMENT BY AUTHOR

This dissertation has been submitted in partial fulfillment of requirements for an advanced degree at Homi Bhabha National Institute (HBNI) and is deposited in the Library to be made available to borrowers under rules of the HBNI.

Brief quotations from this dissertation are allowable without special permission, provided that accurate acknowledgement of source is made. Requests for permission for extended quotation from or reproduction of this manuscript in whole or in part may be granted by the Competent Authority of HBNI when in his or her judgment the proposed use of the material is in the interests of scholarship. In all other instances, however, permission must be obtained from the author.

Rabi Sankar Dutta

(Rabi Sankar Dutta)

DECLARATION

I hereby declare that the investigation presented in the thesis has been carried out by me. The work is original and has not been submitted earlier as a whole or in part for a degree / diploma at this or any other Institution / University.

Rabi Sankar Dutta

(Rabi Sankar Dutta)

DEDICATIONS

To my parents, teachers, mentors and well-wishers

ACKNOWLEDGEMENTS

I would like to express my deep sense of gratitude to my guide Dr. R. Tewari and co-guide Dr. Ashok Kumar Arya for their valuable guidance, keen interest and encouragement during the course of the study. I am extremely thankful to Dr. G.K. Dey, Dr. U.D. Kulkarni and Dr. I.G. Sharma for their encouragement and fruitful discussion during this work. I am indebted to Dr. S. Majumdar for his valuable suggestions, cooperation during the experiments and subsequent analysis and detailed discussions on various aspects.

My sincere thanks to my colleagues Shri B. Paul, Dr. A. Laik, Dr. P. Sengupta, Dr. K. Singh and Shri B. Vishwanadh for their help and cooperation during the experiments and subsequent analysis. I would like to take this opportunity to thank Dr. R.K. Mishra, Dr. C.P. Kaushik, Shri C. Yusufali, Shri P.K. Limaye, Dr. R.J. Kshirsagar for their valuable suggestions, help and cooperation during the experiments.

I am very grateful to all the members of Materials Group related to this study for their help and support throughout these years.

I am also thankful to all the members of the Doctoral Committee for their critical comments during periodic review of this work and suggestions in preparing the manuscript.

Finally, I would like to thank my wife Mrs. Chaitali Dutta and son Rupam Dutta for their moral support during the course of this study.

CONTENTS

CHAPTER 1: INTRODUCTION

CHAPTER 2: LITERATURE REVIEW

CHAPTER 3: EXPERIMENTAL METHOD

CHAPTER 5: PROPERTIES OF ALUMINIZED COATINGS

CHAPTER 6: OXIDATION BEHAVIOUR OF ALUMINIZED SUPERALLOYS AND EVALUATION OF STABILITY OF ALUMINIZED AND OXIDIZED SUPERALLOY 690

Page Number

CHAPTER 7:

SYNOPSIS

HOMI BHABHA NATIONAL INSTITUTE

Ph. D. PROGRAMME

1. **Name of the Student: Rabi Sankar Dutta**
2. **Name of the Constituent Institution: BARC, Mumbai**
3. **Enrolment No. : ENGG01200904024**
4. **Title of the Thesis: Aluminizing of Alloy 690 and Alloy 800, their microstructural characterization and property evaluation**

5. **Board of Studies: Engineering Sciences**

SYNOPSIS

Motivation of the study

Alloy 690 is a solid solution-strengthened, austenitic, high chromium low iron containing Ni-based superalloy. It is an attractive material for coal-gasification units, burners and ducts for processing sulfuric acid, furnaces for petrochemical processing and steam generator (SG) tubes in nuclear power generation [1,2]. Superalloy 690 is also used as material of construction for process pot and susceptor in metallic melter pot furnace as well as electrodes in Joule-heated ceramic melter pot employed for high level nuclear waste immobilization process. However, due to formation of thick, continuous Cr_2O_3 layer at the alloy/molten borosilicate glass interface, the alloy adjacent to the interface has been reported to be depleted in Cr resulting to almost half of its initial content in the alloy [3,4]. Besides this, flaking off continuous Cr-oxide layer can take place due to the development of compressive stresses because of its high thickness and convective motion within borosilicate melt pool adjacent to the region. These phenomena can lead to leaching out of Cr from the alloy ultimately leading to premature failure of metallic melter pot furnaces. Therefore, it is of prime importance to develop effective diffusion barrier coatings on the alloy so that the life of the components can be extended. Aluminides are found to be very effective in functioning as diffusion barrier coatings as they form a protective layer of Al_2O_3 when exposed to high temperature. Keeping this in view, a systematic and detailed study on development of diffusion barrier coatings consisting of aluminization of superalloy 690 substrates followed by their microstructural characterization and property evaluation along with ab-initio modeling of Ni(Cr)/NiAl interface has been undertaken to understand the protectiveness of the aluminide coatings in a rigorous manner, which has not been attempted so far.

Alloy 800 is an austenitic, high nickel moderate chromium containing Fe-based superalloy. It is generally used in solid solution-strengthened condition. In chemical and petrochemical processing, the alloy is used for heat exchangers. It is used as a material for construction where resistance to chloride stress corrosion cracking is needed. In nuclear power plants, superalloy 800 is extensively used as SG tube material. In petroleum processing, the alloy is used for heat exchangers, which air cool the process stream. Besides this, digester-liquor heaters in paper pulp industry are often made of this alloy [5,6]. As compared to the number of studies reported on superalloy 800 in SG related issues, there are only a few on the development of aluminide coatings on this alloy for applications at elevated temperatures [7-9]. Miller et al. [7] have used different Cr-Al masteralloys and alkali halide vapours to form an interdiffusion zone enriched in Cr and Al for Alloy 800, but have not succeeded to achieve the desired one.

Investigation by Haanappel et al. [8] has indicated that aluminide coatings formed on Alloy 800H can provide resistance to sulphidation up to 823 K. Vokál et al. [9] have reported the formation of (Ni,Fe)Al and Fe_2Al_5 phases on top surface of Alloy 800 after pack cementation and have noticed degradation of (Ni,Fe)Al coating after the exposure of coated specimens in 50 mol% KCl + 50 mol% K_2SO_4 at 923 K. Hence, an investigation relating to development of aluminide coatings for applications at elevated temperatures is of immense importance. Therefore, a study on the formation of aluminide coatings on high nickel and moderate chromium containing Fe-based austenitic superalloy 800 followed by their microstructural characterization and property evaluation has been undertaken along with superalloy 690.

Objective of the study

For superalloy 690, the objective of the present investigation is primarily to develop diffusion barrier coatings on the alloy surface for enhanced service life of metallic melter pot as well as electrode in Joule-heated ceramic melter pot in nuclear waste immobilization process. In addition, to explore the possibility of uses of aluminide coatings at elevated temperatures by evaluating their different properties. In case of superalloy 800, the main objective of the present study is to examine various aspects of aluminides formed on the alloy surface for the development of aluminide coatings for applications at elevated temperatures. In doing so, the substrates of the said superalloys have been subjected to pack aluminization as this technique is not only useful but also inexpensive one. Pack aluminization of the substrates has been followed by microstructural characterization, microanalysis, microhardness tests, friction tests, wear tests, adherence tests and finally oxidation tests. In order to understand the nature of interfacial interactions pertaining to superalloy 690 substrates, an attempt has also been made to determine the stability of NiAl phase and adhesion strength of Ni(Cr)/NiAl interface by employing first-principle computational approach. The nature of bonding across the interface and its structure has also been attempted. For superalloy 690 substrates, evaluation of stability of pre-oxidized aluminide coatings in sodium borosilicate melt at 1248 K has also been undertaken that is pertinent to its application. The novelty of the present study is that it deals with the development of aluminide coatings on Ni-based Alloy 690 and Fe-based Alloy 800 in Ni-Cr-Fe alloy system, which has not been systematically carried out so far for applications at elevated temperatures.

Summaries of chapters

The present thesis comprises 7 chapters. Chapter 1 briefly discusses compositions and applications of Ni-, Fe- and Co-based superalloys along with superalloys 690 and 800, motivation of the study as well as objectives of the study. Chapter 2 gives a brief account of literature review pertinent to the present topic. Chapter 3 contains details of materials and the experimental methods employed in the present study. Chapter 4 is on phase evolution of aluminized alloys giving the detailed results on microstructure and microanalysis relating to aluminization of superalloys 690 and 800. In this chapter the results of pack aluminization of the superalloys have been discussed at a length as this technique of aluminization has been extensively used in the present study. Chapter 5 deals with the properties of aluminized substrates of superalloys 690 and 800 summarizing the results on microhardness, wear and friction coefficient and adhesion of aluminides. Besides this, it summarizes the results on modeling of Ni(Cr)/NiAl interface and its adhesion strength (relevant to superalloy 690) determined by employing first-principle computational approach. It also discusses the nature of bonding across the interface and its structure. Chapter 6 discusses the results on thermal oxidation resistance of aluminides. In addition, it discusses the results on stability of pre-oxidized aluminide coatings, formed on superalloy 690 substrates, in molten sodium borosilicate melt at 1248 K pertinent to the application of the superalloy 690. Finally, chapter 7 summarizes the main conclusions of the study. A summary of each chapter pertaining to experimental results are given in the following sections:

CHAPTER 4: Phase evolution in aluminized superalloys

Results on aluminization of superalloys 690 and 800 substrates primarily done by employing pack aluminization (pack cementation) process at 1273 K in argon atmosphere using high Al-containing (10 wt.% Al) pack have been presented in this chapter. For superalloy 690 specimens, results on low Al-containing (2 wt.% Al) pack have also been stated. The findings of different phases in respective alloy system have been discussed from the perspective of Ni-Al and Fe-Al alloy systems and results of other investigators [9,10]. In addition, mechanisms for formation of phases in high Al- and low Al-containing packs have been discussed. Figs. 1 and 2 demonstrate multilayer of aluminides formed on superalloys 690 and 800 substrates respectively.

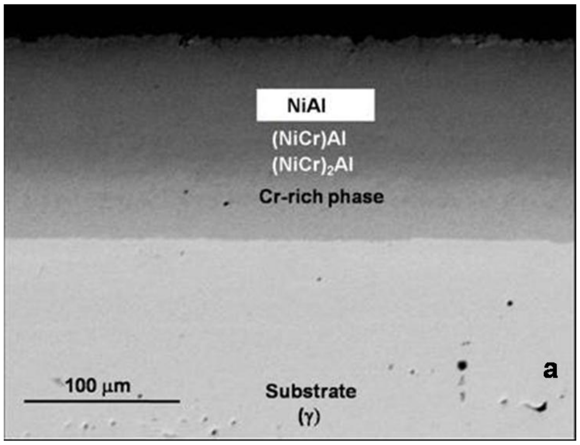

Fig. 1 Scanning electron microscopy along with energy dispersive X-ray analysis along the cross-section of pack aluminized (2 wt.% Al) superalloy 690 substrate revealing multilayer of aluminides.

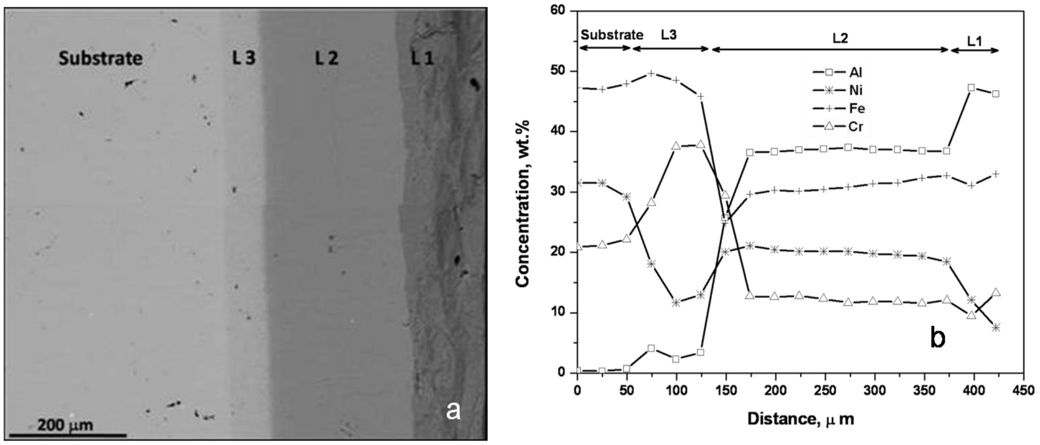

Fig. 2 Cross-section of pack aluminized (10 wt.% Al) superalloy 800 revealing multilayer L1, L2 and L3 along with the substrate under back-scattered electron image mode and (b) concentration profiles of Al, Ni, Fe and Cr at different points covering substrate and three layers.

Based on experiments and understanding, a few important points of this study can be summarized as:

(a) Pack aluminization of substrates of superalloy 690 with high Al-containing pack (10 wt.% Al) at 1273 K results in the formation of multilayer consisting of (NiCr)Al + Cr_5Al_8, Ni_2Al_3 +Cr_5Al_8, NiAl and γ phases that is attributed to inward diffusion of Al and outward diffusion of Ni and Cr. Alloy substrate pack aluminized in low Al-containing pack (2 wt.% Al) indicates formation of NiAl type phase on the uppermost surface with adjoining (NiCr)Al, $(NiCr)_2Al$ and subsequently Cr-rich layer adjacent to alloy substrate, which is attributed to outward diffusion of Ni. The uppermost surface is found to contain nanoparticles of nickel aluminide.

(b) For superalloy 800 substrates, pack aluminization with high Al-containing pack (10 wt.% Al) at 1273 K shows formation of multilayer. The outermost layer is found to consist of FeAl + Fe_2Al_5 type phases. The second layer is composed of FeAl type phase. The innermost layer, which is a solid solution zone, is found to consist of ~ 43 at.% Fe, 38 at.% Cr, 11 at.% Ni containing about 6 at.% Al. It is indicative of the fact that inward diffusion of Al and outward diffusion of Fe, Ni and Cr have led to the formation of multilayer.

CHAPTER 5: Properties of aluminides

Properties of aluminides formed on substrates of superalloys 690 and 800 by using pack aluminization process with high Al-containing (10 wt.% Al) pack at 1273 K in argon atmosphere discussed here are of relevance to development of materials related to applications at elevated temperatures. For aluminized superalloy 690 substrates, the properties those have been stated are microhardness along the cross-section while friction coefficient, wear rate and adherence along the topmost surface. In case of superalloy 800 specimens, those have been microhardness, friction coefficient and adherence along the cross-section. Besides this, similar results have been discussed on aluminides that formed on superalloy 690 substrates with low Al-containing pack (2 wt.% Al). Fig. 3 demonstrates the values of microhardness and penetration depth along the cross-section of aluminides for superalloys 690 and 800 respectively.

All these findings of the present work have been rationalized from the viewpoint of existing microstructure and compared with the results of other researchers [11,12]. Based on experimentation and understanding, a few salient points of this investigation is summarized as:

(a) A variation of microhardness from 225 to 1142 Knoop hardness number along the cross section of pack aluminized (10 wt.% Al) sample of superalloy 690 indicates high hardness values of the aluminides. In dry medium, wear rates of aluminized (10 wt.% Al) 690 specimen and WC ball increase with the frequency at 15 N load. Wear tests of aluminized (10 wt.% Al) 690 specimen at load level of 15 N with the frequencies at 10, 15 and 20 Hz indicate good adherence of surface coating.

(b) In case of superalloy 690 sample pack aluminized with low-Al containing pack (2 wt.% Al), microhardness values have been found to higher for aluminides as compared to the substrate. Multilayer exhibits an increase in microhardness with Al-content. Multilayer shows lower penetration depth than alloy substrate along with a good adherence indicated by scratch test carried out at a constant load level of 2 N along the cross-section of aluminized specimen.

(c) For superalloy 800 substrate pack aluminized with 10 wt.% Al, a variation of microhardness from 213 to 1098 Knoop hardness number along the cross-section has been obtained indicating high hardness values for aluminides as compared to substrate. The microhardness of aluminide increases with Al-content. Scratch test along the cross-section at load levels ranging from 0.9 to 10 N with a loading rate of 30 N/min showed a maximum penetration depth of 12 μm indicating a good adherence of aluminide coatings.

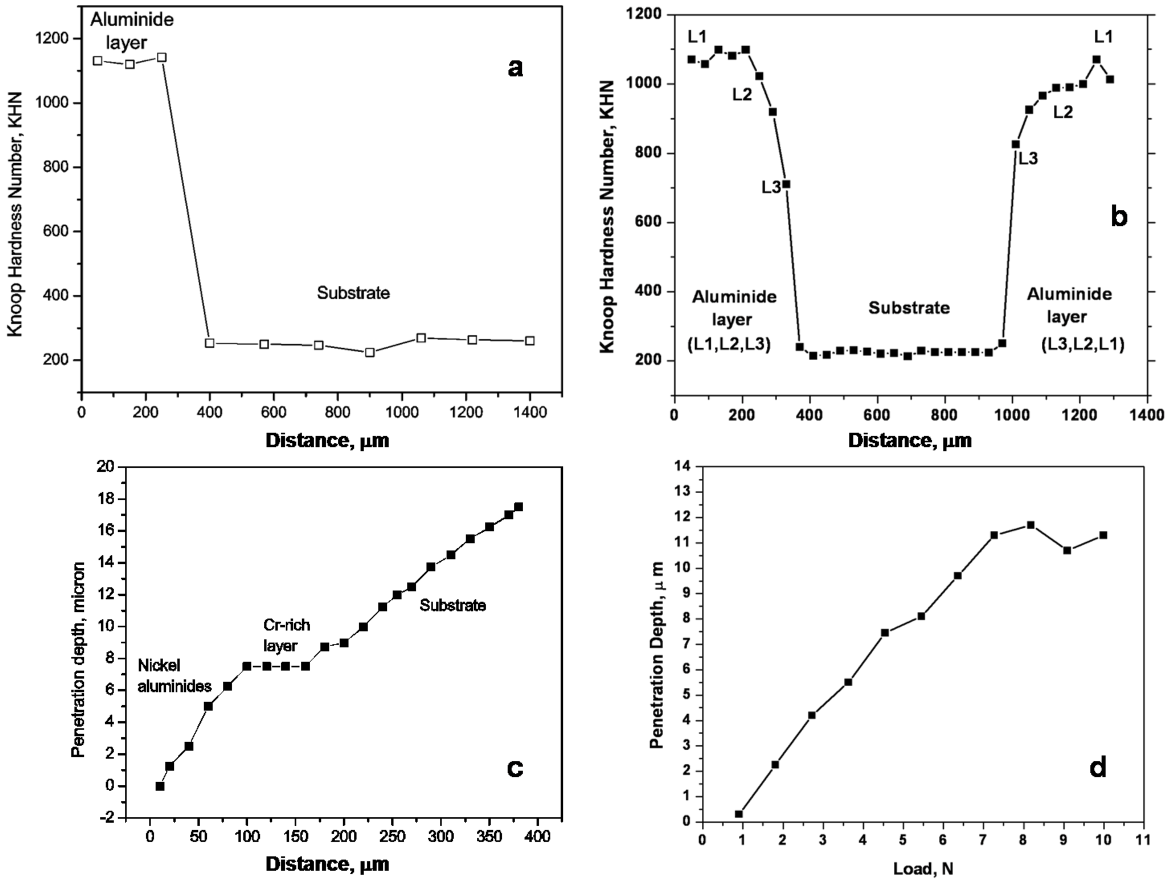

Fig. 3 Variation of (a) microhardness in pack aluminized (10 wt.% Al) superalloy 690 substrate, (b) microhardness in pack aluminized (10 wt.% Al) superalloy 800 substrate, (c) penetration depth with scratch length along the cross-section of pack aluminized (2 wt.% Al) superalloy 690 substrate and (d) penetration depth with load for pack aluminized (10 wt.% Al) superalloy 800 specimen during scratch test along the cross-section.

Modeling of Ni (111)/NiAl(110) interface structure for aluminized superalloy pertaining to development of aluminide coatings on superalloy 690 substrate for applications at elevated temperatures has dealt with first-principle calculations [13]. Good adhesion of the Ni(111)/NiAl(110) interface and Cr-doped interface has been correlated with the experimental results of scratch test for the alloy that indicates good adherence of multilayer and interface. Table-1 demonstrates the results of ab-initio simulations. For Cr-doped interface where 2 Ni atoms at the interface plane replaced by 2 Cr atoms and 1 Ni atom replaced by 1 Cr atom below the interface plane, ideal work of adhesion for the interface has been obtained as 3523.57 mJ/m^2.

Table 1: Calculated surface and interface energies and ideal work of adhesion for unrelaxed and fully relaxed slabs.

Slab	Unrelaxed slab		Relaxed slab	
	Energy, eV	W^{ad}(ideal), mJ/m^2	Energy, eV	W^{ad}(ideal), mJ/m^2
Ni(111)	-292.441	-	-292.443	-
NiAl(110)	-87.464	-	-87.80	-
Ni(111)/NiAl(110)	-382.867	1106.77	-390.092	3683.58

Based on the computational results and understanding, a few important points of these ab-initio simulations can be summarized as:

(a) First-principle calculations on Ni(111)/NiAl(110) interface has indicated strong adhesion.

(b) Ideal work of adhesion, W^{ad} (ideal) = 3684 mJ/m^2 ; lowest bound value.

(c) Strong metallic Ni *d* Ni *d* interaction and covalent Ni *d* Al *p* mixing of states give rise to strong adhesion at the Ni(111)/NiAl(110) interface.

(d) For Cr-doped interface, ideal work of adhesion, W^{ad} (ideal) = 3524 mJ/m^2 that is slightly lower as compared to that with pure Ni substrate.

CHAPTER 6: Oxidation behaviour of aluminized superalloys and evaluation of stability of aluminized and oxidized superalloy 690

Thermal oxidation resistance of aluminides formed on substrates of superalloys 690 and 800 using aluminization process at 1273 K in argon atmosphere has been discussed here as it is of immense importance to work related to the development of diffusion barrier coatings for applications at elevated temperatures. All the results of the present investigation have been discussed and compared with the findings of other investigators [14,15,16] to justify the oxidation resistance of the superalloys 690 and 800 and the stability of pre-oxidized aluminide coatings on superalloy 690. Fig. 4 shows some result on thermal oxidation of superalloy 690.

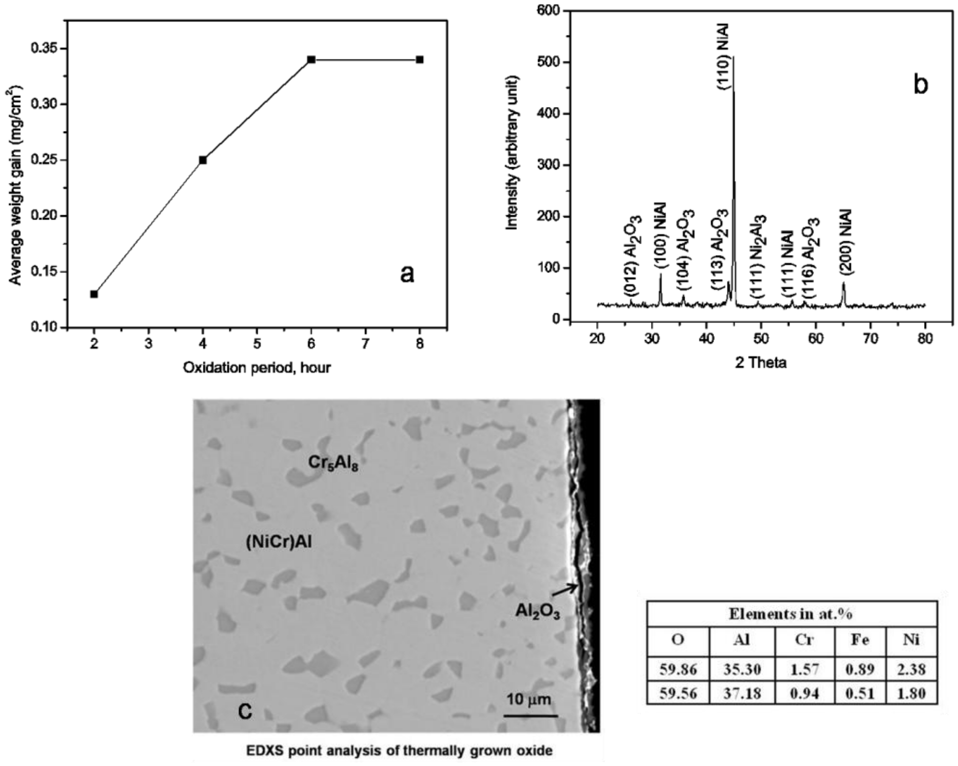

Elements in at.%				
O	Al	Cr	Fe	Ni
59.86	35.30	1.57	0.89	2.38
59.56	37.18	0.94	0.51	1.80

EDXS point analysis of thermally grown oxide

Fig. 4 Variation of weight gain with oxidation period for pack aluminized (2 wt.% Al) superalloy 690 is shown in 4a while 4b demonstrates the presence of Al_2O_3 phase along with predominantly NiAl type phase in thermally oxidized specimen (1273 K for 8 hours). The presence of (NiCr)Al + Cr_5Al_8 types aluminides and Al_2O_3 type layer along with EDXS analysis of oxide is shown in 4c for aluminized (10 wt.% Al) and thermally oxidized (1273 K for 4 hours) superalloy 690.

Based on experimental evidences and understanding, a few important points of the present work can be summarized as:

(a) Good oxidation resistance has been noticed for pack aluminized superalloy 690 substrates at 1273 K in air, which is attributable to formation of a thin Al_2O_3 layer. A fairly good oxidation resistance has also been exhibited by pack aluminized superalloy 800 specimens under similar experimental conditions.

(b) In borosilicate melt, superalloy 690 is oxidized and a thick, continuous Cr_2O_3 layer forms at the glass/alloy interface because of low solubility of Cr_2O_3 in borosilicate melt. A good stability of aluminide coatings with Al_2O_3 layer for superalloy 690 substrates in borosilicate melt at 1248 K is attributed to modification of glass composition at the coating/glass interface that is believed to have induced by partial dissolution of alumina from preexisting Al_2O_3 layer.

Concluding remarks

An attempt has been made in the present study to cover aluminization, microstructural characterization and property evaluation of superalloys 690 and 800 substrates, which can be put in the category of Ni-Cr-Fe based alloys in a broader sense. First-principle calculations have been performed on Ni(Cr)/NiAl interface to estimate ideal work of adhesion between Ni and NiAl and to understand the nature of bonding across the interface. Besides this, the stability of thermally oxidized aluminide coatings of superalloy 690 in borosilicate melt has been evaluated. All these aspects of superalloys 690 and 800 are of relevance to the development of diffusion barrier coatings for applications at elevated temperatures. The results of the present work have been found to be quite promising. There is ample scope to pursue the work in future to evaluate the stability of nickel-alumides/ (nickel + chromium)-aluminides/iron-aluminides coatings for applications at elevated temperatures in oxidizing/non-oxidizing and aggressive environments and to optimize the compositions of aluminides accordingly.

References:

[1] Special Metals, Alloy 690, web: www.specialmetals.com.

[2] R.S. Dutta, in: I.S. Wang (Ed.), Corrosion Research Trends, Nova Science Publishers, Inc., NY, 2007, pp 349-365.

[3] V. Kain, P. Sengupta, P.K. De, S. Banerjee, ‘Case Reviews on the Effect of Microstructure on the Corrosion Behavior of Austenitic Alloys for Processing and Storage of Nuclear Waste’, Metall. Mater. Trans. A 36 A (2005) 1075-1084.

[4] P. Sengupta, C.P. Kaushik, G.B. Kale, D. Das, K. Raj, B.P. Sharma, ‘Evaluation of alloy 690 process pot at the contact with borosilicate melt pool during vitrification of high-level nuclear waste’, J. Nucl. Mater. 392 (2009) 379-385.

[5] Special Metals, Alloy 800, web: www.specialmetals.com.

[6] R.S. Dutta, ‘Corrosion aspects of Ni–Cr–Fe based and Ni–Cu based steam generator tube materials’, J. Nucl. Mater. 393 (2009) 343-349.

[7] D. M. Miller, S. C. Kung, S. D. Scarberry, R. A. Rapp, ‘Simultaneous Chromizing-Aluminizing Coating of Austenitic Stainless Steels’, Oxidation of Metals 29 (1988) 239-254.

[8] V. A. C. Haanappel, B. Geerdink, T. Fransen, P. J. Gellings, ‘The corrosion and mechanical behaviours of aluminide, FeCrA1Y and CoCrA1Y coatings in aggressive environments’, Mater. Sci. and Engg. A 148 (1991) 131-139.

[9] V. Vokál, V. Rohr, M. J. Pomeroy, M. Schütze, ‘Corrosion of alloys and their diffusion aluminide coatings by KCl: K_2SO_4 deposits at 650^o C in air’, Mater. and Corr. 59 (2008) 374-379.

[10] S.R. Levine, R.M. Caves, ‘Thermodynamics and Kinetics of Pack Aluminide Coating Formation on IN-100’, J. of Elec. Soc. 121 (1974) 1051-1064.

[11] C. Sierra, A.J. Vázquez, ‘Dry sliding wear behaviour of nickel aluminides coatings produced by self-propagating high-temperature synthesis’, Intermetallics 14 (2006) 848.

[12] J. Xia, C. X. Li, H. Dong, 'Hot-stage nano-characterisations of an iron aluminide', Mater. Sci. and Eng. A 354 (2003) 112-120.

[13] G. Kresse, J. Furthmueller, 'Efficient iterative schemes for ab initio total-energy calculations using a plane-wave basis set', Phys. Rev. B 54 (1996) 11169-11186.

[14] P. Sengupta, J. Nucl. Mater. 'Interaction study between nuclear waste-glass melt and ceramic melter bellow liner materials', 411 (2011) 181-184.

[15] M.W. Brumm, H.J. Grabke, 'The oxidation behavior of NiAl I. Phase-transformations in the alumina scale during oxidation of NiAl and NiAl-Cr Alloys', Corr. Sci. 33 (1992) 1677-1690.

[16] D. Zhu, C.W. Kim, D.E. Day, 'Corrosion behavior of Inconel 690 and 693 in an iron phosphate melt', J. Nucl. Mater. 336 (2005) 47-53.

Publications:

a. Published

1. 'Characterization of aluminides formed on superalloy 690 substrate'

   R. S. Dutta, S. Majumdar, P. K. Limaye, U. D. Kulkarni and G. K. Dey, Trans. IIM, vol. 64, Issues 1 & 2, February-April 2011, pp 31-36.

2. 'Formation and characterization of aluminide coatings on Alloy 800 substrate'

   R. S. Dutta, S. Majumdar, A. Laik, K. Singh, U. D. Kulkarni, I. G. Sharma and G. K. Dey, Surface & Coatings Technology, vol. 205, 2011, p 4720-4725.

3. 'Thermally grown oxide layer on aluminized superalloy 690 substrate and its stability in nitrate-based environment'

   Rabi Sankar Dutta, Chelakkattu Yusufali, Sanjib Majumdar, Raman Kumar Mishra, Chetan Parkash Kaushik, Rohidas Jagannath Kshirsagar, Ulhas Digambar Kulkarni and Gautam Kumar Dey, Materials Science Forum, vol. 710, 2012, pp 733-738.

4. 'Formation of diffusion barrier coating on superalloy 690 substrate and its stability in borosilicate melt at elevated temperature'

R.S. Dutta, C. Yusufali, B. Paul, S. Majumdar, P. Sengupta, R.K. Mishra, C.P. Kaushik, R.J. Kshirsagar, U.D. Kulkarni and G.K. Dey, Journal of Nuclear Materials, vol. 432, 2013, pp 72-77.

5. ‘Formation of aluminides on Ni-based superalloy 690 substrate, their characterization and first-principle Ni(111)/NiAl(110) interface simulations’

   R.S. Dutta, A. Arya, C. Yusufali, B. Vishwanadh, R. Tewari, G.K. Dey, Surface & Coatings Technology, vol. 235, 2013, pp 741-747.

Signature of Student:

Date:

Doctoral Committee:

Serial No.	Name	Designation	Signature	Date
		Chairman		
		Convener		
		Member		
		Member		
		Member		
		Member		

LIST OF FIGURES

LIST OF TABLES

LIST OF ABBREVIATIONS

Face-centered cubic	FCC
Body-centered cubic	BCC
Steam generator	SG
Chemical vapour deposition	CVD
Physical vapour deposition	PVD
Electron beam physical vapour deposition	EBPVD
Air plasma spraying	APS
Argon-shrouded plasma spraying	ASPS
Scanning electron microscopy	SEM
Electron probe microanalysis	EPMA
Secondary electron	SE
Back-scattered electron	BSE
Wavelength dispersive spectroscopy	WDS
X-ray diffraction	XRD
Energy dispersive X-ray spectroscopy	EDXS
Transmission electron microscopy	TEM
Selected area diffraction	SAD
Vienna Ab-initio Simulation Package	VASP
Density functional theory	DFT
Knoop hardness number	KHN
Vickers hardness number	VHN

CHAPTER 1: INTRODUCTION

1.1 Background

1.1.1 Superalloys and their categories

Superalloys are high-performance alloys those exhibit a combination of mechanical strength and resistance to surface degradation at elevated temperatures. In the beginning, superalloys were Fe-based alloys, which were used under cold wrought condition [1]. In the decade of 1940, investment casting of Co-based superalloys was introduced and this increased operating temperatures considerably. Later in the 1950s with development of vacuum melting techniques, very fine control of chemical compositions of superalloys and reduction in contamination were possible. This, in turn, led to a revolution in processing techniques such as directional-solidification of alloys and single crystal superalloys [1]. With the advancement on each melting and processing technique, a variety of superalloys, catering wide range of technical needs, has been introduced. Based on their solvent elements, superalloys can be broadly classified into three categories, which are Ni-, Fe- and Co-based alloys. Each category of superalloys has its own strength and weakness. In the following subsections, each category has been briefly discussed.

Ni-based superalloys

Ni-based superalloys are the most widely used ones for the parts those experience very high temperature and are the most important ones among superalloys [2]. They currently constitute over 50% of the weight of advanced aircraft engines. The principal characteristics of nickel as an alloy base are the high phase stability of the face-centered cubic (FCC) nickel matrix and the capability to be strengthened by a variety of direct and indirect means. Further, the stability of surface film is readily improved by alloying with chromium and/or aluminum.

The Ni-based superalloys are considered to be complex as they contain quite a good number of elements. In addition to perhaps 10 to 12 more tramp and trace elements such as Mn, Si, P, S, oxygen, and nitrogen must be controlled through appropriate melting practices. Besides this, other trace elements such as Bi, Pb, must be controlled to very small (ppm) levels in critical parts. Many nickel-based superalloys contain 10 to 20% Cr, up to about 8% Al and Ti and small amounts of boron, zirconium, and carbon. Other optional additions are Co, Mo, Nb, W and Ta [2]. Table 1.1 shows the chemical compositions of some nickel-based superalloys [3,4,5]. Ni-based superalloys shown in Table 1.1 can be broadly classified into solid solution-strengthened and precipitation-hardenable varieties. The alloys like Inconel 600, Inconel 690, Inconel 625, Hastalloy C-276 etc. are solid solution-strengthened while Inconel X-750, Astroloy, M-252, Nimonic 115, Waspaloy, Udimet 700 etc. are precipitation-hardenable type. Mar M-246 is an equiaxed cast alloy and CMSX-10 is a single crystal superalloy, which are used in gas turbine engine components.

The major phases that may be present in nickel-based alloys are [2]:

Gamma matrix, γ: The continuous matrix is an FCC nickel-base nonmagnetic phase that generally contains a high percentage of solid-solution elements such as Co, Cr, Mo and W.

Gamma prime, γ': Al and Ti are added in amounts and required proportions to precipitate high volume fraction of FCC γ', which precipitates coherently with the austenitic matrix.

Grain boundary γ': For many alloys, heat-treatments have been developed, which bring about a film of γ' along the gain boundaries. This film is believed to improve rupture properties.

Carbides: Carbon that is added in the range of 0.05 to 0.2 wt% often reacts with reactive and refractory elements to form primary metal carbides of MC type. During the heat treatment and in service, these MC carbides decompose and generate other carbides, such as $M_{23}C_6$ and M_6C and populate the grain boundaries.

Topologically close-packed type phases: Plate-like phases such as σ, μ and Laves may form under certain conditions. These cause lowered rupture strength and ductility.

Table 1.1: Major alloying elements in wrought and cast Ni-based superalloys (wt.%) [3,4,5]

Wrought Ni-based alloys						
	Al+Ti+Ta+Nb	Mo+W	Cr	Co	Ni	Other
Inconel X-750	4.2	-	15	-	73	7 Fe
Inconel 600	-	-	15.5	-	76	8 Fe
Inconel 690	-	-	31	-	58	11 Fe
Inconel 625	4.95	10	23	1	58	5 Fe
Inconel 693	7.5	-	31	-	Bal	6 Fe
Inconel 22	-	18	22.5	2.5	Bal	6 Fe
Hastelloy C-276	-	19.7	15.5	-	59	5 Fe
M-252	3.6	10	20	10	55	-
Waspaloy	4.3	4.3	19	13	58	-
Nimonic 115	9.0	3.5	15	15	57	-
Astroloy	7.9	5.2	15	15	57	-
AF 2 IDA	9.1	9.0	12	10	59	-
Cast Ni-based alloys						
Udimet 500	6.0	4.2	19	18	52	-
Udimet 700	7.75	5.25	15	18.5	53.5	
Rene 77	7.9	4.2	14.6	18.5	58	-
713C	8.9	4.2	12.5	-	74	-
IN-738	9.5	4.4	16	8.5	61	-
Rene 80	8.0	8.0	14	9.5	60	-
B-1900	11.0	6.0	8.0	10	64	-
IN-100	10.2	3.0	10.0	15	60	0.9 V
NASA-TRW VI A	15.9	7.8	6.1	7.5	61	0.5 Hf 0.3 Re
CMSX-10	18.2	9.5	4	9	Bal	
Mar M -246	8.5	12.5	9	10	60	
Wax-20 (DS)	6.5	20	-	-	72	1.5 Zr

*Inconel, Waspaloy etc. are the trade names

Fe-based superalloys

Fe-based 16-25-6 (Cr-Ni-Mo) alloy was developed in 1940s [3]. The alloy was extensively used in turbine wheels and remained the dominant one for more than 10 years. In 1950s, a number of precipitation hardenable alloys were developed, which include Discaloy, A-286 and V-57. The said alloys, which offered higher strength, are still in use. Majority of the alloys in this system contain around 25 wt.% Ni to stabilize the austenitic structure and 15 wt.% Cr to impart corrosion resistance. For solid-solution strengthening, Mo is added in moderate amount. More recent alloys contain a total of 2-3 wt.% Al +Ti for achieving precipitation hardening. Table 1.2 shows major alloying elements in iron-based superalloys. These turbine wheel alloys can be operated in the temperature range of 813 K except for V-57 that can be used up to about 1003 K. Conventional wrought alloys for higher temperature of this type are likely to be unacceptable by the industries due to a tendency toward phase instability as the alloy content is increased. This problem can be solved by replacing part of the iron with nickel, thus making highly alloyed and stronger material without the formation of detrimental phases. This has been achieved in nickel-iron alloys such as Incoloy 901, Inconel 718 and D-979. Table 1.2 shows the major alloying elements in wrought Fe- and Ni-Fe based superalloys [3, 4]. Although Incoloy 800 is generally shown under solid-solution variety, it is a precipitation-hardenable type. The precipitation of its γ' phase that is responsible for precipitation hardening effect is very sluggish. Incoloy 909, Incoloy 925, Inconel 706, Inconel 718 etc. are the typical precipitation-hardenable alloys. Incoloy MA 956 possesses excellent strength and fabricability with outstanding resistance to prolonged exposure up to 1573 K. Its exceptional properties result from the mechanical alloying by which it is made. It is a process that allows a fine distribution of yttrium oxide particles into a highly corrosion resistant Fe-Cr-Al alloy.

Table 1.2: Major alloying elements in wrought Fe- and Ni-Fe based superalloys (wt.%) [3,4]

Fe-based alloys						
	Al+Ti+Ta+Nb	Mo+W	Cr	Fe	Ni	Other
16-25-6	-	6	16	51	25	
Discaloy	1.8	2.7	14	54	26	
A-286	2.4	1.3	15	55	26	
V-57	3.2	1.2	15	52	27	
Incoloy 800	1.2	-	23	39.5	35	
Incoloy 909	7.15	-	-	Bal	40	16 Co
Incoloy MA 956	6.35	-	21.5	Bal	0.5	0.7 Y_2O_3
Ni-Fe based alloys						
Pyromet 860	4.2	6	13	29.5	43	
D-979	4	8	15	27	46	
Incoloy 901	3	5.7	12	36	42	
Inconel 706	4.9	-	16	37	41	
Inconel 718	6.3	3.1	19	18	53	
Incoloy 890	1.5	1.5	25	Bal	42.5	
Incoloy 925	3.4	3.5	22.5	22	46	

* Incoloy, Inconel etc. are the trade names

Co-based superalloys

Co-based superalloys were used to a great extent in early aircraft gas turbine engines as blades and vanes [3]. The ability was first shown more than seventy years back when cast Vitallium (Co-27Cr-5.5Mo-2.5Ni-0.25C) turbo supercharger blades were engine tested with success. Modification of said alloy was done later to reduce the tendency for carbide precipitation and subsequent loss of ductility in service. Modified alloy is known as Haynes alloy 21.

Both cast and wrought cobalt-based superalloys are generally FCC (austenite). They are solid solutions containing one or more carbides. Their strength is achieved both by solid-solution hardening by a combination of Ta, Nb, Mo, W and Cr and also through dispersion hardening by carbides of these elements or Zr. The FCC structure of these alloys is stabilized by nickel. Nickel also counterbalances the tendency of the refractory metals to cause transformation to the hexagonal-close-packed structure. The microstructure of cast cobalt-based alloys such as Mar-M 509 contains blocky, script and eutectic carbides in a solid-solution matrix without any intermetallic compounds. Intermetallic compounds are occasionally for strengthening cobalt-based alloys due to their tendency toward instability at elevated temperatures. Popular wrought cobalt-based alloys in past included S-816 that was used in many turbine buckets and L-605 sheet that found application in burners and ducts. Haynes alloy 188, a new wrought alloy, was developed in 1966 that combines the strength of L-605 with improved oxidation resistance and ductility in service. Wrought cobalt alloys often contain less chromium. Table 1.3 shows major alloying elements in wrought and cast Cobalt-based superalloys [3,5]. In wrought variety, MP 35-N, MP 159, Stellite B, UMCo-50 are some of the new solid solution alloys while in cast variety, MAR-M 918, NASA Co-W-Re are the new ones.

Table 1.3: Major alloying elements in wrought and cast Co-based superalloys (wt.%) [3,5]

Wrought Co-based alloys							
	C	Ta+Nb	Mo+W	Cr	Ni	Co	Other
L 605(HA 25)	0.1	-	15	20	10	55	
HA 188	0.1	-	14	22	22	40	0.08La 1 Fe
S 816	0.4	4	8	20	20	44	4 Fe
MP 35-N	-		10	20	35	35	
MP 159	-	0.6	7	19	25	36	9Fe ,3Ti, 0.2Al,
Stellite B	1.0		4.5	30	1	61.5	1Fe
UMCo-50	0.12		-	28	-	49	21Fe
Cast Co-based alloys							
X-45	0.25	-	7.5	25	10	54	2 Fe
FSX 414	0.35	-	7	29.5	10	51	2 Fe
HS-31(X-40)	0.5	-	7.5	25	10	54	2 Fe
WI-52	0.45	2	11	21	-	64	2 Fe
MAR-M 509	0.6	3.5	7	24	10	54	0.5 Zr
MAR-M 322	1.0	4.5	9	21.5	-	61	2.2 Zr
MAR-M 918	0.05	7.5		20	20	52	0.1Zr
AiResist 215	0.35	7.5	4.5	19	0.5	63	4.3Al,0.5Fe 0.1Zr,0.1Y
NASA Co-W-Re	0.4	-	25	3		67.5	1Ti, 1Zr,2Re

1.1.2 Properties of Superalloys

1.1.2.1 Mechanical Properties

The close-packed FCC lattice for superalloys of austenitic compositions has great capability to maintain good tensile, rupture and creep properties to homologous temperatures much higher than for equivalent BCC systems due to several factors, which include excellent modulus and diffusivity of secondary elements in FCC lattice [3]. Probably of utmost importance is the solubility of many elements in austenitic matrix and the ability to regulate the precipitation of intermetallic compounds such as γ' for strength. Strengthening effects can also be achieved by solid solution hardening and carbide precipitation. This capability of Ni-Co-Fe austenite cannot be underrated. It has led to very satisfactory medium- and high-temperature tensile properties for turbine wheels, to very strong compositions for turbine blades for short-lived military aircraft and to high long-time creep-rupture resistant compositions for industrial turbine and for all types of vanes. Besides properties like tensile, stress-rupture and creep, other mechanical properties of superalloys must be taken into account. Ductility under service conditions as well as during processing is of immense importance. Superalloys, in general, demand good ductility. The majority of the superalloys possess very good impact resistance and good resistance to high-cycle and low-cycle mechanical fatigue as well as thermal fatigue [3].

1.1.2.2 Physical Characteristics

The data for physical properties for unalloyed Ni, Co, Fe and Cr are shown in Table 1.4.

1.1.2.2.1 Density

The density of superalloys lies in the range of 0.28 to 0.335 lb/in^3. Fe-based alloys possess the lowest density due to density advantage of Fe over Ni and Co. Ni-based alloys have a range of densities because of wide variation in contents of alloying elements. This can be exemplified as the case for IN-100 (containing about 60% Ni), which shows a density of 0.28

lb/in^3 owing to large amount of low-density Al and Ti contents [3]. On the contrary, some Ni-based alloys containing large amounts of high-density W and Ta have densities as high as 0.326 lb/in^3. For Co-based alloys, W and Ta are the major additions and that is why, these superalloys show high densities in the range of 0.31 to 0.335 lb/in^3. Density is an important consideration particularly in the design of rotating components to minimize centrifugal stress.

Table 1.4: Physical properties of elemental Co, Ni, Fe and Cr [3]

Element	Crystal structure at 298 K	Melting point, K	Density, g.cm^{-3} near 298 K	Thermal expansion at 298 K, µm·m^{-1}·K^{-1}	Thermal conductivity, W·m^{-1}·K^{-1}	Phase stability (alloying tolerance)
Co	HCP	1768	8.9	13.0	100	2
Ni	FCC	1728	8.908	13.4	90.9	1 (most stable)
Fe	BCC	1811	7.874	11.8	80.4	4 (least stable)
Cr	BCC	2180	7.19	4.9	93.9	3

1.1.2.2.2 Thermal Expansion

Ni- and Co-based alloys show similar thermal expansion coefficients those are lower as compared to austenitic Fe-based alloys. Since gas turbines are designed to operate most efficiently with close tolerances, thermal expansion is a design factor of immense importance. In some cases, it necessitates to match coefficients in mating components while in other cases, a low coefficient is desirable to minimize thermal stresses, which result in buckling and thermal fatigue cracking [3].

1.1.2.2.3 Thermal Conductivity

Extensive alloying adversely affects thermal conductivity of superalloys. It is only in the range of 10 to 30% that of pure Fe, Ni, or Co because of the effect of enormous alloying.

Generally, Fe-based alloys are slightly more conductive as compared to Co-based alloys and Ni-based alloys extend the range of each. To dissipate heat and minimize temperature gradients for reducing thermal stress and the tendency for thermal-fatigue failures, it is desirable to have high thermal conductivity in superalloys [3].

1.1.2.2.4 Phase Instability

The individual phases in the microstructure of superalloys have a tendency to change on exposure to high temperatures. Depending upon the temperature and time of exposure, many phase changes can take place. This phase instability is responsible to vary the properties of many of these alloys by heat-treatments those are followed to develop optimum composition, the size, the shape and the volume fraction of carbides and intermetallic phases [3]. In some alloys, phase instability induces formation of phases those can weaken the structure. This can occur when the base metal is highly alloyed with certain elements. In this respect, Ni has an advantage over the other bases as it is having a greater tolerance for alloying additions without the formation of deleterious phases.

1.1.2.3 Surface Stability

Hot section of a gas turbine engine is one of the most harsh environments encountered in service [3]. The high-velocity hot gas stream that is produced by compression and combustion has an enormous capacity in degrading the hot stage parts by oxidation and hot corrosion and that is why, surface stability of the superalloys quite often becomes the limiting service factor.

1.1.2.3.1 Oxidation

In gas turbine industry, the definition of oxidation is the reaction of an alloy with oxygen in the presence of products of combustion of clean fuel, which is mostly devoid of contaminants like Na, S and V. Good oxidation resistance is obtained by the formation of an adherent, continuous surface layer, which serves as a diffusion barrier and does not spall off during thermal cycling [3]. Generally, Ni-Cr alloys containing high amount of Al, such as 713C and B-1900, are known to have excellent resistance to oxidation owing to their ability to form the protective oxides Cr_2O_3 and Al_2O_3. As compared to Ni-based alloys, Co-based alloys possess resistance to oxidation somewhat to a lesser extent. It has been found that the Co-based alloy X-45 suffers about five times the oxidation of a typical Ni-based alloy such as Rene 77 (U-700) in a 2000-hr oxidation test at 1313 K. Minor additions of Y, La or Ce have been reported to promote scale retention and improve the resistance to oxidation of a number of Co-, Fe-, Ni- and Cr-based alloys [3].

1.1.2.3.2 Hot Corrosion

In gas turbine industry, hot corrosion that is occasionally referred as sulfidation is an aggressive attack caused by the combined effects of oxidation and reaction with S and other contaminants ingested with inlet air and content in fuel [3]. It proceeds by a complex series of reactions. One view of its reaction sequence is formation of molten Na_2SO_4 that dissolves the protective oxide facilitating inward movement of S into the base metal followed by a reaction of S with Cr precipitating sulfides.

For Ni- and Co-based alloys, hot corrosion resistance is related to Cr content and is also a function of sulfide properties of these alloy systems. Cobalt sulfide is more refractory as compared to nickel sulfide and Co has a lower diffusivity for S. In addition, most of the Co alloys contain higher amount of Cr as compared to their Ni counterparts. The net result is that Co-based alloys possess superior hot corrosion resistance as compared to Ni-based alloys. Severe hot corrosion is limited to temperatures below around 1253 K as above this temperature Na_2SO_4 volatilizes and hot corrosion does not take place but it is the oxidation that predominates. It is to be mentioned that generalization about comparative oxidation and hot corrosion resistance of Ni- and Co-based alloys must be done carefully as there are wide ranges of resistance within each group and small variations in service conditions may affect the results to a great extent [3].

1.1.3 Superalloys of present study

In the present study, Alloy 690 and Alloy 800 those are superalloys have been considered. Chemical compositions, microstructures and mechanical properties of the said alloys have been briefly discussed in the following subsections.

Alloy 690

Alloy 690 is a solid solution-strengthened high chromium low iron containing Ni-based superalloy. The high chromium content in the alloy makes it very resistant to attack from oxidizing chemicals or hot gases. High concentration of nickel in the alloys improves resistance to stress corrosion cracking in chloride-containing environments as well as to sodium hydroxide solutions [4]. Besides its corrosion resistance, superalloy 690 has high strength, has a high degree of metallurgical stability without forming any embrittling phases during during prolonged (up to 12,000 hours) exposure at 1033 K and exhibits excellent weldability. These combinations of properties make this material useful for several diverse applications. For example, high resistance to sulfur-containing gases makes it an attractive material for coal-gasification units, burners and ducts for processing sulfuric acid, furnaces for petrochemical processing, recuperators, incinerators, and glass vitrification equipments for radioactive waste disposal. Superalloy 690 is extensively used for steam generator tubes, baffles, tubesheets, and hardware in nuclear power generation [4,6].

Superalloy 690 has single phase (FCC; austenitic) microstructure. The alloy has a low solubility for carbon and its microstructure normally contains carbides. The major carbide present in the alloy is $M_{23}C_6$. The abundance of the phase varies with carbon content and thermal exposure of the material. Other phases normally present are titanium nitrides and carbonitrides. This alloy has been found to contain primary TiC (small, spherical-shaped) and TiN (large, faceted) particles randomly distributed in the austenite matrix. Figure 1.1, for example, shows a typical micrograph of mill-annealed superalloy 690 revealing primary TiN particle and secondary Cr-carbides. Thermal treatment of the alloy at 973 K for 4 hours followed by air cooling forms discrete grain boundary Cr-carbide precipitation along with intragranular Cr-carbides, whereas ageing treatment for 16 hours results in intragranular and near continuous intergranular Cr-carbide precipitation. These secondary Cr-carbides are of $M_{23}C_6$ type and large, faceted TiN particle/matrix interface has been reported to act as a precipitation site during ageing of the alloy.

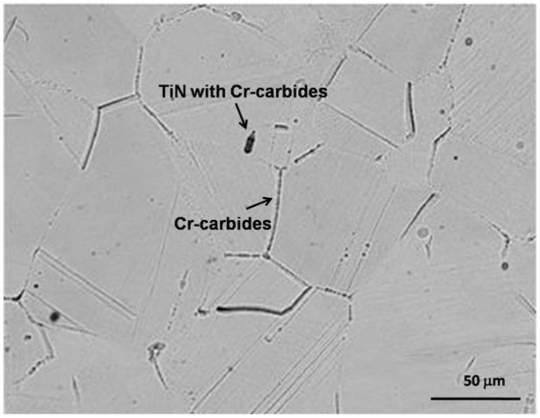

Figure 1.1 Superalloy 690 in mill-annealed condition revealing primary TiN particle and secondary Cr-carbides.

The hardness of Alloy 690 (skin hard) is reported to vary from B85 to B88 (Rockwell B scale) at 298 K. For annealed Alloy 690, yield strength decreases from 325 to 150 MPa with the increase in temperature from room temperature (RT) to 1273 K. The tensile strength changes from 700 to 600 MPa with the increase in temperature from RT to 723 K and finally comes down to 150 MPa at 1273 K. The elongation remains at a value of about 50 to 40 % over a range of temperature from RT to 873 K and increases to 90% at about 1073 K and remains constant up to 1273 K. The creep rate (%/h) of annealed Alloy 690 is found to vary from 0.001 to 0.6 over a range of stress level from 5 to 10 MPa at 1253 K [4].

Alloy 800

Alloy 800 is austenitic, high nickel moderate chromium containing Fe-based superalloy. It is extensively used as a material for heat-treating equipment, heat-exchangers, piping systems, digester-liquor heaters, which require resistance to corrosion as well as heat, strength and stability for services up to 1089 K. The alloy possesses general corrosion resistance to many aqueous environments and resists stress corrosion cracking by virtue of its high nickel content. It offers resistance to oxidation, carburization and sulfidation along with rupture and creep strength at elevated temperatures [4].

The chromium in the alloy imparts both aqueous and heat resistance while resistance to internal oxidation (that could be due to readiness with which chromium is oxidized) is provided by iron. The high nickel content maintains a ductile, austenitic structure enabling the alloy to be readily formed, welded and machined [4].

Superalloy 800 has got various applications, which involve exposure to corrosive media and high temperature. It is used for heat-treating equipment. In chemical and petrochemical processing, the alloy is used for heat exchangers. It is used as material for construction where resistance to chloride stress corrosion cracking is needed. In nuclear power plants, superalloy 800 is extensively used as steam generator tube material. In petroleum processing, the alloy is used for heat exchangers, which air cool the process stream. Besides this, digester-liquor heaters in paper pulp industry are often made of this alloy [4,7].

Superalloy 800 is generally used in solid solution-strengthened condition. The alloy contains minor alloying elements like Ti and Al those are added to this alloy to bring about precipitate of $Ni_3(Ti,Al)$, known as γ', on longer ageing to induce precipitation hardening effect. This alloy contains primary TiC (small, spherical-shaped) and TiN (large, faceted) particles randomly distributed in the austenite matrix. Figure 1.2 shows mill-annealed superalloy 800 revealing secondary Cr-carbides and a few randomly distributed TiN particles. Ageing of the alloy at 973 K for specific periods followed by air cooling brings about grain boundary Cr-carbide precipitation. The primary nitride particles have been found to act as precipitating sites for secondary Cr-carbides, which are of $M_{23}C_6$ type.

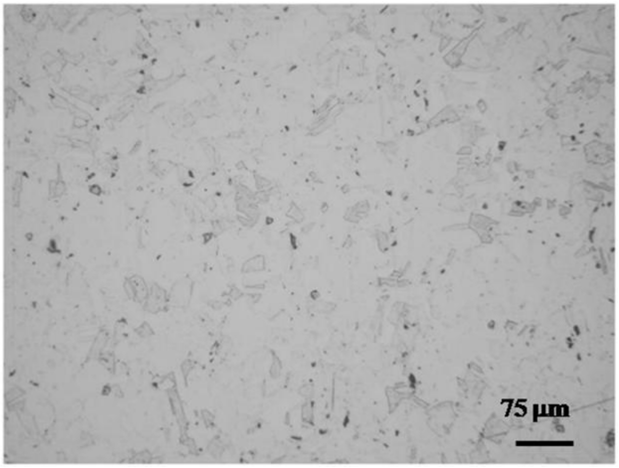

Figure 1.2 Superalloy 800 in mill-annealed condition revealing a few randomly distributed primary TiN particles and secondary Cr-carbides.

The hardness of annealed Alloy 800 at 298 K is reported as 138 BHN. For annealed Alloy 800 yield strength is found to decrease from 300 to 100 MPa with the increase in temperature from RT to 1073 K. The tensile strength changes from 600 to 500 MPa with the increase in temperature from RT to 823 K and finally comes down to 150 MPa at 1073 K. The elongation remains in the vicinity 40 % over a range of temperature from RT to 873 K and increases to 90% at about 1073 K. The creep rate (%/h) of annealed Alloy 800 is found to vary from 0.00001 to 0.4 over a range of stress level from 25 to 150 at 978 K [4].

1.1.4 Motivation of the study

Alloy 690 is a solid solution-strengthened, austenitic, high chromium low iron containing Ni-based superalloy. It is an attractive material for coal-gasification units, burners and ducts for processing sulfuric acid, furnaces for petrochemical processing and steam generator (SG) tubes in nuclear power generation [4,6]. Superalloy 690 is also used as material of construction for process pot and susceptor in metallic melter pot furnace as well as electrodes in Joule-heated ceramic melter pot employed for high level nuclear waste immobilization process. However, due to formation of thick, continuous Cr_2O_3 layer at the alloy/molten borosilicate glass interface, the alloy adjacent to the interface has been reported to be depleted in Cr resulting to almost half of its initial content in the alloy [8,9]. Besides this, flaking off continuous Cr-oxide layer can take place due to the development of compressive stresses because of its high thickness and convective motion within borosilicate melt pool adjacent to the region. These phenomena can lead to leaching out of Cr from the alloy ultimately leading to premature failure of metallic melter pot furnaces. Therefore, it is of prime importance to develop effective diffusion barrier coatings on the alloy so that the life of the components can be extended. Aluminides are found to be very effective in functioning as diffusion barrier coatings as they form a protective layer of Al_2O_3 when exposed to high temperature. Keeping this in view, a systematic and detailed study on development of diffusion barrier coatings consisting of aluminization of superalloy 690 substrates followed by their microstructural characterization, property evaluation along with ab-initio modeling of Ni(Cr)/NiAl interface and evaluation of thermal oxidation resistance as well as stability in borosilicate melt is intended to undertake to understand the protectiveness of the aluminide coatings in a rigorous manner, which has not been attempted so far. As the service temperature of the component (superalloy 690 as metallic melter pot) is close to 1273 K, similar temperature for thermal oxidation will be chosen and an attempt will also be made to evaluate the behaviour of oxidation. For aluminized and thermally oxidized specimens of superalloy 690 specimens, temperature of exposure to borosilicate melt will be chosen at 1248 K for a prolonged duration (in the vicinity of 200 hours or so) to evaluate the stability of the coatings since these conditions closely simulate the service conditions of metallic melter pot.

Apart from Alloy 690, one more alloy that is Alloy 800 has also been considered in the present study. Alloy 800 is an austenitic, high nickel moderate chromium containing Fe-based superalloy. It is generally used in solid solution-strengthened condition. In chemical and petrochemical processing, the alloy is used for heat exchangers. It is used as a material for construction where resistance to chloride stress corrosion cracking is needed. In nuclear power plants, superalloy 800 is extensively used as SG tube material. In petroleum processing, the alloy is used for heat exchangers, which air cool the process stream. Besides this, digester-liquor heaters in paper pulp industry are often made of this alloy [4,7]. As compared to the number of studies reported on superalloy 800 in SG related issues, there are only a few on the development of aluminide coatings on this alloy for applications at elevated temperatures [10-12]. Miller et al. [10] have used different Cr-Al masteralloys and alkali halide vapours to form an interdiffusion zone enriched in Cr and Al for Alloy 800, but have not succeeded to achieve the desired one. Investigation by Haanappel et al. [11] has indicated that aluminide coatings formed on Alloy 800H can provide resistance to sulphidation up to 823 K. Vokál et al. [12] have reported the formation of (Ni,Fe)Al and Fe_2Al_5 phases on top surface of Alloy 800 after pack cementation and have noticed degradation of (Ni,Fe)Al coating after the exposure of coated specimens in 50 mol% KCl + 50 mol% K_2SO_4 at 923 K. Hence, an investigation relating to development of aluminide coatings for applications up to ~ 1273 K where tensile strength of the alloy is not of primary consideration is of importance. It is also of importance to develop Fe_2Al_5 and FeAl coatings [12] and to characterize their various parameters for possible application as coating material to form Al_2O_3 on it for fusion reactor programme. Therefore, a study on the formation of aluminide coatings on high nickel and moderate chromium containing Fe-based austenitic superalloy 800 followed by their microstructural characterization and property evaluation will be undertaken along with superalloy 690. For aluminizing the substrates of superalloys 690 and 800, pack cementation (pack aluminization) method will be employed as this method is an effective as well as inexpensive one.

1.2 Objective of the study

For superalloy 690, the objective of the present investigation is primarily to develop diffusion barrier coatings on the alloy surface for enhanced service life of metallic melter pot as well as electrode in Joule-heated ceramic melter pot in nuclear waste immobilization process. In addition, to explore the possibility of uses of aluminide coatings at elevated temperatures (up to 1273 K) by evaluating their different properties where tensile strength is of secondary consideration. In case of superalloy 800, the main objective of the present study is to examine various aspects of aluminides formed on the alloy surface for the development of aluminide coatings for applications at elevated temperatures (up to 1273 K) where tensile strength is not of primary consideration. In doing so, the substrates of the said superalloys have been subjected to pack aluminization as this technique is not only useful but also inexpensive one. Pack aluminization of the substrates has been followed by microstructural characterization, microanalysis, microhardness tests, friction tests, wear tests, adherence tests and finally oxidation tests. In order to understand the nature of interfacial interactions pertaining to superalloy 690 substrates, an attempt has also been made to determine the stability of NiAl phase and adhesion strength of Ni(Cr)/NiAl interface by employing first-principle computational approach. The nature of bonding across the interface and its structure has also been attempted. For superalloy 690 substrates, evaluation of stability of pre-oxidized aluminide coatings in sodium borosilicate melt at 1248 K has also been undertaken that is pertinent to its application. The novelty of the present study is that it deals with the development of aluminide coatings on Ni-based Alloy 690 and Fe-based Alloy 800 in Ni-Cr-Fe alloy system, which has not been systematically carried out so far for applications at elevated temperatures.

1.3 Structure of the Thesis

In this dissertation, Chapter 2 gives a brief account of literature review covering features of Ni- and Fe-aluminides, structure of NiAl and FeAl, different types of coating like diffusion, overlay and thermal barrier coatings, various coating techniques like pack aluminization, hot dip aluminization, gas phase aluminizing and thermal spray processes and thermodynamic analysis of phase transformation during aluminization, which all are relevant to the present topic. Chapter 3 contains details of materials and the experiments employed in the present study. Chapter 4 is on phase evolution of aluminized alloys giving the detailed results on microstructure and microanalysis relating to aluminization of superalloys 690 and 800. In this chapter the findings of pack aluminization of the superalloys have been discussed at a length as this technique of aluminization has been extensively used in the present study. Chapter 5 deals with the properties of aluminized substrates of superalloys 690 and 800 summarizing the results on microhardness, wear and friction coefficient and adhesion of aluminides. Besides this, it summarizes the results on modeling of Ni(Cr)/NiAl interface and its adhesion strength (relevant to superalloy 690) determined by employing first-principle computational approach. It also discusses the nature of bonding across the interface and its structure. Chapter 6 discusses the results on thermal oxidation resistance of aluminides. In addition, it discusses the results on stability of thermally oxidized aluminide coatings, formed on superalloy 690 substrates, in molten sodium borosilicate melt at 1248 K pertinent to the application of the superalloy 690. Finally, chapter 7 summarizes the conclusions of the study.

CHAPTER 2: LITERATURE REVIEW

2.1 Features of nickel and iron aluminides

Over the last a few decades, ordered intermetallics, based on aluminides of transition metals such as nickel, iron, titanium, niobium, and cobalt, have become a prime topic of research for their possible use as high-temperature structural materials [13]. Aluminides of transition metals contain adequate concentrations of aluminium as shown in Table 2.1 to form a continuous, fully adherent Al_2O_3 layer on the surface on exposure to air or oxygen atmospheres. The amount of aluminium present in aluminides is considerably higher as compared to that in conventional alloys and superalloys. For nickel and iron aluminides, the Al_2O_3 layer that formed on the surface of the materials is responsible for their excellent resistance to oxidation and carburization even at temperatures higher than 1273 K. Therefore, aluminides unlike conventional steels and superalloys based on nickel, iron, and cobalt, do not necessarily need chromium to form an oxide layer on the surface of the material to protect against high-temperature oxidation and corrosion. Al_2O_3 is much more thermodynamically stable at high temperatures than Cr_2O_3. It is interesting to note that the chemistry of aluminides is much simpler than superalloys; subsequently, they form long-range ordered crystal structures. Besides their resistance to oxidation and carburization, aluminides possess lower densities, high-melting points, and exhibit interesting mechanical properties because of their ordered crystal structures. The strength of some intermetallics increases with temperature instead of exhibiting a decrease; thus, they are ideally suited for high-temperature applications. Advantages of intermetallics based on Ni_3Al, Fe_3Al, and FeAl are listed below [13]. The major advantages, which can be derived from the use of nickel aluminides (Ni_3Al) are:

1. Good tensile and compressive yield strengths in the temperature range of 923-1373 K, as opposed to many nickel-based superalloys.
2. Superior fatigue resistance as compared to nickel-based superalloys, resulting from the elimination of second-phase particles such as carbides.
3. Superior creep strength that is highly grain size dependent. For the best creep resistance, coarse grain size is needed.
4. Excellent wear resistance at high temperatures (> 873 K).
5. The formation of Al_2O_3 on the surface by preoxidation provides good chemical compatibility for many environments.
6. Resistance to oxidation and carburization in both oxidizing and reducing carburizing atmospheres up to1373 K.

The major advantages that can be obtained from the use of iron aluminides include:

(1) Lower density than that of many stainless steels and, therefore, better strength-to-weight ratio can be obtained.

(2) Much better resistance to sulfidation in H_2S and SO_2 gases as compared to that of any other iron- or nickel-based alloys.

(3) High electrical resistivity that increases with temperature.

(4) Good corrosion resistance in many aqueous environments.

Despite the above attractive features, low ductility, brittle fracture, and processing problems have posed problems in commercial use of these intermetallics for several decades. A number of reviews, symposium proceedings and books describe the recent advances in alloy design, processing and mechanical properties of intermetallics. Excellent accounts of historical perspectives on the development of intermetallics have been provided by a few researchers [13]. The tensile properties of aluminides based on Ni_3Al and Fe_3Al have been compared with superalloys like Haynes 214 (NiCrAl alloy), HU (FeNiCr alloy) and Incoloy MA-956 (FeCrAl alloy with yittria dispersion) and presented in Table 2.2. A comparison of creep data between Ni_3Al-based alloys and superalloys (Haynes 214 and HU) shows better creep resistance of Ni_3Al-based alloys. The Larson-Miller plot indicates superior creep resistance of Ni_3Al-based alloy as compared to HU alloy by a factor of 2-4 even at high temperatures. A comparison of creep data has shown superior creep resistance of MA-956 alloy as compared to Fe_3Al-based alloys.

Table 2.1: Weight percentages of aluminium and melting points of intermetallics [13]

Intermetallic	wt.% of Al	Melting point (degree Celsius)
Ni_3Al	13.28	1395
NiAl	31.49	1639
Ni_2Al_3	40.81	1133
$NiAl_3$	57.96	854
Fe_3Al	13.87	1502
FeAl	32.57	1215
$FeAl_2$	49.1	1164
Fe_2Al_5	54.70	1171

Table 2.2: Tensile properties of aluminides based on Ni_3Al and Fe_3Al and a few superalloys[13]

Alloy	Temperature, K	Yield strength (0.2% offset), MPa	Tensile strength, MPa	Elongation, %
Ni_3Al-based alloy IC 50	RT-873	500-600 MPa	1200-700	40-<5
	873-1273	600-200 MPa	700-200	<5-90
Ni_3Al-based alloy IC-218LZr	RT-873	500-600 MPa	1300-900	40-15
	873-1273	600-200 MPa	900-250	15-40
Haynes 214	RT-873	500-600 MPa	950-850	40-35
	873-1273	600-50 MPa	850-100	35-75
Fe_3Al-based alloy FAS	RT-873	400-300	850-350	15-45
	873-1073	300-50	350-50	45-75
Fe_3Al-based alloy FAL	RT-873	450-350	950-400	20-50
	873-973	350-100	400-100	50-100
Incoloy MA-956	RT-873	550-200	600-250	10-25
	873-1073	200-100	250-150	25-10

2.2 Structure of NiAl and FeAl

The exceptional properties of intermetallic alloys are related to their ordered structures [14]. An ideal AB ordered structure can be defined as a structure where all the nearest neighbours of a B atom are only A atoms and vice versa. In the body-centered cubic (BCC) lattice, we get according to this definition, a B2 structure as shown in Figure 2.1 [14], in which all the nearest neighbours of an A atom are only B atoms. However, when we put the A atoms on all the nearest neighbour sites of a B atom in the FCC lattice we get Ll_2 structure as demonstrated in Figure 2.2 [14]. The stoichiometry of this structure is not AB but A_3B and therefore, all the neighbouring atoms of an A atom cannot be B atoms. In this sense, the Ll_2 structure is not ideally ordered. Actually, we can say that the ideally ordered AB structure cannot exist on the FCC lattice. For example, in the Ll_0 structure, which is composed of A and B alternating (001) atomic layers, each B atom has only 8 A and 4 B neighbours and vice versa. It can be said that a strong ordering tendency of two atomic species on the FCC lattice results in the instability of this lattice and in its transition into a BCC base ordered structure [14]. Despite the fact that Ni and Al are FCC metals, the ordered NiAl structure is B2 with the BCC basic lattice. Because of high ordering energy, the B2 structure is stable up to the melting temperature that is higher than the melting temperature of both pure elements Ni and Al, and of their other intermetallic structures as well. In a relatively narrow composition range as shown in Figure 2.3 [14], the Ni_3Al alloy has the Ll_2 structure that is also stable up to the melting temperature. Therefore, the mechanical properties are not affected by a loss of order up to very high temperatures. The complete Al-Ni binary diagram with different phase regions is shown in Figure 2.4 [15].

The Fe-Al system has a qualitatively different phase diagram as shown in Figure 2.5 [14]. There are only bcc based ordered phases in the iron-rich part, B2 down to about 20 at.% Al and

$D0_3$ with the maximum transition temperature of only about 820 K (0.46 T_m). It can be noted that the $D0_3$-B2 phase transition can be affected by the magnetic ordering. The Curie temperature of the transition from the ferro- into paramagnetic state is marked by the dashed-dot line in Figure 2.5. The complete Fe-Al binary diagram with different phase regions is shown in Figure 2.6 [16].

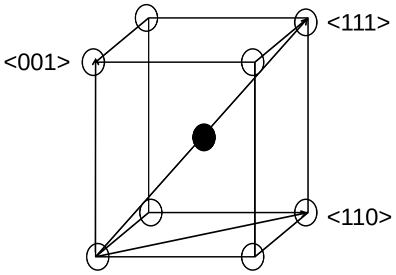

Figure 2.1 An elementary cell of the B2 structure of an AB ordered BCC alloy. The open circles denote the positions of A atoms and the full circles indicate the positions of B atoms. The arrows show the shortest lattice vectors [14].

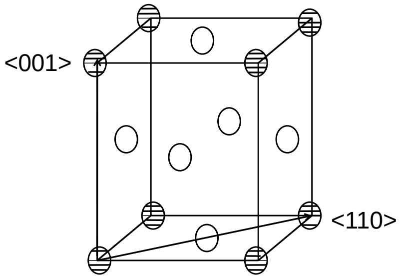

Figure 2.2 An elementary cell of the LI_2 structure of an A_3B ordered FCC alloy. The open circles indicate the positions of A atoms and the dashed circles mark the positions of B atoms. The arrows show the shortest lattice vectors [14].

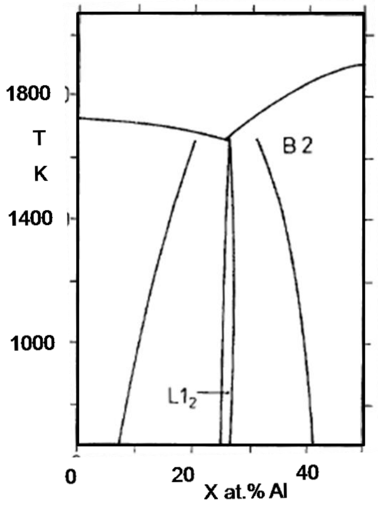

Figure 2.3 Ni-rich part of the Ni-Al phase diagram. The details near the melting temperature of the LI$_2$ phase are not depicted [14].

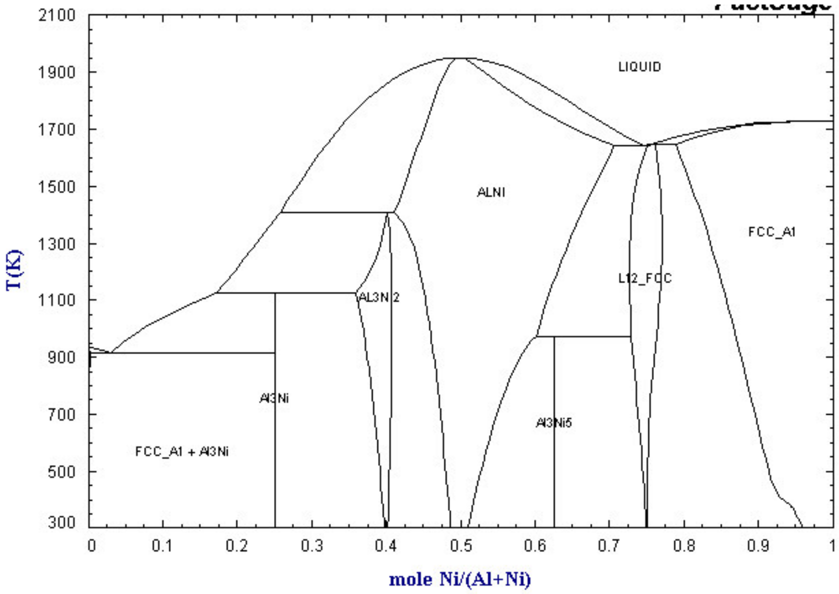

Figure 2.4 Al-Ni binary diagram with different phase regions [15].

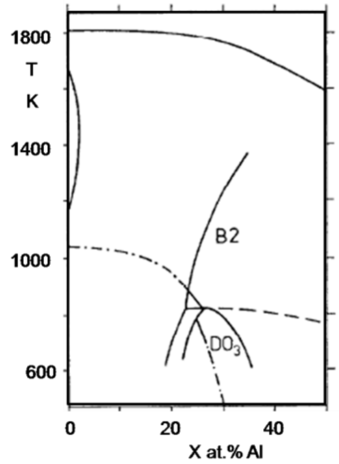

Figure 2.5 Fe-rich part of the Fe-Al phase diagram. The dot-dashed line is the ferro-paramagnetic transition. The dashed line denotes the temperature of the flow stress peak [14].

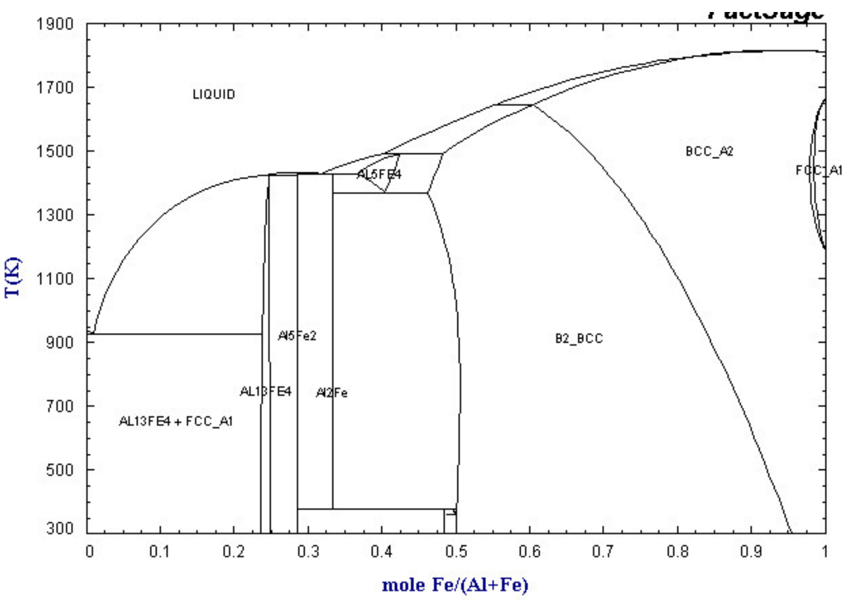

Figure 2.6 Fe-Al binary diagram with different phase regions [16].

2.3 Classification of coatings

2.3.1 Diffusion coatings

These comprise intermetallic compounds, usually aluminides. They are most often produced via chemical vapour deposition (CVD) technique, with formation generally controlled by diffusion mechanisms [17]. In this regard, pack cementation and gas phase coating are used extensively.

Goward [18] has highlighted the development of protective coatings for superalloy airfoils starting with simple aluminides, followed by modifications with silicon, chromium and platinum, then MCrAlY overlay and finally ceramic thermal barrier coatings. It is worth mentioning some highlights from his article. According to him, a qualitative description of diffusion mechanisms for the formation of aluminide coatings on nickel-base superalloys was put forward by Goward and his co-worker in 1971 [18,19]. Their findings enabled classification of coatings as either inward or outward diffusion types, based on the motion of aluminum in Ni_2Al_3 and high aluminum NiAl or higher rate of diffusion of nickel in low aluminum NiAl. Despite getting microstructural variations by varying the activities of source material, this simple classification has been found to be useful. It is indicated that in the end of 70s, some investigators demonstrated that diffusion of nickel predominates in nickel-rich NiAl; rates of diffusion of nickel and aluminum are equal at about 51 at.% of aluminum; and aluminum diffusion predominates in aluminum-rich NiAl as reported by Goward and his co-worker [18-20]. It is revealed that the studies by a few researchers on the thermodynamics and kinetics of pack aluminization laid a foundation for further progress of the technology [18]. The refinement of details in regard to kinetics of coating processes was done during the work on activators for aluminizing and chromizing while the activity coefficients of aluminum in Ni–Al, Co–Al and Fe–Al systems those were published helped in selection of source compositions for pack aluminization and out-of-contact processes, whereas thermodynamic details were reported on processes for co-deposition of chromium, silicon, yttrium, hafnium with aluminum [18].

As far as mechanisms of protection and degradation are concerned, Pettit defined mechanisms of oxidation for Ni-Al and Ni-Cr-Al alloys [18,21,22]. The importance of interdiffusion of aluminides with base alloys in decreasing coating life has been reported [18] along with the effect of small amount of hafnium in a substrate alloy in aiding adherence of protective alumina on coatings. In addition, some interesting results are also highlighted [18,23,24]. Investigation on hot corrosion revealed the effects of substrate elements on the hot corrosion resistance of aluminide coatings. It was indicated from the studies on chromium modified aluminide coatings that the best coatings contained chromium, from chromizing, in the outer layer of inward diffusion aluminide coatings. Two-phase ($PtAl_2$ in NiPtAl) platinum-modified aluminide coatings was found to have good resistance to high temperature (Type I) but comparatively a lesser resistance to low temperature (Type II) hot corrosion. This is related to Na_2SO_4-induced hot corrosion (90 Na_2SO_4 + 10 K_2SO_4 (mol%) melt at 1173 K in air). Type I generally refers to hot corrosion in the range between 1073-1223 K while type II refers to that one in the range between 943-1023 K.

With the knowledge that diffusion aluminide coatings can be used as bond coats for thermal barrier coatings, the aim has been to provide resistance to spalling of alumina to permit use of prime reliant thermal barrier coatings with the capability of reducing blade airfoil cooling air flow to gain higher turbine efficiency [18]. Reduction in sulfur contents of diffusion coatings reported to improve the adherence of alumina and the knowledge of the effects of platinum as well as various forms of active metals and their oxides was expected to improve the use of diffusion aluminide systems as thermal barrier bond coats [18,25-31].

2.3.2 Overlay coatings

These comprise complex alloys based upon the M-Cr-AI-X system (M = Ni, Co, Ni-Co, Co-Ni; X = active element addition(s) such as Y, Si, Ta, Hf etc.). Deposition of these systems is generally achieved via plasma spraying or physical vapour deposition (PVD) techniques [17].

Majority of the research in this area has focused around the active element effect. Understanding prior to 1950s on active element-doped nickel–chromium alloys and from cyclic oxidation tests, it was assumed that the Cr_2O_3 scales spalled less due to pegging (mechanical keying or interlocking) by active element oxides [18]. Similar conclusions were drawn during the work on oxidation of FeCrAl alloys doped with yttrium and scandium and it was continued to support the pegging mechanism later on and also shown that active elements minimize void formation at the scale metal interface [18,32]. In addition, it was demonstrated that fine dispersions of active element oxides improve adherence of alumina to NiCrAl and CoCrAl. Goward in his article mentioned that in 1986, pegging explanation was apparently dropped and it was assumed only that active elements may assist in the formation of strong chemical bonds between oxide scales and the metal substrates. The article [18,33] further reported that in 1983 and later in 1985, some researchers showed that small amounts of impurities like sulfur can segregate to the alumina–metal interface and lower the interface bond strength. It followed that active elements must react with tramp sulfur to prevent this segregation. However, a review [18,34] of that subject asserted that such effects are not consistent with the fact that active element oxide dispersions also improve scale adhesion. It was also indicated that active elements like yttrium diffuse through grain boundaries in alumina scales and lower scale growth rates. A dynamic segregation theory was proposed to explain lower scale growth rates and improved scale adhesion that involves segregation of active element ions to scale boundaries and to the oxide–metal interface. The search progresses in this way while the practical benefits of the active element effect have been commercially utilized for more than five decades [18,35,36].

2.3.3 Thermal barrier coatings

These comprise a low thermal conductivity ceramic layer over a M-Cr-AI-X (overlay) bond-coated substrate. The ceramic is generally deposited via plasma spraying or PVD techniques [17].

Contrary to the science base of first and second types of coatings as mentioned above, the early development work to improve the durability of thermal barrier coatings was done by experimentation and evaluation by testing in burner rigs and actual engines as highlighted by Goward [18]. To understand thermal barrier systems in helping the development of more durable coatings, the research has been going on for last two decades. According to Goward, initial improvements in durability involving the use of MCrAlY bond coats were based upon prior knowledge of good oxidation and hot corrosion resistance and oxide adherence of these coating alloys. The improved durability of partially stabilized zirconia ($8\%Y_2O_3–ZrO_2$) was shown in 1979 while the beneficial effects of micro-cracked and/or segmented ceramic layers were also demonstrated in the same year as per the review. The fact that electron beam physical vapour deposition (EBPVD) produces columnar grain structures in MCrAlY coatings led to exploration of the properties of columnar grained EBPVD zirconia-based thermal barrier coatings [18]. Findings that active elements in nickel-base superalloys and/or platinum modifications resulted in improved scale adherence in diffusion aluminide coatings might have led to the use of these coatings as bond coats. The possibility of attaining large beneficial effects in gas turbine efficiency by using thermal barriers, e.g. up to 443 K lowering of blade material temperature, have triggered a revival in research on scale adherence and failure mechanisms involved in loss of ceramic layers [18]. It is expected that extensive research will lead to improvements in scale adherence [37-41].

2.4 Different coating techniques

2.4.1 Pack cementation (pack aluminization)

Aluminide diffusion coatings are generally applied by pack cementation method to Ni-base superalloy turbine components to improve their oxidation resistance [42]. Halide-activated pack cementation is a high temperature closed-system chemical vapor deposition batch process in which the pack consists of three mixed powdered components: (i) a masteralloy powder of the element to be deposited (Al/Cr/other), (ii) a halide salt activator (NaCl/NaF/NH_4Cl), and (iii) an inert filler powder ($A1_2O_3$). The parts to be coated are embedded in this powder mixture and heated in a vented retort. A controlled atmosphere, generally Ar or H_2/Ar, surrounds the pack as it is heated to an elevated temperature (1173-1423 K), at which the masteralloy reacts with the halide salt activator to form volatile metal halide species of significant partial pressures according to the following reaction

$$\mathrm{Me(alloy)} + \mathrm{AX_x(l, v)} = \mathrm{MeX_x(v)} + \mathrm{A(l, v)}$$

where, Me stands for Cr or Al; A is NH_4; and X is Cl. Several different vapour species may be formed for each element (e.g., Al, AlX, AlX_2 and AlX_3; Cr, CrX_2, CrX_3 and CrX_4). Partial pressure gradients that support vapour transport for each vapour species to the substrate surface, result from the higher thermodynamic activity for the metallic component in the powdered masteralloy compared to its activity at the substrate surface. At the surface, deposition of the desired coating element occurs via the dissociation of the halide molecules or by a displacement reaction with the substrate [42]. Ultimately, the coating element reacts and interdiffuses with the metallic substrate, producing some specific phase, composition and microstructure at the surface.

2.4.2 Hot dip aluminizing

Hot dip aluminizing is a diffusion coating formation process, which has been extensively employed to deposit high temperature oxidation- and corrosion-resistant coatings on stainless steels and low-alloy steels [43,44]. It has the advantages of high volume, low capital and operating costs and is applicable for large-size work pieces. The first aluminizing of Ni-base turbine blades by hot dip process was done in 1952 [44]. During the hot dip aluminizing process, which is generally performed at around 973 K for short durations, silicon is normally added (usually Al–7 wt.% Si) to the melt to reduce the thickness of the intermetallic layer. Besides this, silicon has been reported to be beneficial in improving hot corrosion resistance of high temperature coatings. However, its ability to provide total protection against high temperature oxidation and increase in lifetimes of nickel-base superalloy components needs proper explanation [44]. From a practical viewpoint, the adherence of scale may also be affected by cyclic thermal stresses generated during heating and cooling, which are often a primary cause of degradation of the protective external oxide scale.

2.4.3 Gas phase aluminizing process

The coating apparatus used for the gas phase aluminizing process is shown schematically in Figure 2.7 [45]. This coating apparatus consists of two main parts: the powder and the coating chambers, which are placed in an electrical furnace. Inert gas is circulated in the chambers to keep an inert atmosphere and acts as the carrier gas for the coating process Typical pack compositions used in single step high temperature high activity gas phase aluminizing process is shown in Table 2.2 [45].

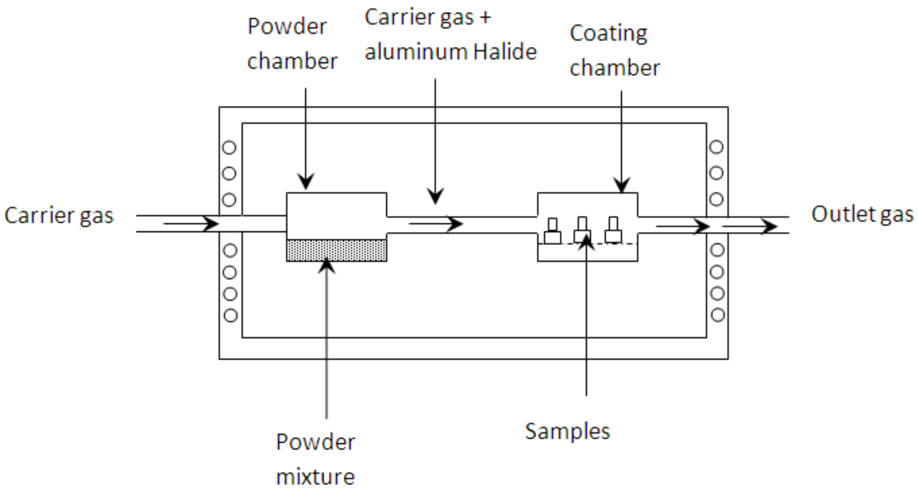

Figure 2.7 Schematic diagram showing the coating equipment that is used for the gas phase aluminizing process [45].

Table 2.3: Typical chemical composition of powder mixtures used in the single step high temperature high activity gas phase aluminizing process [45].

Pack	Composition (wt.%)		
	Al	NH_4Cl	Al_2O_3
1	10	5	Bal
2	30	5	Bal
3	10	15	Bal
4	30	15	Bal

In gas phase aluminizing process, according to the following reactions aluminum halides $AlCl_n$ ($n<3$) are formed at temperatures above 1073 K [45]. The aluminum halide $AlCl_n$ will react with the surface of the Ni-based superalloy in the coating chamber to form $AlNi_y$ (y is an index) compounds at temperatures above 1073 K. All these reactions are reversible.

$$NH_4Cl = HCl + NH_3 \quad (1)$$

$$2Al + 6HCl = 2AlCl_3 + 3H_2 \quad (2)$$

$$Al + AlCl_3 = AlCl_n \ (3)$$

$$AlCl_n + Ni = AlNi_y + AlCl_3 \ (4)$$

It is suggested [45] that $AlCl_n$ is more stable thermodynamically as compared to $AlCl_3$ as the temperature increases. The activator of the reactions, $AlCl_3$, is a product in Equation 4 that is reproduced during the reactions. The reproduced $AlCl_3$ can then react with aluminum again to form an $AlCl_n$ compound. These reactions indicate why increasing the amount of Al and/or NH_4Cl increases the coating thicknesses. Increasing either the amount of Al and/or NH_4Cl favours the formation of $AlCl_3$ during the coating process. The more $AlCl_3$ is produced in the powder chamber, the more $AlCl_n$ is transferred to the coating chamber and hence, a higher amount of $AlNi_y$ will be produced at the surface of the specimens during the coating. The driving force for the formation of $AlNi_y$ intermetallic is provided by the energy release due to the reaction of $AlCl_n$ and Ni [45].

2.4.4 Thermal spray processes

A number of thermal spray processes are available for the deposition of surface coatings for aero engine applications. Among these, the principal techniques are combustion flame spraying, arc wire spraying, high velocity combustion and plasma spraying [46]. The principal characteristics of these techniques are summarized in Table 2.3 [46].

Table 2.4: Principal characteristics of thermal spray deposition processes [46].

Process	Consumable material	Heat source	Flame temperature around (K)	Particle velocity in the range (ms^{-1})
Flame	Powder/Wire	Chemical reaction	3273	90-180
Arc	Wire	Electric arc	4273	240
D-Gun	Powder	Controlled explosion	4273	750
Plasma	Powder	Inert gas plasma	4773-20273 K	240-600

2.4.4.1 Combustion flame spraying

In this process [46], an oxygen-acetylene mixture is passed through a nozzle and ignited for forming a combustion flame. Coating powder or wire is fed into the flame, accelerated and projected on the specimen/job to form deposit. The combustion flame temperature is limited to around 3273 K and gas-particle velocities are relatively on the lower side. The deposit itself is porous, poorly bonded and metallic coatings may contain high amount of oxide. Among the thermal spray processes, flame spraying is the cheapest one and it can be used in specific applications, particularly, where porosity (oil retention for bearings) or high oxide contents (hard molybdenum coatings for piston rings) provide specific benefits. Besides this, it can be employed to deposit self-fluxing systems such as Ni-Cr-B-Si that can be fused to form wear-resistant layers.

2.4.4.2 Arc wire spraying

This process [46] involves the production of molten particles at the tips of two consumable wires via resistance heating. The material is subsequently atomized and projected on the substrate by a compressed air jet. The process is limited to the spraying of conductive wires, with the spray material being initially fully molten and reaching higher velocities as compared to those in flame spraying. The coatings deposited by this process are more dense and highly bonded than those in flame spraying. The arc wire process is relatively cheap and can achieve high deposition rates.

2.4.4.3 High velocity combustion processes

A number of high velocity combustion processes are employed in the aero engine industry including the following.

The Detonation Gun: D-Gun:

The D-Gun is a process [46] that utilizes the energy released by a controlled series of detonations of oxygen-acetylene to heat and accelerate the coating powder to high velocities and to propel the powder on job surface to form coatings. Measured volumes of oxygen and acetylene are fed into a combustion chamber at the breech of a gun barrel. Fine coating powder is introduced through a separate port. The gas mixture is ignited by an electric spark. A detonation occurs that results in a temperature rise to around 4273 K. The high temperature gases leaving the gun along the barrel cause the particles to be accelerated, plastically deformed and ejected from the gun at around 750 ms^{-1}. During the impact on the target, their high kinetic energy produces a strong bond with the substrate/previously coated layer. After detonation, the D-Gun is purged with nitrogen and the process is repeated to build up the coating of desired thickness. Gas temperatures associated with the D-Gun are 1273 K hotter than with conventional oxy-acetylene torches but jobs to be coated are cooled during processing by supplementary cooling. This process produces highly dense and high quality coatings with low contents of oxide and unprocessed particles.

Super D-Gun:

This is a new system representing an improvement over the D-Gun [46]. In essence, the mass of gas in the gun barrel prior to each detonation is increased without reducing the final temperature. This increases the pressure of the gas to a large extent as well as its post-detonation exit velocity that consequently provides a considerably increased force to the powder particles. One of the main advantages reported for this type of coatings is that due to the increased deposition velocities the coating powder particles self-peen during deposition, thereby leaving residual compressive stresses in the final coating rather than the more usual residual tensile stresses.

Diamond Jet System:

The Diamond Jet System uses an oxygen-fuel mixture of either propylene or hydrogen to produce dense, low porosity highly bonded coatings [46]. Fuel gases are mixed in proprietary siphon system in the front portion of the type DJ Diamond Jet Gun. The gases are thoroughly mixed, ejected from a nozzle and ignited externally to the gun. Ignited gases form a circular flame configuration that surrounds the spray powder as it flows through the gun into the flame. The circular flame shapes the powder stream to provide uniform heating and melting. Heated powder particles are then accelerated by a high velocity flow of compressed air. Typical aero engine applications include WC-Co coatings for wear control in compressors.

2.4.4.4 Plasma spraying processes

The plasma gun [46] consists of a copper anode and tungsten cathode both of which are water cooled. An inert gas, generally argon, flows around the cathode and through the anode that is shaped as a constricting nozzle. Gases other than argon, such as nitrogen, helium or hydrogen (used as a secondary gas), can also be used. A d.c. arc is struck between the electrodes by a high voltage discharge, which ionizes the gas resulting in a plasma coming out of the gun through the nozzle, thereby producing a high velocity jet. The coating material in fine powder form is injected into the plasma and is accelerated and propelled on to the job so that the particles deform and adhere on impact to form a coating.

In air plasma spraying (APS), the powder particles are accelerated to 200-400 ms^{-1} before being deposited as relatively dense coating. The principal limitation of this technique is the incorporation of air in the plasma jet that results in depositing coatings with significant oxide content. However, when oxide contamination in coatings is tolerable (e.g. air-sprayed M-Cr-Al-X bond coats for thermal barrier systems used in combustion chambers in aero engines), or when oxides are deposited as coatings (e.g. the ZrO_2 - 8%Y_2O_3 layer of thermal barrier coatings), the APS process provides satisfactory coatings. In argon-shrouded plasma spraying (ASPS), the use of an argon gas shield around the plasma gun and work piece provides protection against the deleterious effects of air encountered with the APS technique. The ASPS coatings are clean, well bonded and relatively oxide free as compared with APS deposits. Typical applications of ASPS include M-Cr-Al-X systems (both as overlay coatings and bond coats for thermal barrier systems) for turbine vane and blade applications, combustion chamber sections and hot gas path seals [46]. The vacuum plasma spraying (or low pressure plasma spraying) process has several advantages over APS. The problems associated with air contamination of the plasma jet are eliminated. The plasma jet is longer than in air and can achieve 400-600 ms^{-1} particle velocities with the overall result being the deposition of highly dense, high purity deposits with good adhesion. In vacuum, a transferred arc can be utilized to sputter clean the substrate surface prior to coating, giving a very clean substrate/coating interface, thereby improving adhesion. Besides this, the use of a vacuum chamber allows the heating of the job to high temperatures to promote diffusional bonding without oxidation problems. Typical uses of vacuum plasma spraying - low pressure plasma spraying in aero engines include M-Cr-Al-X systems (overlays and thermal barrier bond coats), hot gas path seal systems and WC-Co coatings for wear protection in compressor applications [46].

2.5 Thermodynamic analysis during aluminizing

The work of Ivanov [47] has dealt with thermodynamic analysis during aluminizing of steels and nickel alloys and also in the process of operation. The change in the Gibbs free energy of formation of aluminides has been given by the approximate formula:

$\Delta G^0 = \Delta G_{al} + \Delta G^0_{melt}$, where ΔG_{al} (aluminide) = $\Delta H_{298} - T\Delta S_{298}$; ΔG^0_{melt} is the change in Gibbs free energy with melting of aluminium in the respective aluminide.

The heats of formation and the calculated values of entropy of iron and nickel aluminides are given in Table 2.4. From these data, with the melting of aluminium taken into consideration, the changes of Gibbs free energy have been calculated with formation of iron and nickel aluminides per g-atom of aluminium. Table 2.5 indicates that in calculations per g-atom of aluminum in the Fe-Al system, the most probable is the formation of the FeAl and Ni_3Al in the Ni-Al system. The enthalpy of formation of Fe_3Al per g-atom of aluminium and the change of entropy are much higher than those in other compounds. Above 730 K, the formation of this compound is not possible as the change of Gibbs free energy of this compound is positive [47].

Table 2.5: Values of enthalpy and entropy for Fe-Al and Ni-Al systems [47].

System	Aluminide	$-\Delta H_{298}$, $kJmol^{-1}$	S^0_{298}, $J\ mol^{-1}\ K^{-1}$
Fe-Al	Fe_3Al	57	27.8
	FeAl	48.4	50.6
	$FeAl_2$	81.5	72.9
	Fe_2Al_5	201.3	165.9
	$FeAl_3$	111.4	95.1
Ni-Al	Ni_3Al	157.1	103.6
	NiAl	142.1	42.3
	Ni_2Al_3	28.4	122.8
	$NiAl_3$	15.8	113.8

Table 2.6: Gibbs free energy calculated with formation of iron and nickel aluminides [47].

System	Aluminide	ΔG^0, $kJmol^{-1}$
Fe-Al	Fe_3Al	-57+0.079T/-67.5+0.09T
	FeAl	-49.6+0.004T/-58.8+0.015T
	$FeAl_2$	-40.7+0.005T/-51.2+0.016T
	Fe_2Al_5	-40.2+0.005T/-50.7+0.017T
	$FeAl_3$	-37+0.056T/-55.8+0.016T
Ni-Al	Ni_3Al	-157.1+0.018T/-159.2+0.029T
	NiAl	-142.1+0.015T/-152.5+0.026T
	Ni_2Al_3	-94.7+0.007T/-105.2+0.018T
	$NiAl_3$	-52.9+0.0002T/-63.4+0.011T

Note: Numerators refer to 298-933 K, while denominators refer to 933-1500 K

As atoms of aluminium continue to arrive the aluminides are transformed from low-aluminium to high-aluminum aluminides. The change of Gibbs free energy with the interaction of iron and nickel aluminides with aluminum is given in Table 2.6. Chemical compounds $FeAl_2$ and Ni_2Al_3 are metastable and thus at aluminizing temperatures the probability of their formation is minimal since with increasing temperatures they are dissociated by reactions

$$3FeAl_2 \rightarrow Fe_2Al_5 + FeAl; \;\; 2Ni_2Al_3 \rightarrow NiAl_3 + 3NiAl$$

Therefore, in the process of aluminization at 700-1500 K, depending upon the activity of aluminium in the saturating medium and its arrival at the substrate, the formation of FeAl, Fe_2Al_5 and $FeAl_3$ phases in Fe-Al system while Ni_3Al, NiAl, and $NiAl_3$ phases in Ni-Al system is expected. In the aluminized layer, one would expect phases matching those in the phase diagrams of these systems. The calculation of thermodynamic probability of formation of aluminides has been reported to be in accordance with the mechanism of reactive diffusion [47]. With the arrival of aluminium atoms at the steel/nickel substrate, a solid solution begins to form. With increasing time of a constant aluminium supply at a given temperature the concentration of aluminium in the solid solution will increase and FeAl phase will be precipitated out from it in the Fe-A1 system and Ni_3Al in the Ni-A1 system. Continued arrival of aluminium atoms at the substrate will lead to formation of Fe_2A1_5 and $FeA1_3$ in steels and NiAl and $NiAl_3$ in nickel alloys. For equilibrium calculations, it is necessary to know the change of Gibbs free energy characterizing the difference between the standard condition of aluminium and its condition in a given phase [47]. Consequently, the data in Table 2.6 require to be recalculated to take into account the increasing change of Gibbs free energy with formation of aluminides. The results of these calculations are shown in Table 2.7. With constant arrival of aluminium atoms at the substrate, it is most probable that high-aluminium containing phases will be formed. Therefore, depending upon the activity of aluminium in the powdered mixture and its arrival at the substrate, aluminides with a given concentration of aluminium are formed.

Table 2.7: Change of Gibbs free energy for interaction of aluminides with aluminium[47]

System	Reaction	ΔG^0 (kJmol^{-1}) at:	
		293-933 K	933-1500 K
Fe-Al	1/2 Fe_3Al +Al = 3/2 FeAl	-44-0.032T	-50.3-0.021T
	FeAl + Al = $FeAl_2$	-33.1+0.005T	-43.5+0.017T
	2 $FeAl_2$ + Al = Fe_2Al_3	-38.2+0.008T	-48.7+0.019T
	Fe_2Al_5 + Al = 2 $FeAl_3$	-21+0.004T	-31.5+0.015T
Ni-Al	1/2 Ni_3Al + Al = 3/2 NiAl	-13.3+0.014T	-149.2+0.025T
	2 NiAl + Al = Ni_2Al_3	-0.009T	-10.4+0.001T
	1/3 Ni_2Al_3 + Al = 2/3 $NiAl_3$	-11.2-0.006T	-23.3+0.004T

Table 2.8: Gibbs free energy change for aluminides at two temperature ranges [47].

System	Aluminide	ΔG^0 (kJmol^{-1}) at:	
		293-933 K	933-1500 K
Fe-Al	Fe_3Al	-57+0.079T	-67.5+0.09T
	FeAl	-86.4+0.029T	-101.1+0.046T
	$FeAl_2$	-119.5+0.035T	-140.7+0.063T
	Fe_2Al_5	-157.7+0.043T	-189.3+0.083T
	$FeAl_3$	-168.3+0.045T	-205+0.091T
Ni-Al	Ni_3Al	-157.1+0.018T	-167.5+0.029T
	NiAl	-166.1+0.032T	-177.1+0.046T
	Ni_2Al_3	-166.1+0.022T	-187.6+0.047T
	$NiAl_3$	-183+0.012T	-222.7+0.054T

2.6 Summary

A review on literature as discussed above covers topics, which are pertinent to the present study that is development of diffusion barrier coatings for high temperature applications. It deals with features of nickel and iron aluminides followed by discussion on structures of NiAl and FeAl. Classification of coatings those are diffusion coatings, overlay coatings and thermal barrier coatings have been stated along with different coating techniques like pack cementation (pack aluminization), hot dip aluminization, gas phase aluminization and thermal spray processes including combustion flame spraying, arc wire spraying, high velocity combustion processes and plasma spraying processes. Finally, thermodynamic analysis during aluminizing of Ni-Al and Fe-Al systems has been discussed.

CHAPTER 3: EXPERIMENTAL METHOD

3.1 Aluminization of substrates of superalloys 690 and 800

3.1.1 Pack aluminization of substrates of superalloys at 1173-1273 K in argon atmosphere

Commercially available superalloys 690 and 800 were used as substrate materials in the present investigation. The alloys were available in mill-annealed condition. The typical chemical compositions of the alloys are shown in Table 3.1.

Table 3.1: Typical chemical compositions of superalloys 690 and 800 (wt.%)

Alloy	Ni	Cr	Fe	C	Mn	Si	Cu	Ti	Al	S	P	N
690	Bal	28.0	9.6	0.03	0.17	0.04	0.05	-	-	0.001	-	-
800	30.0	19.5	Bal	0.03	0.7	0.4	-	0.5	0.3	0.01	0.01	0.02

Pack aluminizing process was used to form aluminide coating on superalloys 690 and 800 specimens having initial dimensions 15 mm x 10 mm x 5 mm and 15 mm x 10 mm x 1.5 mm respectively. All the sides of the specimens were ground up to 600 grit emery paper, cleaned, dried, and weighed. In pack aluminizing process, the pack mixture was composed of 10 wt.% Al powder (particle size finer than 200 micron), 5 wt.% NH_4Cl and 85 wt.% Al_2O_3 powder. In alumina crucibles, the substrate specimens were embedded in the pack mixture one by one after proper ramming of the space in-between. After putting each alumina lid, the entire crucible was covered with high temperature cement and kept for drying for two days. The pack cementation was carried out at 1173-1273 K in a resistance heating horizontal type furnace having a constant temperature zone of about 200 mm. Prior to carrying out pack cementation experiments, the temperature range was optimized. Low-temperatures (lower than 1173 K) pack aluminization leads to the formation of Ni_2Al_3 due to lower diffusivities of the elements. In the case of pack aluminization above 1273 K, kinetics of NiAl formation are very fast. Keeping this in view, pack cementation in the present study was done between 1173 K and 1273 K with different pack compositions and soaking periods. As service temperature for metallic melter pot is in the vicinity of 1273 K, aluminizing parameters for superalloy 690 have been optimized around 1273 K. For the sake of comparison, the aluminizing parameters of superalloy 800 have also been optimized at similar range of temperature. That is why, aluminizing experiments on Alloys 690 and 800 involving temperatures other than 1273 K were not included. The process was standardized at 1273 K with a soaking period of 10 hours for superalloy 690 and 8 hours for superalloy 800. Each process was carried out in argon atmosphere with a heating and cooling rate of 4 K/min. After each treatment, the crucible was allowed to cool to room temperature under controlled atmosphere (argon). After cooling, the specimens were removed from the pack, cleaned, dimensions were measured and weighed. In order to find out the type of Ni-aluminide that formed using a low aluminium-containing pack and to examine its properties as well as the performance of diffusion barrier coating, pack aluminization was also standardized on superalloy 690 substrates (of initial dimensions about 10 mm x 10 mm x 4 mm) with a pack mixture consisting of 2 wt.% Al powder, 2 wt.% NH_4Cl and 96 wt.% Al_2O_3 at 1273 K in argon atmosphere with a soaking period of 4 hours. The other experimental conditions of pack aluminization were similar to those as mentioned earlier.

3.2 Microstructural characterization of aluminides

Scanning electron microscopy (SEM) and electron probe microanalysis (EPMA) were carried out on metallographically polished aluminized (with pack mixture containing 10 wt.% Al) specimens of the superalloys 690 and 800 along the cross-section. SEM using secondary electron (SE) image mode was used to examine the surface morphologies of the aluminized samples, whereas back-scattered electron (BSE) image mode was chosen to examine the cross-section of aluminized substrates. For EPMA, X-ray profiles for different elements were acquired across the cross-section to determine the difference in composition and wavelength dispersive spectroscopy (WDS) mode was used. Chemical compositions of various layers were determined by using quantitative chemical analysis on point-to-point basis and pure elemental standards were used for calibration of the spectrometer. For compositions of phases, values were obtained in wt.% (±1%), which were converted to at.%.

For aluminized superalloy 800 substrates, X-ray diffraction (XRD) studies were performed along the top surface after controlled grinding layer by layer using emery paper of grit number 80 up to 400. Digital micrometer screw gauge was used to measure the reduction of specimen thickness. Readings were taken on a number of locations of specimen surface and an average value was considered. The first XRD scan was taken on the metallographically ground surface after removing a layer of 140 μm. The second XRD scan was done after removal of 100 μm layer, whereas the third one was taken after removal of 300 μm layer. XRD studies at room temperature were performed by using CuK_{α} radiation of wavelength 1.5406 Å with a scan rate of 0.02^0/s in 2θ range of 20^0 to 100^0. All the XRD peak intensities were converted to normalized values and the peaks were ascertained by using 1998 JCPDS-International Centre for Diffraction Data.

For specimens of superalloy 690 those were aluminized with pack mixture containing 2 wt.% Al, XRD at ambient temperature was carried out on the surface of an aluminized sample. SEM was performed along with energy dispersive X-ray spectroscopy (EDXS) analysis along the cross-section of metallographically polished specimen. Point analysis was done at various locations along the cross-section. To resolve the aluminide at a finer scale, transmission electron microscopy (TEM) was conducted. For preparing sample of cross-sectional transmission electron microscopy, very thin sections containing the aluminides and the substrates were cut precisely.

The portions of the thin sections containing the aluminides were held together face to face tightly using a 3 mm diameter Ti grid and by applying a non-reactive glue. The 3 mm diameter disc (Ti grid containing glued specimen) was then subjected to dimple grinding. After the dimple grinding of the specimen from both the sides of the disc, further thinning was done using argon ion gun operated initially at 4 kV and finally at 6 kV for a very short duration. TEM examination was performed on the specimen using bright-field and dark-field image conditions. Selected area diffraction (SAD) patterns were obtained from certain locations. EDXS analysis was performed on a few points. Besides this, high-solution TEM was performed.

3.3 Microhardness of aluminides

Microindentation method, suitable for thin sheet, was used to measure microhardness values of metallographically polished aluminized (with pack mixture containing 10 wt.% Al) specimens of superalloys 690 and 800 along the cross-section. Knoop hardness values were measured for the specimens at specific distances along the cross-section. A load of 50 gm was applied each time for 10s to determine the micohardness value. A magnification of 400X was chosen during the measurements. Adequate gap (about 50 µm) was maintained between two successive indentations and sufficient margins were left on either side while measuring microhardness values to avoid error due to edge effects. For specimens of superalloy 690 those were aluminized with pack mixture containing 2 wt.% Al, Vickers hardness values were measured along the cross-section of the sample by applying a load of 100 gm at each time for 5s to determine the microhardness.

3.4 Wear, friction and adherence tests of aluminides

Wear and friction tests were carried out in a dry medium using reciprocating sliding wear and friction machine on the aluminized (with pack mixture containing 10 wt.% Al) specimen of superalloy 690 using 6 mm diameter grade 10 tungsten carbide (WC) ball at the load level of 15 N and varying the frequency values at 10, 15 and 20 Hz resulting sliding speed of 20, 30, and 40 mm/s respectively. Sliding amplitude was 1 mm. The duration of test at each frequency was 1800s. The coefficients of friction both static and dynamic were measured during the tests. The wear was measured for the WC ball as well as for the aluminized specimen at the three selected frequencies. After each test, the wear scar on specimen was scanned with a Taylor Hobson Form Telesurf Series-2 profilometer and the wear volume was calculated from the 3D-profile of the wear track. The ball scars were also examined using an optical microscope.

In order to evaluate the adherence of aluminide coatings, scratch tests were performed on metallographically polished aluminized samples of superalloys 690 and 800 by CSM Scratch tester using a Rockwell indenter of 200 micron tip radius. For superalloy 690 aluminized with 10 wt.% Al, a length of 3 mm was chosen on the surface, whereas for aluminized superalloy 800, a length of 1 mm along the cross-section was taken into consideration. The load levels chosen for the alloys were 0.9 to 20 N and 0.9 to 10 N respectively with a loading rate of 30 N/minute to evaluate the adherence of aluminides. The load sensor had a resolution of 0.003 N, while depth sensor was having a resolution of 7.5 nm. For superalloy 690 aluminized with 2 wt.% Al, a scratch length of 0.4 mm was considered along the cross-section keeping a constant load level of 2 N. Friction curves and depth penetration curves were recorded for the specimens of the superalloys. Appearances of scratched surfaces at different regions with different loads were recorded using a light microscope that was attached to the instrument. Selections of type of test and test parameters were done based on the dimensions of the specimens of the alloys, type of previous test and applications of the superalloys.

3.5 Modeling of Ni (111)/NiAl(110) interface structure for aluminized superalloy 690 substrate

First-principle calculations on Ni(111)/NiAl(110) interface were performed to estimate ideal work of adhesion (W^{ad}(ideal)) between Ni and NiAl and to understand nature of bonding across the interface and its structure. The purpose of selection of Ni(111) and NiAl(110) surfaces to form the respective interface was to get lowest bound values on the interfacial adhesion as these are the most closed packed planes in their respective systems. The methodology consisted of understanding cohesion in the bulk structures, *viz.,* Ni (fcc, Fm-3m) and NiAl (B2, Pm-3m) and then studying Ni(111)/NiAl(110) interface between the substrate (Ni(111)) and the coating (NiAl(110)) surfaces. All the calculations were performed using the plane wave based Vienna Ab-initio Simulation Package (VASP) [48,49]. VASP is based on the density functional theory (DFT) and generalized gradient approximation was used for the exchange and correlation potentials as parameterized by Perdew, Burke and Ernzerhof [50]. The projector augmented wave potentials [51] were used for the ion-electron interactions. The Brillouin-zone integration was done using the Monkhorst-Pack [52] k-point mesh. The Methfessel-Paxton technique [53] was used for free energy calculations with a modest smearing of 0.1 eV, which resulted in a very small entropy term (<0.1 meV/atom) in all the cases. Full optimization was carried out with respect to E_{cut} and k-point meshes to ensure convergence of total energy to within a precision of 1 meV/atom. The total energy was optimized with respect to volume (or lattice parameter), c/a ratio and atomic positions as permitted by the space group symmetry of the crystal structure ensuring that residual force on each atom was less than 1 meV/Å. Slab model was used for the interface simulations. Seven mono-layers of Ni(111) substrate were taken to ensure no interaction between the top and bottom surfaces in the isolated surface slab. The substrate slab consists of 56 Ni atoms with surface area of 42.85 Angstrom^2. Three monolayers of NiAl(110) containing 12 atoms (6 atoms each of Ni and Al, respectively) were used as coating on Ni(111) substrate. In the present simulations, all the atoms of the NiAl(110) coating and atoms in only three topmost monolayers of Ni(111) in the interface slab were allowed to relax. Similar calculations have also been performed by replacing 2 Ni atoms by 2 Cr atoms at the interface plane and by replacing 1 Ni atom by 1 Cr atom below the interface plane and determining ideal work of adhesion for the interface.

3.6 Oxidation test

Pack aluminized (with pack mixture containing 10 wt.% Al) samples of superalloys 690 and 800 were ground up to 320 grit emery paper to remove particles, which got adhered to the surface during aluminization treatment and to have a surface that was neither very rough nor very smooth. The specimens were cleaned and weighed. Thermal oxidation of aluminized specimens was conducted at 1273 K for 2 hours in each time with a total period of 4 hours in a resistance heating horizontal furnace without using any controlled atmosphere followed by air cooling. After each oxidation treatment, the specimens were cleaned and weighed. For samples of superalloy 690 those were aluminized with pack mixture containing 2 wt.% Al, thermal oxidation was performed at 1273 K for a total period of 8 hours (4 x 2-hour) in a resistance heating horizontal furnace without using any controlled atmosphere. After every 2 hours of holding at 1273 K, the samples were taken out and allowed to cool in air. Weight gains were recorded for the first 3 x 2-hour cycles during thermal oxidation while that was negligible during last 2-hour cycle. As the service temperature of the component (superalloy 690 as metallic melter pot) has been close to 1273 K, similar temperature for thermal oxidation was chosen and an attempt has also been made to evaluate the behaviour of oxidation. Similar oxidation tests were also conducted on bare superalloy substrates for a total period of 12 hours (6 x 2-hour) to compare the oxidation behaviour of aluminized substrates of superalloys with those of bare substrates.

3.7 Characterization of oxide layer for aluminized superalloy 690

Aluminized (10 wt.% Al) and oxidized (1273 K for 4 hours) superalloy 690 substrate containing thermally grown oxide layer was examined along the cross-section using SEM under BSE as well as SE image modes. EDXS analysis was also carried out for elements on a quantitative basis at different locations along the cross-section of the specimen on point-to-point basis. XRD studies at room temperature were carried out on pack aluminized (with pack mixture containing 2 wt.% Al) sample thermally oxidized in air at 1273 K for 8 hours. It is to be mentioned that for aluminized superalloy 800 substrates, investigation was kept restricted up to evaluation of oxidation resistance.

3.8 Evaluation of stability of thermally oxidized aluminides in borosilicate melt

To evaluate the stability of the coating, aluminized superalloy 690 substrates (pack aluminized with either 10 wt.% or 2 wt.% Al in the pack mixture) with thermally grown oxide layer were exposed in sodium borosilicate melt at 1248 K for a total period of 192 hours. This exposure was restricted to superalloy 690 samples but not conducted with superalloy 800 specimens keeping in view the applications of the alloys. The composition of borosilicate glass used in the present investigation is shown in Table 3.2.

Table 3.2: Composition of borosilicate glass

Compositions of oxides, wt.%					Compositions of elements, at.%					
SiO_2	B_2O_3	Na_2O	TiO_2	Fe_2O_3	Si	B	Na	Ti	Fe	O
48.0	26.0	12.0	9.5	4.5	14.94	13.95	7.24	2.2	1.04	60.59

The glass composition is of interest. The glass formulation for immobilization of high level radioactive liquid waste is judiciously chosen to ascertain optimal waste loading, modest processing requirements and desirable product characteristics. About 6 g of sodium borosilicate glass beads were taken in one set of sillimanite crucibles of internal diameter of about 17 mm and height of 18 mm and the crucibles were placed inside a pre-heated (1248 K) chamber type furnace in air atmosphere. The samples were dipped in the glass when it reached molten state and the temperature of the molten glass was maintained at 1248 K for a total period 192 hours. In each crucible, the volume of molten glass was around 6 times to that of the specimen. Superalloy 690 bare substrates were also kept in another set of crucibles under identical experimental condition for comparison of results.

After the exposure of the specimens in borosilicate melt, the cross-section of the specimens (aluminized + thermally oxidized and bare alloy samples) with adhered glass were metallographically polished and microstructural characterization was carried out using SEM under BSE as well as SE image modes. EDXS analysis using a polymer-based thin window for detector entrance allowing detection of X-rays down to 100 eV was performed for elements on a quantitative basis at various locations along the cross-section on point-to-point basis for the specimens. The analyses of substrates for the samples and aluminides were found to be reproducible and accurate. EDXS analysis of glass phase excluding B was carried out only in close vicinity of specimen/glass interface. The glass phase in each case that was far away from interface was not considered to avoid possibility of any contamination from crucible surface. Besides this, some overestimation of elements only in glass phase because of omission of B was kept in mind.

XRD studies at ambient temperature were performed on the surface of aluminized (10 wt.% Al) and thermally oxidized superalloy 690 substrate after exposure in borosilicate melt.

CHAPTER 4: PHASE EVOLUTION IN ALUMINIZED SUPERALLOYS

4.1 Background

Over the past a few decades, intermetallic compounds have been a prime topic of research for high temperature structural applications owing to their high melting points, mostly low density, good wear resistance and good resistance to aggressive environments at elevated temperatures [13,18,54-61]. In this regard, NiAl, FeAl and Fe_3Al have been found to be quite promising [13,54-57,59,60]. High temperature oxidation resistance of these materials is attributed to the formation of a continuous, adherent Al_2O_3 layer on exposure to air or oxygen atmosphere that provides a good diffusion barrier [13,58,59,61-68]. However, these intermetallic compounds have got some deficiencies. In case of FeAl-based alloys, the limitations are low ductility in air and relatively low high-temperature strength, whereas for NiAl these are low fracture toughness at low temperatures and low strength and low creep resistance at high temperatures [69,70]. However, it has been possible to improve, to some extent, the properties of Fe_3Al by controlling the composition and process parameters [54]. Improvement of oxidation resistance by the addition of alloying elements in the bulk is not always beneficial as this quite often adversely affects the mechanical properties of the materials. That is why, surface treatments are widely practiced to overcome this shortcoming [58]. Various methods used for surface coatings are chemical vapour deposition, thermal spraying, pack cementation, physical vapour deposition, magnetron sputtering, laser cladding and plasma spraying [58]. Among these, pack cementation is not only useful but also inexpensive and that is why, it is generally applied to steels and superalloys for improving their resistance to oxidation and sulphidation at elevated temperatures [58,71-73]. High chromium low iron containing Ni-based superalloy 690 and high nickel moderate chromium containing Fe-based superalloy 800 find high temperature service applications besides their wide uses as SG tube materials as mentioned earlier. As compared to the number of studies carried out on these alloys in SG related issues, a few [5,10-12] have been dealt with aluminization of the alloys relating to development of diffusion barrier coatings for high temperature applications. Therefore, an investigation on formation of aluminide coatings on superalloys 690 and 800 substrates by aluminization process followed by their microstructural characterization has been undertaken from the perspective of development of materials for high temperature applications. In this study, aluminization of the substrates of superalloys 690 and 800 has been primarily done by pack aluminizing (pack cementation) process. This has been followed by microstructural analysis employing SEM, EDXS, EPMA, XRD and TEM. Prior to presentation of the results on pack aluminization of the alloys, it is relevant to briefly discuss the diffusion coefficients of Ni, Cr, Fe and Al at the elevated temperatures.

4.2 Results

4.2.1 Calculated diffusion coefficients of elements

The diffusion coefficients of Ni, Cr, Fe and Al have been calculated and are given below in tabular form.

Table 4.1: Calculated diffusion coefficients of Ni, Cr, Fe and Al

Matrix	Diffusing element	Diffusion coefficient, m^2/s	Temperature, K
Nickel	Ni (self diffusion)	1.016×10^{-16}	1212
		3.811×10^{-16}	1273
		2.604×10^{-15}	1373
		1.509×10^{-14}	1478
Nickel	Al (as tracer impurity)	6.225×10^{-16}	1212
	Cr (as tracer impurity)	4.679×10^{-15}	1373
	Fe (as tracer impurity)	3.011×10^{-14}	1478
Iron	Cr (as tracer impurity)	1.147×10^{-15}	1273
	Ni (as tracer impurity)	2.379×10^{-16}	1273

The diffusion coefficients shown in the above table have been calculated from the pre exponential factors and activation energies reported [74] for the elements over the ranges of temperatures. The values correspond to either in self diffusion (predominantly for Ni) or as tracer impurities of the elements in nickel and iron matrices, which are of relevance in the present context. It is indicative from the table that Ni is the slowest diffusing element among the four elements in nickel matrix. In iron, the diffusion of Ni is also slower than Cr.

4.2.2 Pack aluminization

4.2.2.1 Surface morphology

Figure 4.1 is an SEM micrograph showing the surface morphology of aluminized (10 wt.% Al) specimen of superalloy 690. It reveals the presence of 160-200 nm spherical particles inside each granular particle indicating that the deposition is particulate in nature. Figure 4.2a and b show the surface morphologies of pack aluminized (10 wt.% Al) superalloy 800. Figure 4.2a demonstrates the presence of lath kind of structure in some locations and granular particle formation in other part of the surface. Figure 4.2b indicates the formation of coating with spherical morphology.

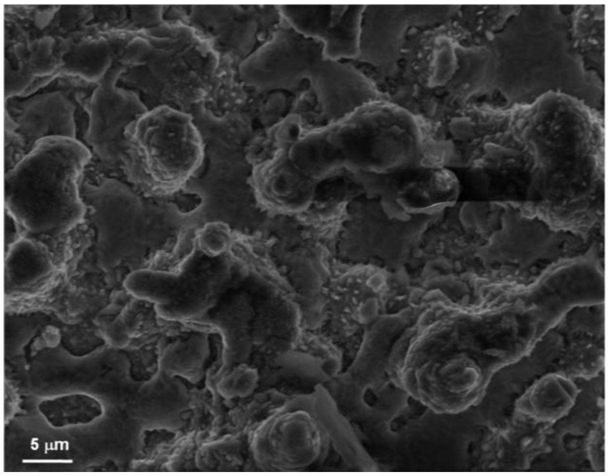

Figure 4.1 Surface morphology of aluminized (10 wt.% Al) superalloy 690 specimen showing the presence of 160-200 nm spherical particles inside each granular particle indicating the deposition is particulate in nature.

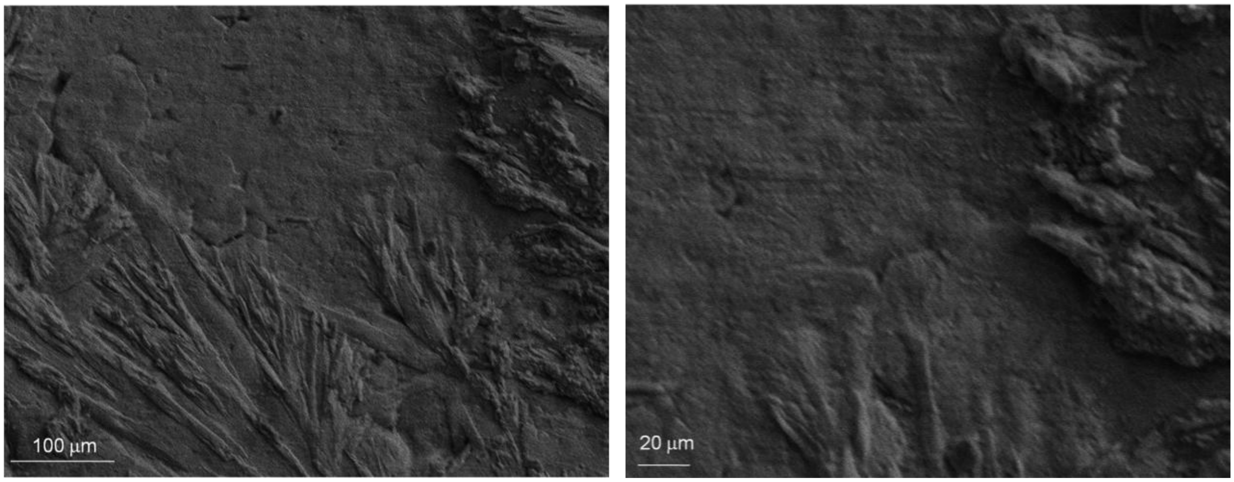

a b

Figure 4.2 Surface morphology of pack aluminized superalloy 800 substrate indicating (a) presence of lath kind of structure in some regions and the formation of granular particles in other part of the surface and (b) formation of coating with spherical morphology revealing fine globular or spherical granular particles.

4.2.2.2 Microstructure, microanalysis and XRD

Cross-sectional microstructure examined by SEM has revealed that aluminides formed in multilayer on aluminized (10 wt.% Al) superalloy 690 substrate (along the cross-section) as is evident from Figure 4.3. The concentration of elements in different phases along the cross-section covering the layers and substrate is shown in Table 4.2, which summarizes the results of SEM and EPMA. It is indicated that the top layer (15 micron thick) consists of (NiCr)Al type and Cr_5Al_8 type phases. The adjoining layer (second layer; 300 micron thick) is also having two distinct regions comprising Ni_2Al_3 + Cr_5Al_8 type phases. The third one, a homogeneous layer (50 micron thick), comprises of a phase, which is of NiAl type. The fourth one, the innermost layer (10 micron thick), is a solid solution of Ni, Cr, Fe and Al showing a compositional difference of less than 1 wt.% with respect to the substrate composition.

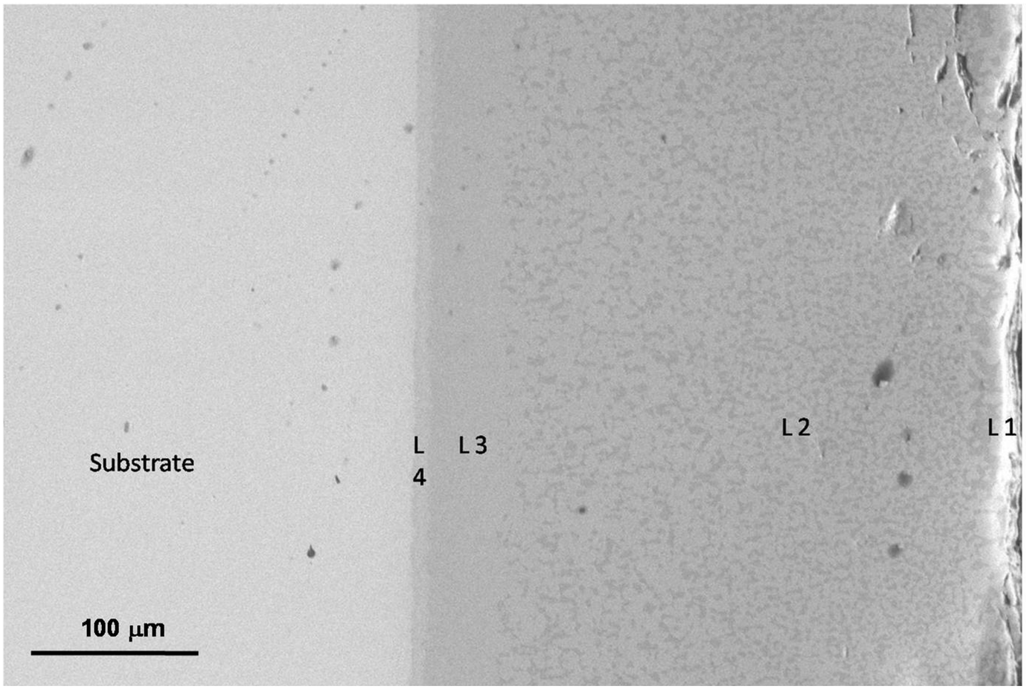

Figure 4.3 Multilayer in aluminized (10 wt.% Al) superalloy 690 substrate (along the cross-section). Substrate is shown along with four layers L1, L2, L3 and L4.

It is to be mentioned that the different phases (data points 1-7) as stated above and shown in Table 4.2 have been chosen by examining the phase contrast under back-scattered electron image mode of SEM. It is further mentioned that data points 1 and 2 from layer 1, points 3 and 4 from layer 2, point 5 from layer 3, point 6 from layer 4 and point 7 from substrate have been selected, their compositions are analyzed and shown in Table 4.2. On SEM micrograph, L1, L2, L3 and L4 indicate layer 1, layer 2, layer 3 and layer 4 respectively. It is to be mentioned that the volume fraction of Cr_5Al_8 type phase in layer 1 is more than (NiCr)Al type phase but as one moves towards the austenite substrate, the volume fraction of Cr_5Al_8 type phase decreases.

Table 4.2: Summary of SEM and EPMA results on aluminized (10 wt.% Al) superalloy 690 substrate along the cross-section.

Material	Thickness, micron & data point number	Compositions of representative phases, wt.%				Compositions of representative phases, at.%				Possible phases
		Al	Cr	Fe	Ni	Al	Cr	Fe	Ni	
Layer 1	~15 Data points 1,2	45.72	43.83	6.94	3.52	62.2	31.02	4.56	2.21	Cr_5Al_8
		35.63	19.24	5.67	39.47	53.59	15.02	4.1	27.28	(NiCr)Al
Layer 2	~300 Data points 3,4	39.64	14.07	5.44	40.85	58.03	10.66	3.83	27.47	Ni_2Al_3
		43.03	40.77	6.31	9.9	59.88	29.53	4.25	6.33	Cr_5Al_8
Layer 3	~50 Data point 5	36.65	6.88	6.63	49.83	55.31	5.37	4.79	34.52	NiAl
Layer 4	~10 Data point 6	0.28	31.49	10.2	58.03	0.56	33.85	10.18	55.4	γ
Substrate	Data point 7	0.24	30.94	10.08	58.74	0.5	33.33	10.08	56.08	γ

Microscopic examinations of aluminized (10 wt.% Al) superalloy 800 substrate along the cross-section indicated the formation of a multilayer having different phases. Figure 4.4 demonstrates the micrograph of aluminized superalloy 800 substrate in back-scattered electron image mode. The thickness of the top layer was found to be about 150 micron, whereas the second one was around 250 micron. A thickness of about 60 micron was noticed for the innermost layer. Figure 4.5 shows the EPMA profile of multilayered superalloy 800 specimen along the cross-section.

Figure 4.6a, b and c show X-ray diffractograms of first layer, second layer and substrate of superalloy 800 respectively. Table 4.3 summarizes EPMA and XRD results on multilayer of the alloy. XRD has revealed that the outermost layer consists of FeAl + Fe_2Al_5 type phases, whereas adjoining layer consists of FeAl type phase. FeAl is cubic (ordered body centered cubic structure), whereas Fe_2Al_5 is orthorhombic. In the present investigation, a slight deviation of lattice parameters (first or second decimal place) for FeAl and Fe_2Al_5 phases as compared to 1998 ICDD has been observed. This could be attributed to the presence of Cr and Ni in intermetallic phases FeAl and Fe_2Al_5 as revealed by microanalyses (partial replacement of Fe by Cr and Ni). EPMA has also indicated that the outermost layer consists of two types of phases with the variation of Al-content in the range of 63-64 at.%, while the second layer consist of one type of phase containing Al in the vicinity of 55 at.%. EPMA has revealed that the innermost layer, which is a solid solution zone, has been found to compose of ~ 43 at.% Fe, 38 at.% Cr and 11 at.% Ni containing about 6 at.% Al. The substrate has been found to have a composition of ~ 47 at.% Fe, 22 at.% Cr, 29 at.% Ni and 0.7 at.% Al. XRD confirmed that the substrate is austenite (face centered cubic structure) and its lattice parameter has been obtained as 3.58 Å.

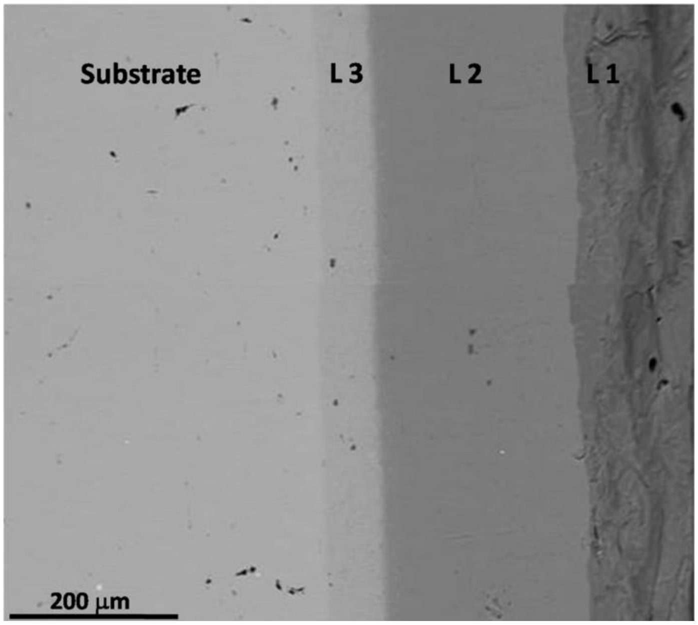

Figure 4.4 Cross-section of aluminized superalloy 800 revealing multilayer L1, L2 and L3 along with the substrate under back-scattered electron image mode.

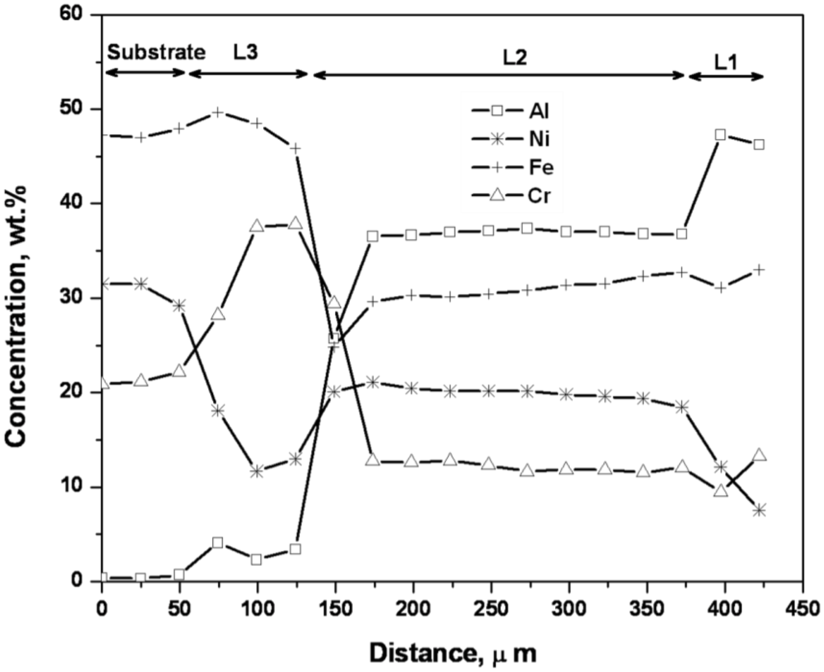

Figure 4.5 Concentration of Fe, Ni, Cr and Al at different points covering substrate and three layers as shown in Figure 4.4. Position of substrate is shown along with three layers L1, L2 and L3 in the profile.

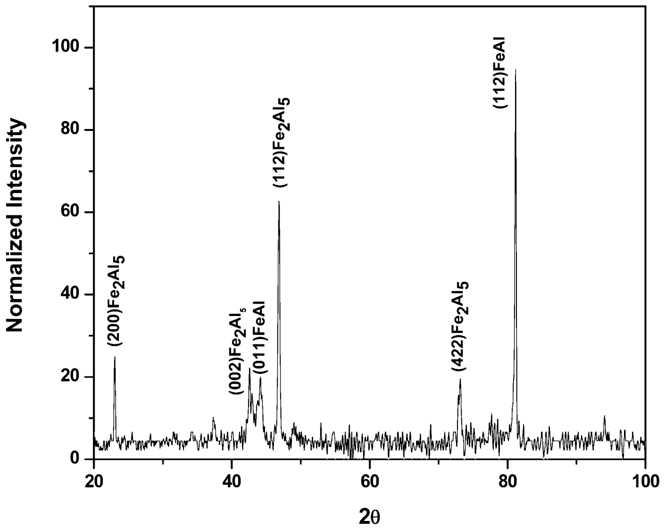

a

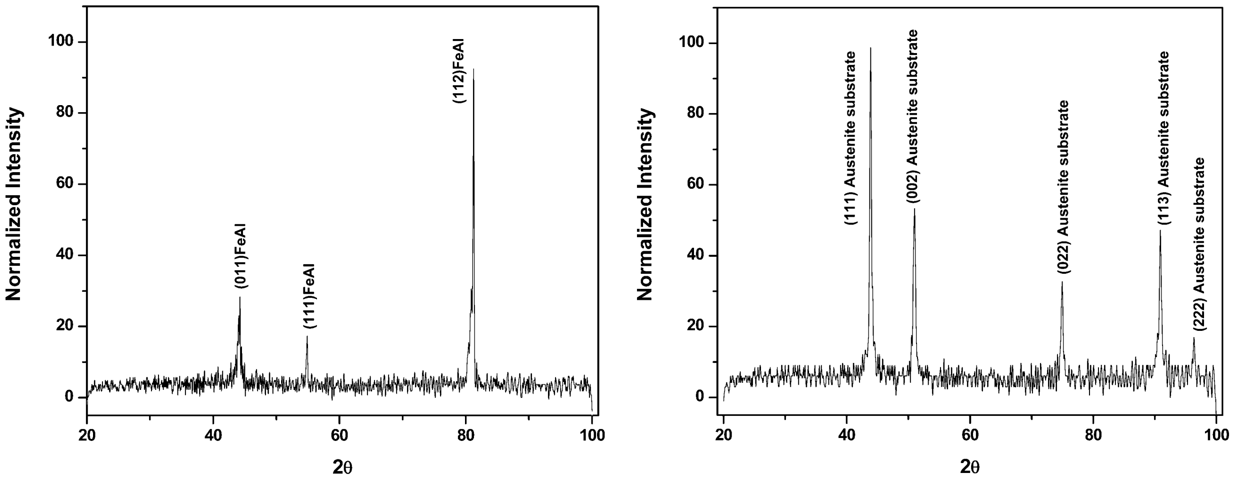

b

c

Figure 4.6 X-ray diffractograms indicating the presence of (a) FeAl type and Fe_2Al_5 type phases in layer 1, (b) FeAl type phase in layer 2 of aluminized superalloy 800 substrate and (c) austenite phase in superalloy 800 substrate. These are achieved by controlled grinding of layers followed by XRD studies.

Table 4.3: Summary of EPMA and XRD results on aluminized superalloy 800 substrate

Material	Thickness, micron	Compositions of representative phases, wt.%				Compositions of representative phases, at.%				Major phases identified by XRD
		Al	Cr	Fe	Ni	Al	Cr	Fe	Ni	
Layer 1	~150	46.25	13.22	32.96	7.57	63.79	9.45	21.96	4.8	Fe_2Al_5, FeAl
		47.29	9.47	31.11	12.13	64.94	6.75	20.67	7.64	
Layer 2	~250	37.12	12.31	30.42	20.15	55	9.48	21.8	13.72	FeAl
Layer 3	~60	3.4	37.82	45.84	12.94	6.65	38.38	43.35	11.62	Solid solution
Substrate		0.36	20.87	47.3	31.47	0.72	22.32	47.13	29.83	γ

For samples of superalloy 690, aluminized with pack mixture containing 2 wt.% Al, SEM examination with EDXS analysis along the cross-section of aluminized superalloy 690 substrate indicated formation of multilayer. The uppermost layer consisted of NiAl type phase (~45 μm), while adjoining one composed of (NiCr)Al and $(NiCr)_2Al$ types layer (~25 μm) and subsequently Cr-rich layer (~ 35 μm) adjacent to substrate. Al-content was found to increase while moving from Cr-rich layer towards outer layer. Figure 4.7 shows different layers, whereas Table 4.4 summarizes SEM-EDXS analysis at various points of the aluminized specimen along the cross-section. XRD pattern of the aluminized specimen obtained from the coating surface (Figure 4.8) revealed peaks of B2 crystal structure with lattice parameters matching with NiAl phase. This identification of the phase was consistent with the SEM-EDXS analysis of the top layer. Figure 4.9 demonstrates the results obtained on examining the uppermost layer of cross-sectional sample under TEM. EDXS along with SAD pattern analysis has confirmed that the uppermost layer comprises of NiAl type phase as demonstrated in Figure 4.9a and b respectively. Streaks in the spots of the SAD pattern (Figure 4.9b) appear to have induced from strains during sample preparation. The EDXS measurement was done at the central region of Figure 4.9a. It is indicated that normalization to 100% introduced a maximum error of 0.002% during EDXS measurements in which adding up all the elements shows 99.998% in three cases, while it shows 99.999% in one case instead of showing 100.00%. The finding of TEM-EDXS analysis is in consistent with SEM-EDXS analysis and XRD results. TEM examination has further revealed that the uppermost surface contains nano particles. High-resolution TEM examination with quantitative analysis has indicated that the nano particles are of nickel aluminide as shown in Figure 4.9c. TEM investigation was confined up to a few micron of the uppermost surface of aluminized alloy substrate.

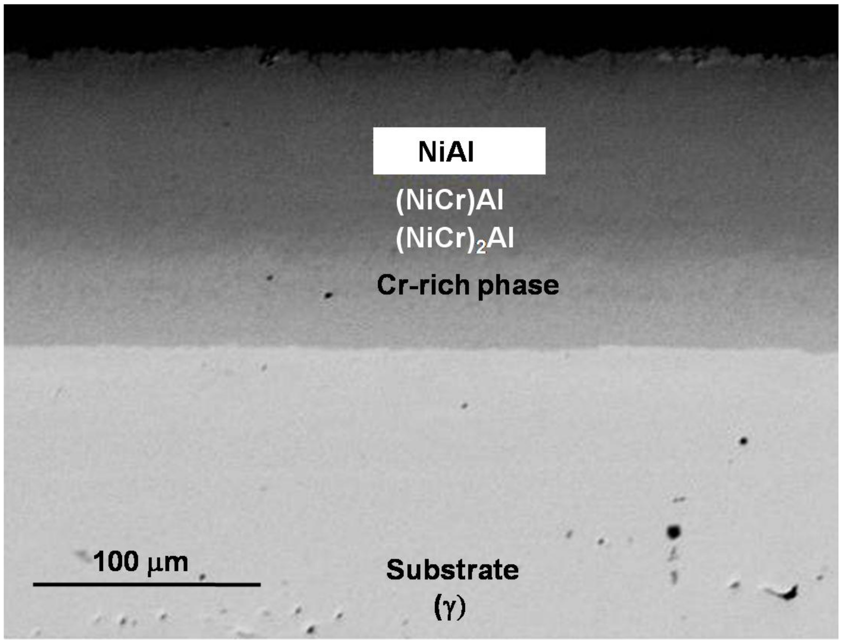

Figure 4.7 Multilayer in aluminized (2 wt.% Al) superalloy 690 substrate along the cross-section.

Table 4.4: SEM-EDXS analysis on aluminized (2 wt.% Al) superalloy 690 substrate along the cross-section.

Location	Analysis point	Elements, at.%					Possible phase
		Al	Cr	Fe	Ni	O	
Layer 1	1	56.71	5.26	4.96	33.08	-	NiAl NiAl
	2	55.55	5.85	4.72	31.89	1.99	
Layer 2	3	48.23	11.71	3.24	36.82	-	(NiCr)Al
Layer 3	4	30.76	31.78	5.35	32.11	-	(NiCr)$_2$Al
Layer 4	5	12.93	54.55	10.60	21.93	-	Cr-rich phase Cr-rich phase
	6	15.33	53.69	8.97	22.01	-	
Substrate	7	-	32.48	10.32	57.20	-	γ

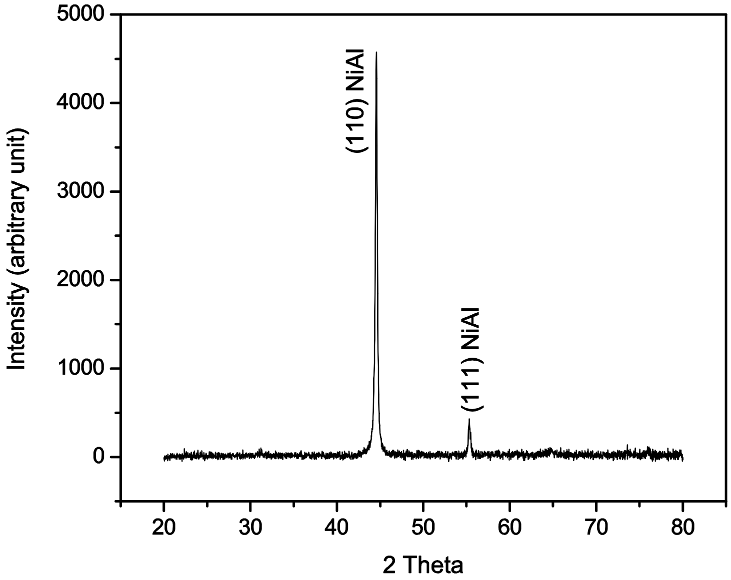

Figure 4.8 X-ray diffractogram of aluminized (2 wt.% Al) superalloy 690 revealing NiAl phase.

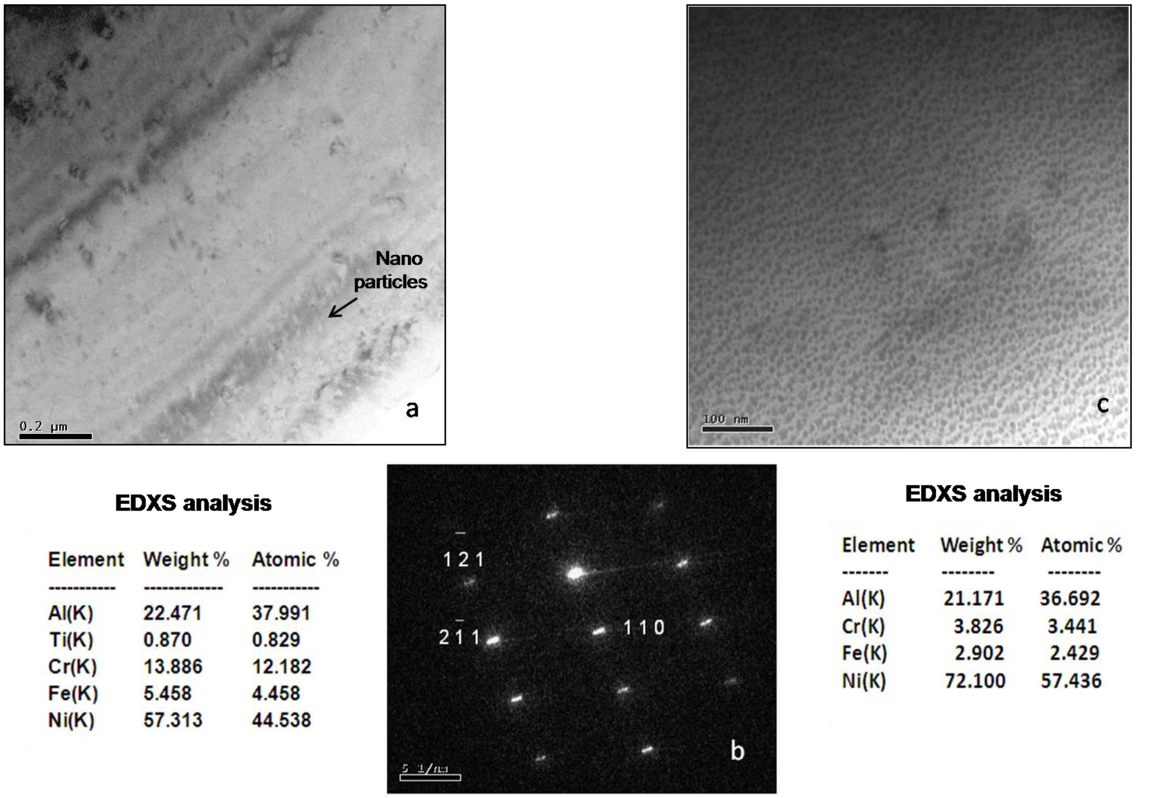

EDXS analysis

Element	Weight %	Atomic %
-----------	-------------	-----------
Al(K)	22.471	37.991
Ti(K)	0.870	0.829
Cr(K)	13.886	12.182
Fe(K)	5.458	4.458
Ni(K)	57.313	44.538

EDXS analysis

Element	Weight %	Atomic %
-------	--------	--------
Al(K)	21.171	36.692
Cr(K)	3.826	3.441
Fe(K)	2.902	2.429
Ni(K)	72.100	57.436

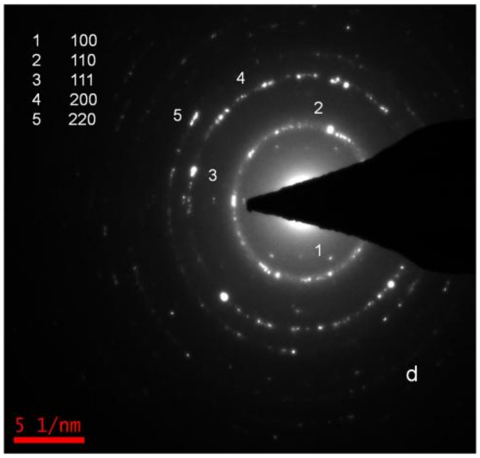

Figure 4.9 Cross-sectional TEM micrographs revealing (a) NiAl type phase along with EDXS (on central region), (b) SAD pattern of NiAl along zone axis $[\bar{1}\ 1\ 3]$, (c) nano particles with quantitative analysis and (d) SAD pattern of nano particles showing rings of different planes.

4.3 Discussion

According to the binary Al-Ni phase diagram by Okamoto [75], $NiAl_3$ forms at 25 at.% Ni. The phases Ni_2Al_3 and NiAl are found to be stable in the composition range of 37 to 42 and 42 to 69 at.% Ni respectively, while the phases Ni_5Al_3 and Ni_3Al exist at higher and higher composition of Ni [75]. Levine and Caves [76] have studied thermodynamics and kinetics of pack aluminide coating formation on nickel-based superalloy IN-100 in one-step packs containing Al at unit activity. The ammonium halides were primarily used to activate 1366 K, 16-hour packs. According to the investigators [76], pack temperature rather than pack Al activity controls the principal coating phase. Gaseous diffusion was found to control the rate of coating formation in NH_4Cl-activated packs containing 1 wt.% Al. The kinetics of coating formation were found to be near parabolic. The major phase has been reported to be NiAl as detected by X-ray diffraction [76]. Thevand et al. [77] have studied formation and growth mechanisms of various intermetallic phases in Al-Ni system during pack aluminization of Ni with respect to Al activity in the pack. According to them [77], a Ni-rich NiAl coating formed by outward diffusion of Ni in a low activity pack. Houngninou et al. [58] have investigated pack aluminization on pure Ni mainly at 1273 K in argon atmosphere. They have reported the formation of intermetallic phases such as Ni_2Al_3 and NiAl as first layer followed by interdiffusion layer indicating inward diffusion of Al and outward diffusion of Ni. According to the investigators [58], the diffusivity of Al and Ni was not adequate at the chosen aluminizing condition for the attainment of equilibrium NiAl phase on pure Ni substrate. Goward [18] has discussed various diffusion mechanisms in Ni-Al system. It has been indicated that diffusion of Ni predominates in Ni-rich NiAl and Al diffusion predominates in Al-rich NiAl. Das et al. [78] have carried out pack aluminization of cast Ni-based superalloy at 1307 K in argon atmosphere. The coatings developed on the alloy surface have been found to consist of NiAl phase without formation of any high Al-containing phases indicating attainment of equilibrium NiAl phase even in very short time because of high diffusivity of Ni and Al under the experimental conditions. Based on the microstructural details of the coatings, the authors [78] have proposed that the growth of the coating takes place initially by inward Al diffusion, followed by an intermediate stage wherein the growth involves both inward Al and outward Ni diffusion and in the final stage, the outward diffusion of Ni dominates coating formation. Da Costa et al. [79] have studied co-deposition of chromium-aluminide coatings on a Ni-based superalloy in a cementation pack at 1393 K in argon atmosphere. Based on the investigation, a simplified mechanism involving a combined parabolic accumulation of β-NiAl and two-stage linear accumulation of α-Cr has been proposed by the investigators [79]. According to them, as the system was partially open, a uniform thermodynamic equilibrium could not be achieved. Huang et al. [80] have examined first-stage aluminized coating formed on pure Ni-Cr alloy by pack aluminizing at 1023 K in argon atmosphere and have observed multilayer formation comprising polygonized γ, γ'-Ni_3Al, β-NiAl + α–Cr, δ–Ni_2Al_3 and δ–Ni_2Al_3 + Cr_5Al_8 layers. According to the binary Al-Cr phase diagram by Murray [81], the phases $CrAl_7$, Cr_2Al_{11} and $CrAl_4$ are found to be stable in the composition range of 12.4 to 13.7, 15.2 to 17 and 18.5 to 20 at.% Cr respectively, while the phases Cr_4Al_9 and Cr_5Al_8 are found to exist in the range of 30 to 33.5 and 35.5 and 42 at.% Cr respectively. In the present study, pack aluminization of superalloy 690 with 10 wt.% Al indicated formation multilayer comprising (NiCr)Al + Cr_5Al_8, Ni_2Al_3 + Cr_5Al_8, NiAl and γ phases. These findings seem to be in accordance with the results of other investigators [15,58,76-81]. Multilayer formation on superalloy 690 substrate appears to have taken place by inward diffusion of Al and outward diffusion of Ni and Cr [58]. Ni and Cr having similar atomic weights diffuse in a similar manner giving rise to Ni-rich and Cr-rich phases at different depths. However, existence of Ni-rich phase (layer 3) very close to substrate could be attributed to marginally higher atomic weight of Ni as compared to Cr leading to Ni being slightly less fast diffusive element than Cr. In case of pack aluminization of superalloy 690 with 2 wt.% Al, the formation of NiAl type phase on the topmost surface and existence of Cr-rich phase adjacent to superalloy 690 substrate appear to have taken place by outward diffusion of Ni in low Al-containing pack [77]. The formation of nano particles of nickel aluminide on the uppermost surface indicates that the deposition is particulate in nature. This can be explained as follows. Deposition that takes place in pack aluminization (pack cementation) resembles chemical vapour deposition process. $AlCl_x$ vapours that form during pack aluminization process come in contact with the surface of the substrate and dissociates into Al and Cl_2. Therefore, it is evident from the deposition process during pack aluminization that pack aluminized surface leaves the signature of particulate nature of deposition. Afterwards, for high Al-containing pack (10 wt.% Al), multilayer of aluminides form by inward diffusion of Al and outward diffusion of alloying elements of the substrate (Ni,Cr). In case of low Al-containing pack (2 wt.% Al), multilayer forms by outward diffusion of Ni.

According to the binary Fe-Al phase diagram by Kattner and Burton [82], Fe_3Al phase is stable in the composition range between 23 and 34 at.% Al, whereas FeAl exists between 23.3 and 55 at.% Al. $FeAl_2$, Fe_2Al_5 and $FeAl_3$ phases have been found [82] to exist at higher composition of Al. Palm [83] has also discussed the occurrences of various phases in Fe-Al system. According to him [83], two compounds exist between 0 and 54 at.% Al. Below 825 K, Fe_3Al is stable at around 27 at.% Al, whereas FeAl exists between 23 and 54 at.% Al depending on the temperature. In addition, it is evident from the isothermal section of Fe-Al-Cr system at 1273 K [83] that $FeAl_2$, Fe_2Al_5 and $FeAl_3$ phases occur at higher composition of Al as mentioned by Kattner and Burton [82]. Miller et al. [10] have used 70Cr-30Al, 90Cr-10Al and 95Cr-5Al masteralloys (wt.%) with NaF and NaCl as activators to form an interdiffusion zone enriched in Cr and Al for Incoloy 800 during pack cementation at 1273 K for 27 hours either in argon or argon + 5% hydrogen atmosphere. A pack mixture composed of 75 wt.% $\alpha-Al_2O_3$ powder, 23 wt.% Cr-Al masteralloy and 2 wt.% halide activator has been chosen. The auhors [10] could not find a suitable pack composition to achieve the desired interdiffusion zone. Aluminide coatings applied by pack cementation process on Incoloy 800H have been found to provide a good protection against corrosive environment up to 823 K under stress-free condition [11]. Pack cementation of Alloy 800 has been carried out at 1223 K for 8 hours in argon + 10% hydrogen atmosphere by some researchers [12] using a pack mixture consisting of 5 wt.% Al, 0.5 wt.% NH_4Cl and 94.5 wt.% Al_2O_3. The authors [12] have reported the formation of (Ni,Fe)Al and Fe_2Al_5 phases on top surface (15-20 μm). A pack cementation process has been developed to coat commercial 9 wt.% Cr ferritic-martensitic steel by substituting the pure Al masteralloy with Cr-25wt.% Al so that a duplex coating forms at 973 K consisting of thin Fe_2Al_5 outer layer and an inner layer of FeAl [84]. The formation of ~12 μm thick FeAl layer has been reported at 973 K with Cr-15wt.% Al master alloy [84]. Houngninou et al. [58] have carried out synthesis and characterization of pack cemented aluminide coatings on Fe-30 wt.%Cr alloy, pure Fe and pure Ni. Aluminization temperature was mainly chosen at 1273 K and it was carried out in argon atmosphere with a pack mixture composed of 15 wt.% Al powder, 3 wt.% NH_4Cl and 82 wt.% Al_2O_3 powder. The formation of intermetallic phases as first layer followed by interdiffusion zone on Fe-30 wt.% Cr alloy and pure Fe substrates has been reported [58]. For Fe-30 wt.% Cr alloy and pure Fe, the first layer has been found to be composed of FeAl and Fe_3Al. According to the authors [58], the formation of interdiffusion zone in both the cases is indicative of inward diffusion of Al and outward diffusion of Fe and Cr. In the present study on pack aluminization of superalloy 800 with 10 wt.% Al, XRD and EPMA have indicated that the outermost layer consists of FeAl + Fe_2Al_5 type phases, wherein partial replacement of Fe has taken place by Cr and Ni present as alloying elements in Alloy 800. EPMA has indicated the Al-content of first layer is in the range of 63-64 at.%. It is the average Al content of the first layer comprising of FeAl + Fe_2Al_5 type phases. The formation of high Al-containing aluminides that is Fe_2Al_5 on the outermost layer is believed to be attributed to high Al activity in the pack mixture. It is, therefore, evident that the findings of present study are in agreement with the results of other investigators [58,12,16,83,84]. Since major alloying element in Alloy 800 is Fe, the formation of Ni-based intermetallic phases as predominant ones is not expected, only partial replacement of Fe by Ni in intermetallic phases is expected as noticed in microanalyses of present study. The second layer that consists of FeAl type phase with partial replacement of Fe by Cr and Ni is a homogeneous layer having Al-content in the vicinity of 55 at.%. These results indicate that the formation of second layer has taken place by inward diffusion of Al followed by intermetallic formation with Fe, Ni and Cr of Alloy 800, and this is as per the expectation. The formation of innermost layer that is a solid solution zone, comprising ~ 43 at.% Fe, 38 at.% Cr, 11 at.% Ni containing about 6 at.% Al, is also indicative of inward diffusion of Al and outward diffusion of Fe, Ni and Cr that is in agreement with the findings of other investigators [58].

4.4 Summary

The present investigation pertaining to work related to development materials for high temperature applications has dealt with aluminization of superalloys 690 and 800 substrates primarily by employing pack aluminization (pack cementation) process at 1273 K in argon atmosphere using high Al-containing (10 wt.% Al) pack. For superalloy 690 specimens, low Al-containing (2 wt.% Al) pack has also been considered. This is followed by microstructural characterization of aluminized superalloy substrates using XRD, SEM, EDXS, EPMA and TEM. Findings of different phases in respective alloy system have been discussed from the perspective of Ni-Al and Fe-Al alloy systems as well as results of other investigators. Besides this, the mechanisms for formation of phases in high Al- and low Al-containing packs have been discussed. Based on experiments and understanding, a few important points of this study are summarized as follows:

(a) Pack aluminization of substrates of superalloy 690 with high Al-containing pack (10 wt.% Al) at 1273 K results in formation of multilayer including nickel aluminides and chromium aluminide that is attributed to inward diffusion of Al and outward diffusion of Ni and Cr. For low Al-containing pack (2 wt.% Al) of superalloy 690, multilayer predominantly NiAl type phase on the uppermost surface forms due to outward diffusion of Ni.

(b) For superalloy 800 substrates, pack aluminization with high Al-containing pack (10 wt.% Al) at 1273 K shows formation of multilayer including iron aluminides, which could be attributed to inward diffusion of Al and outward diffusion of Fe, Ni and Cr.

CHAPTER 5: PROPERTIES OF ALUMINIZED COATINGS

5.1 Background

For development of aluminide coatings on high chromium low iron containing Ni-based superalloy 690 and high nickel moderate chromium containing Fe-based superalloy 800 for high temperature applications, evaluation of microhardness, wear rate and adherence are of immense importance. Hence, an investigation on measurements of such properties has been undertaken. In this study, the properties of aluminized superalloy 690 substrates, which are microhardness, friction, wear and adherence have been discussed. For superalloy 800, the properties of aluminized substrates those are microhardness, friction and adherence have been stated. During development of aluminide coatings for high temperature applications, understanding the nature of interfacial interactions is of prime importance. Keeping this in view, a study relevant to superalloy 690 has also been undertaken to determine the stability of NiAl phase and adhesion strength of Ni(111)/NiAl(110) interface by employing first-principle computational approach. The bonding across the interface and its structure has also been discussed in this study. Similar calculations have also been conducted by replacing a few Ni atoms by Cr atoms at the interface plane and determining ideal work of adhesion for the interface.

5.2 Results

5.2.1 Microhardness values of aluminides

For aluminized (10 wt.% Al) superalloy 690 substrate, microhardness test along the cross-section indicated a variation of Knoop hardness number (KHN) in the range of 225 to 1142 (±15) indicating aluminide layer formation as revealed by SEM and EPMA. Since the edges of cross-section contain aluminide layers, Knoop microhardness values were high at the edges and low in mid region due to the presence of substrate. It may be noted that adequate margins were left on either side while measuring microhardness values to avoid error due to edge effects. Figure 5.1 demonstrates the variation of microhardness value for aluminized superalloy 690 along the cross-section.

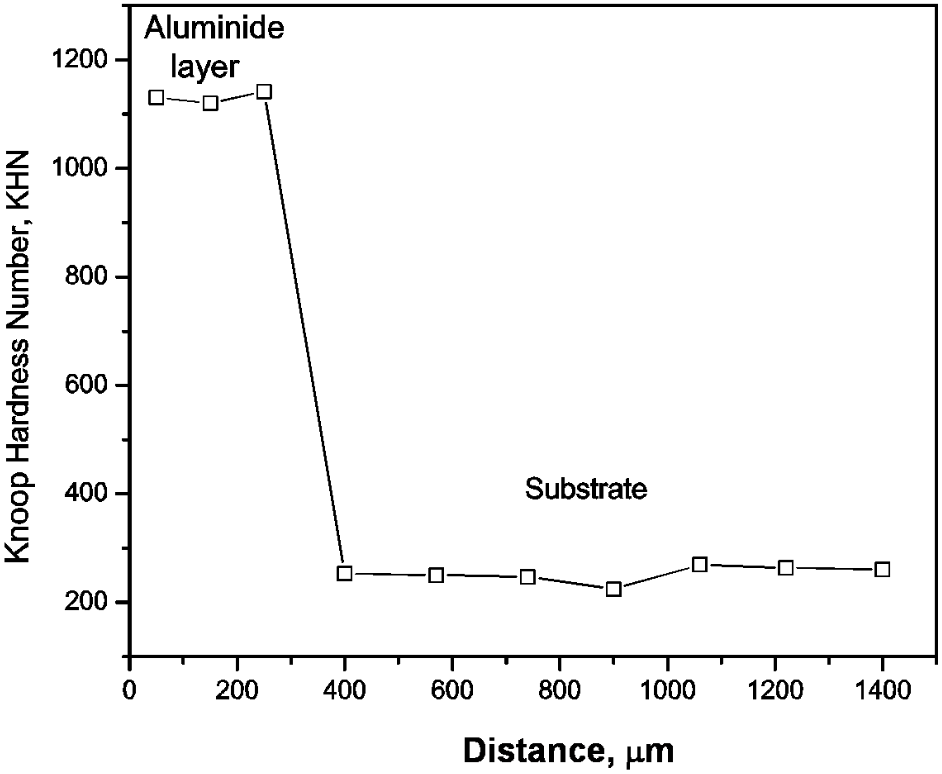

Figure 5.1 Variation of Knoop microhardness number (error ±15) along the cross-section of aluminized (10 wt.% Al) superalloy 690 sample.

A variation of microhardness value in the range from 213 (±5) to 1098 (±15) KHN has been obtained for the aluminized (10 wt.% Al) superalloy 800 substrate along the cross-section as shown in Figure 5.2. Knoop microhardness values are high at the edges and low at mid region with moderate values between the two regions. High and moderate hardness values are due to presence of multilayer of aluminides indicating a decrease in microhardness value with the decrease in Al-content of the aluminide, while low values at mid region are because of substrate.

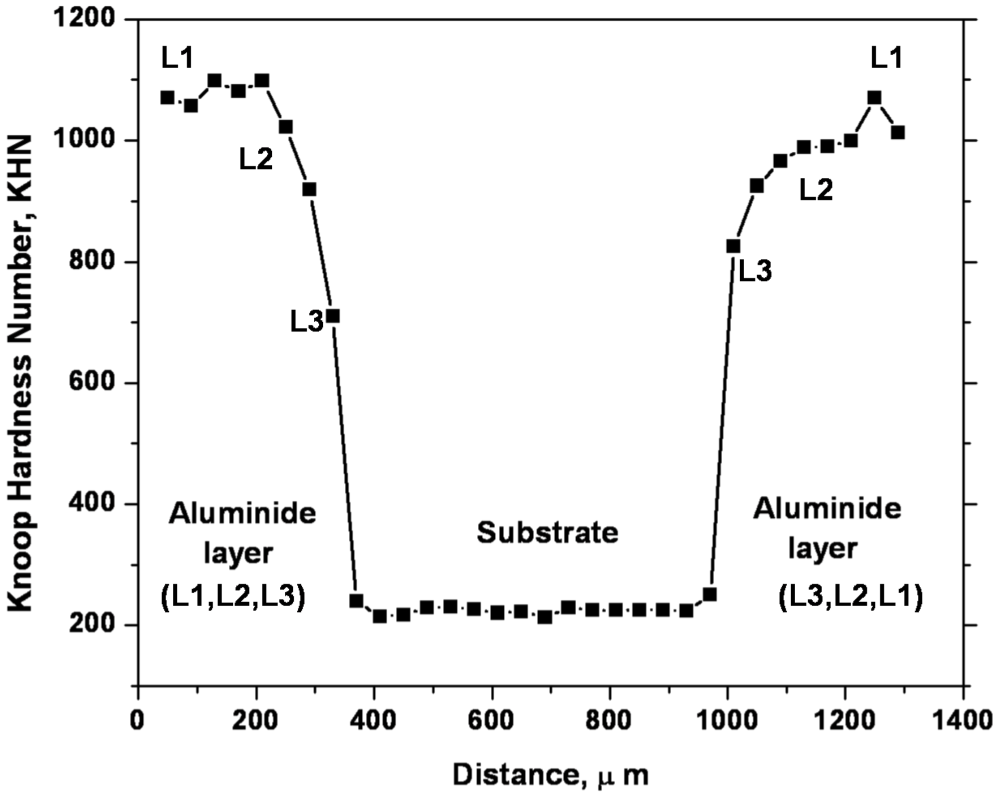

Figure 5.2 Variation of Knoop microhardness number (error ±15) along the cross-section of aluminized superalloy 800 sample. Hardness measurement started from one end and finished at the other end of the cross-section.

For specimens of superalloy 690, aluminized with pack mixture containing 2 wt.% Al, microhardness test along the cross-section of aluminized superalloy 690 substrate indicated a variation of Vickers hardness number (VHN) in the range of 157 to 624 (±10) indicating aluminide layer formation as revealed by SEM with EDXS analysis. Since the edge of cross-section contains aluminide layer, Vickers microhardness values were high at the edge and low in mid region due to presence of substrate. It may be mentioned that sufficient margin was left from the edge while measuring microhardness values to avoid error due to edge effect. The variation of microhardness value for aluminized superalloy 690 along the cross-section is shown in Figure 5.3.

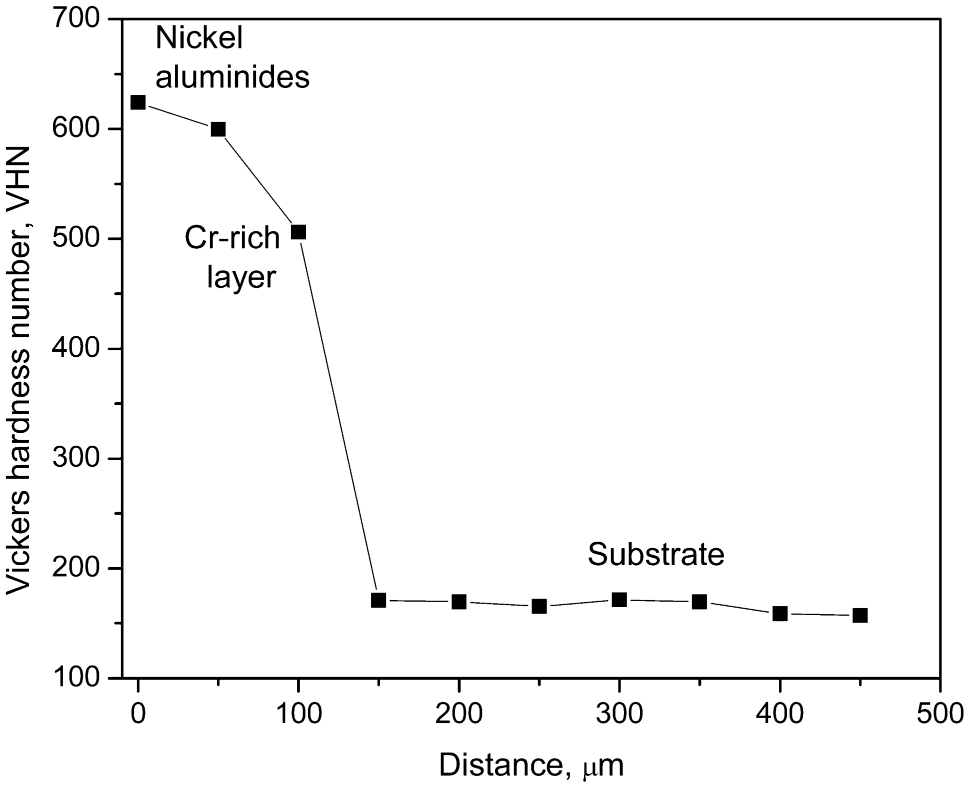

Figure 5.3 Variation of Vickers microhardness number (error (±10) along the cross-section of aluminized (2 wt.% Al) superalloy 690 specimen.

Pack aluminization conditions were different for the superalloy 690 substrates in the two cases (10 wt.% Al and 2 wt.% Al) and the methods of hardness measurement (scales) were also different, therefore, direct comparison was not possible. The consistency of hardness values in each case was checked.

5.2.2 Friction coefficient of aluminides

The coefficients of friction both static and dynamic were measured for the aluminized (10 wt.% Al) specimen of superalloy 690 at load level of 15 N with frequencies at 10, 15 and 20 Hz. The average static values were recorded in the vicinity of 0.2, 0.3 and 0.5, while dynamic values were 0.3, 0.4 and 0.4 respectively. The variation of coefficient of friction with time for the frequencies at 10, 15 and 20 Hz is shown in Figure 5.4, which is characterized by an increase in value of coefficient of friction with frequency and a fluctuation at the lowest frequency. An increase in coefficient of friction with the frequency (sliding speed) appears to have resulted from more adhesion of two counterface materials and lower is the frequency more is the time for surface roughness to stabilize [85].

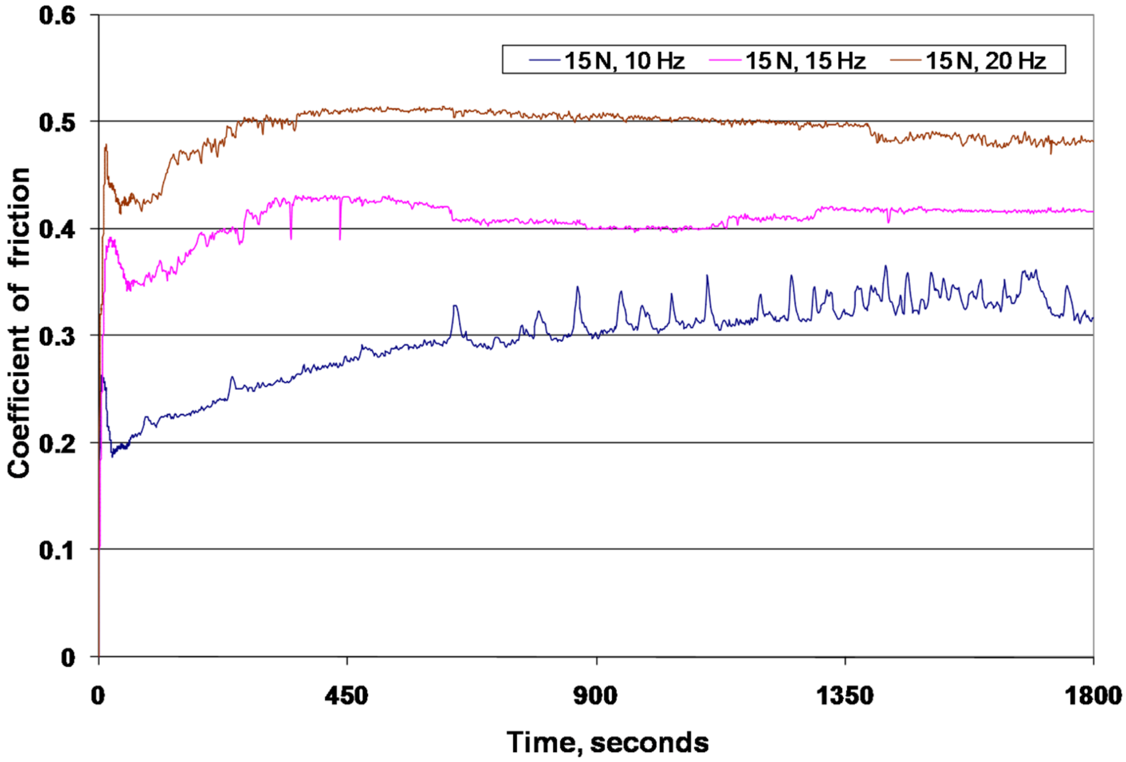

Figure 5.4 Variation of coefficient of friction with time for the aluminized (10 wt.% Al) specimen of superalloy 690 tested at 15 N load with frequencies at 10, 15 and 20 Hz.

5.2.3 Wear rate of aluminides and tungsten carbide ball

Ball wear scar diameter was measured using an optical microscope and was used to calculate its wear volume by using the formula [86],

$$V = \pi d^4/64r,$$

where V is wear volume in mm^3, d is wear scar diameter in mm and r is the ball radius in mm.

Wear volume of the scar in the aluminized (10 wt.% Al) superalloy 690 specimen was measured using 3D-profilometer and was used to calculate wear rate by using following formula,

$$\text{Wear rate} = \text{Wear volume in mm}^3 / (\text{Load in N x Sliding distance in m})$$

Wear rates of the ball and aluminized specimen were calculated for the three selected frequencies and the detailed results are shown in Table 5.1. The values of wear rate for ball and aluminized specimen have indicated a good adherent aluminide coating with an increase in wear rate with the frequency at a load level of 15 N.

Table 5.1: Results of wear tests on aluminized (10 wt.% Al) superalloy 690 sample in a dry medium using WC ball and at 15 N load with different frequencies for duration of 1800s each.

Frequency in Hz	Sliding speed in mm/s	Total sliding distance in mm	Ball scar dia. in mm	Ball wear vol. in mm^3	Wear rate of ball in mm^3/Nm	Aluminized specimen wear scar analysis				
						Length in mm	Width in mm	Depth in micron	Vol. in mm^3	Wear rate in mm^3/Nm
10	20	32175.92	0.5	0.001	1.9×10^{-6}	1.25	0.45	17.6	0.02807	5.8×10^{-5}
15	30	12997.51	0.624	0.0023	1.2×10^{-5}	1.35	0.65	7.39	0.0741	3.8×10^{-4}
20	40	16364.13	0.7	0.0037	1.5×10^{-5}	1.35	0.75	12.10	0.11402	4.6×10^{-4}

Wear scar morphology of aluminized specimen after the test at 15 N load and 10 Hz frequency is shown in Figure 5.5, while Figure 5.6 indicates the corresponding WC ball scar morphology. These two figures are optical micrographs.

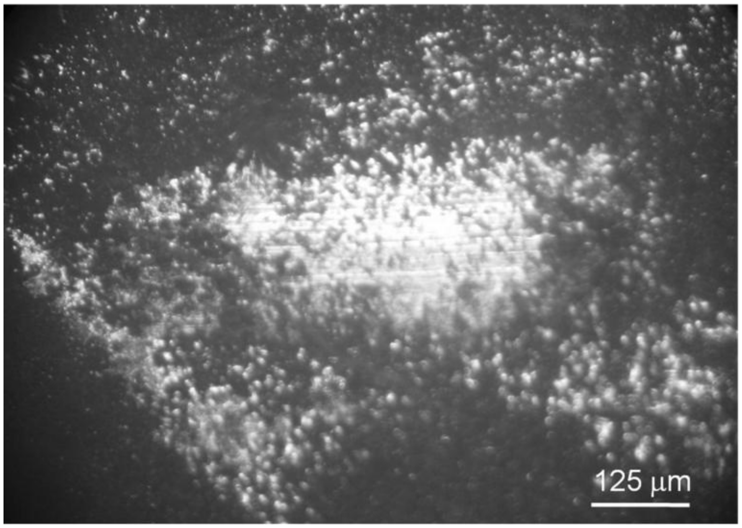

Figure 5.5 Wear scar morphology of aluminized (10 wt.%) specimen of superalloy 690 after the test at 15 N load and 10 Hz frequency.

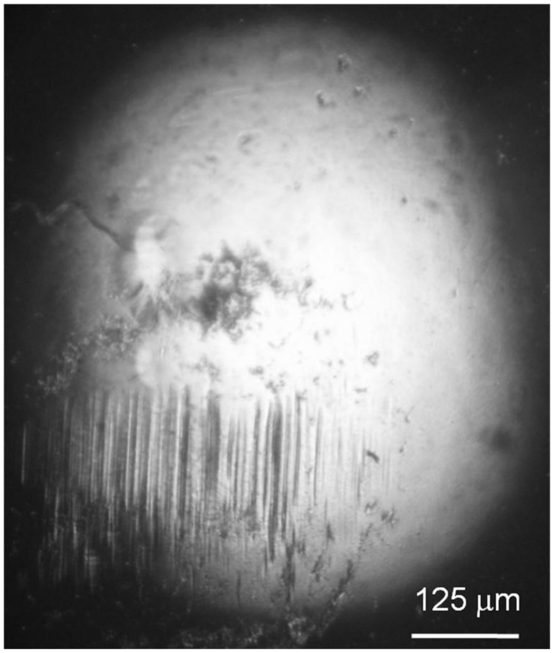

Figure 5.6 Wear scar morphology of WC ball after the test at 15 N load and 10 Hz frequency.

5.2.4 Adherence of aluminides

During scratch test (adherence test), a maximum value of friction coefficient in the vicinity of 0.4 has been obtained for the aluminized (10 wt.% Al) superalloy 690 substrate. For aluminized superalloy 690 specimens, an average penetration of 45 micron was obtained along the top surface for the load value varying between 0.9 to 20 N over a length of 3 mm indicating very good adherence of aluminide coating.

A variation of friction coefficient in the range from 0 to 0.22 has been obtained for the aluminized (10 wt.% Al) superalloy 800 substrate along the cross-section during scratch test as demonstrated in Figure 5.7. These are obtained for load values varying between 0.9 to 10 N over a length of 1 mm. Figure 5.7 depicts a low initial value of the friction coefficient and its subsequent rise to a saturation value of around 0.2 followed by a drop. The value of friction coefficient in the range of 0.2 appears to be that of the substrate, whereas low initial and final values are for the aluminide layers at the edges. A decrease in friction coefficient with the load for aluminides after a value in the vicinity of 0.2 seems to have resulted from wear debris [85]. Figure 5.8 shows the variation of penetration depth with load values along the cross-section of aluminized superalloy 800 samples. It is evident that a maximum penetration depth of around 12 micron has been obtained for the aluminized alloy substrate. It may be mentioned here that the aluminized superalloy 800 specimens used for microhardness test and scratch test were symmetrical in nature where both the ends of the cross-section contain coating layers of FeAl and Fe_2Al_5 and substrate is lying at the middle portion. In such samples during scratch testing under higher value of loading (>7 N in the present case), tip starts interacting with other side of aluminide coating as soon as it crosses the first half. Because of such effects, penetration depth shows saturation behaviour. Microscopic examination of the scratched surface with the load range of 0.9 to 10 N did not reveal any peeling off either at the aluminide or at the substrate or at aluminide/substrate interface. Figure 5.9 shows the appearances of scratched surface covering aluminide layers, substrate and their interface at the completion of scratch test. The scratch contour does not indicate any peeling off either at the substrate/aluminide interface or at the aluminide layers at the load values up to around 10 N.

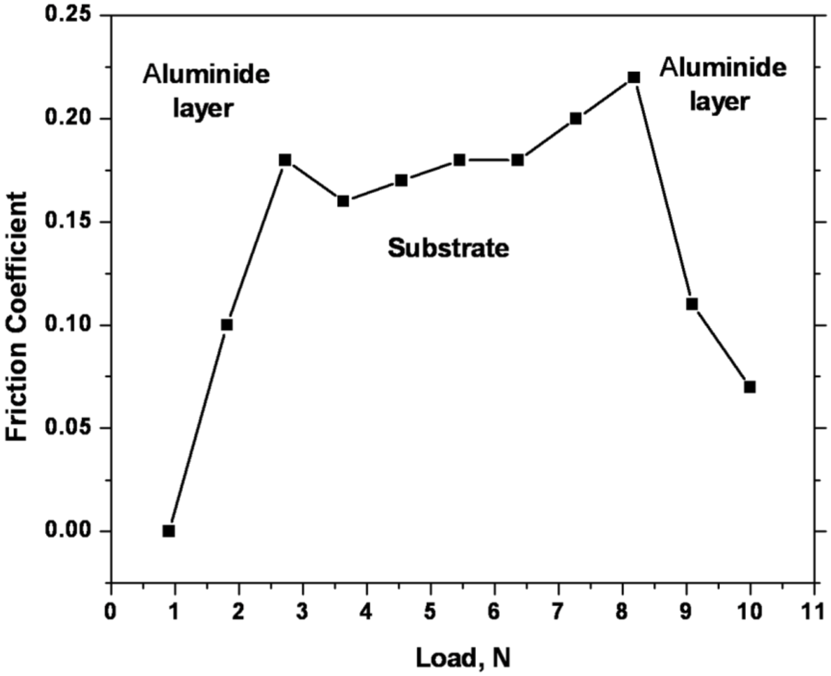

Figure 5.7 Variation of friction coefficient with load for aluminized (10 wt.% Al) superalloy 800 sample during scratch test along the cross-section.

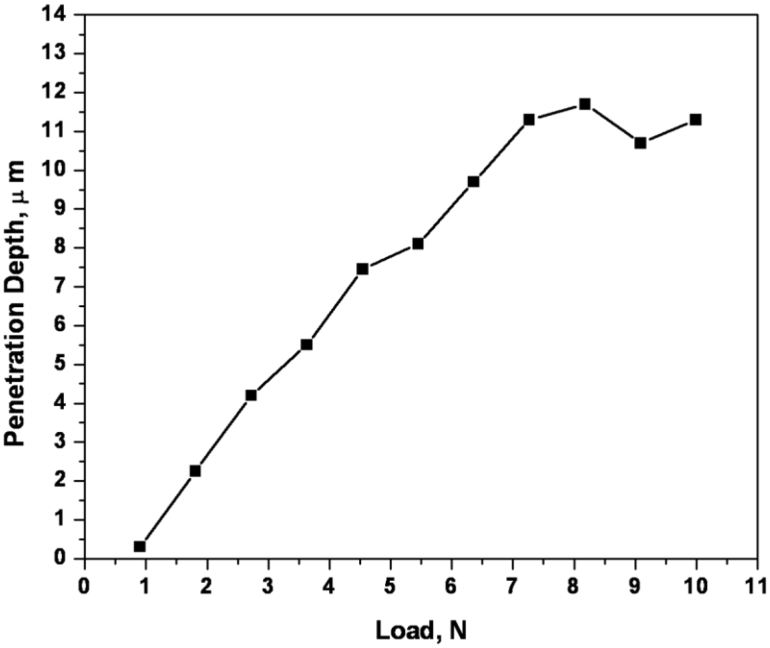

Figure 5.8 Variation of penetration depth with load for aluminized (10 wt.% Al) superalloy 800 specimen during scratch test along the cross-section.

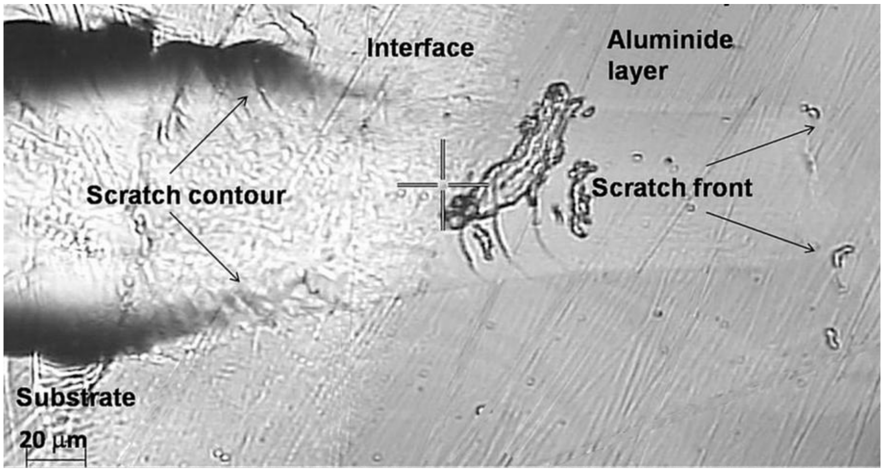

Figure 5.9 Scratched surface along the cross-section of substrate (superalloy 800), aluminide layer and their interface. The load value at cross region was recorded around 10 N.

In case of aluminized (2 wt.% Al) superalloy 690, scratch test results, which have been obtained at a scratch length of 0.4 mm along the cross-section at a constant load level of 2 N can be presented as follows. Figure 5.10 demonstrates the variation of friction coefficient with the scratch length for multilayered substrate. For the portion of multilayered coating, a large variation in friction coefficient has been noticed that could be attributed to compositional variation, whereas for the portion of alloy substrate the variation has not been appreciable. The variation of penetration depth with scratch length is shown in Figure 5.11. Multilayered portion has been found to have experienced comparatively lower penetration as compared to alloy substrate. In multilayered region, Cr-rich phase has exhibited constant penetration depth and the behaviour has been found to be consistent. Figure 5.12 demonstrates the appearance of scratched surface covering aluminides, Cr-rich phase, substrate and interfaces. The scratch contour does not indicate any peeling off at any region.

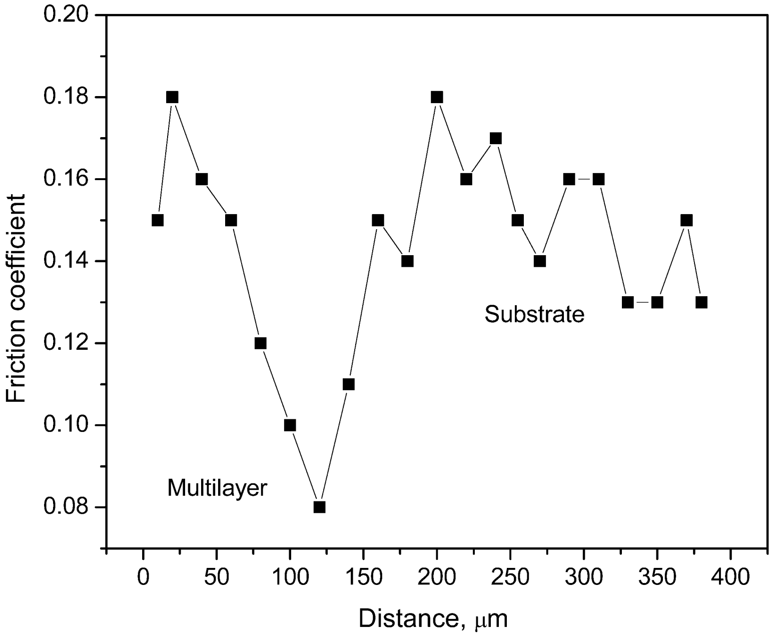

Figure 5.10 Variation of friction coefficient with load for aluminized (2 wt.% Al) superalloy 690 sample during scratch test along the cross-section.

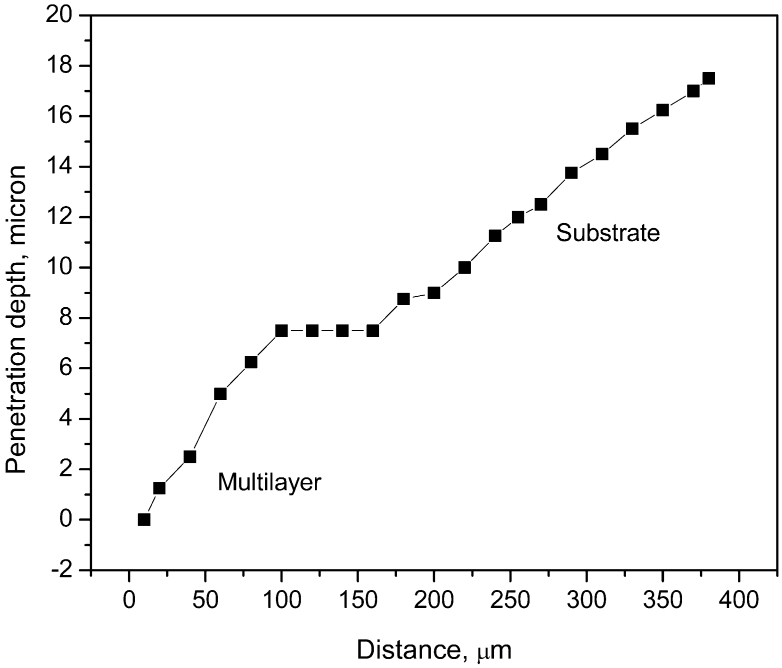

Figure 5.11 Variation of penetration depth with load for aluminized (2 wt.% Al) superalloy 690 specimen during scratch test along the cross-section.

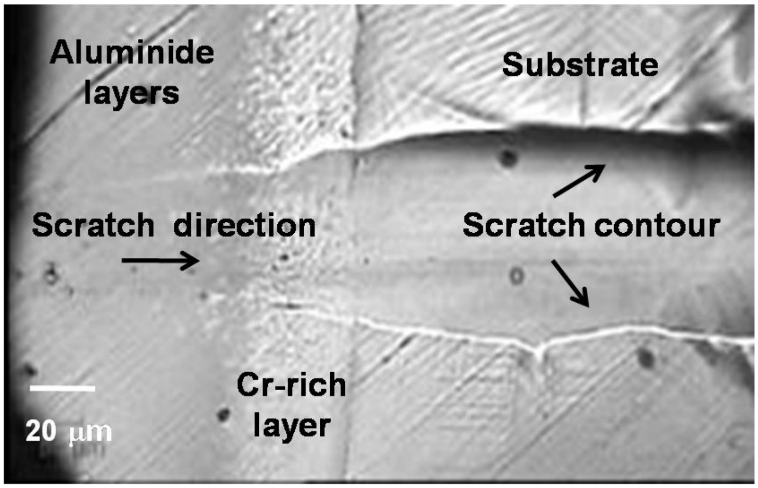

Figure 5.12 Appearance of scratched surface covering aluminides, Cr-rich layer and interfaces for aluminized (2 wt.% Al) superalloy 690.

5.2.5 Computational results on ab-initio modeling of Ni(Cr)/NiAl interface structure

Fully converged calculations on the bulk structures yielded lattice parameters of Ni as 3.5171 Å, Al as 4.0523 Å and NiAl as 2.8931Å, in very good agreement with the experimental values of 3.524 Å, 4.0488 Å and 2.8864 Å respectively [87]. Our spin-polarized calculations yielded net magnetic moment of 0.627 Bohr-Magneton for Ni (fcc) and a negligibly small value for NiAl. The value of magnetic moment for Ni appears to be in agreement with that of reported by Ernst et. al [88]. The energy of formation for bulk NiAl was computed as -0.662 eV/atom as compared to experimental value of -0.614 eV/atom [87] using calculated values of cohesive energies of -10.542, -5.478 and -3.740 eV for NiAl (B2), Ni (fcc) and Al (fcc), respectively. Figure 5.13 a, b and c show unrelaxed isolated Ni(111) substrate slab, unrelaxed isolated NiAl(110) coating slab and relaxed Ni(111)/NiAl(110) interface slab respectively. The results of ab-initio simulations on isolated Ni(111) and NiAl(110) surface slabs and Ni(111)/NiAl(110) interface slab are given in Table 5.2. Our spin-polarized calculations gave net magnetic moment of 0.634 Bohr-Magneton per atom, and 0.451 BM per atom for Ni(111) and the interface slab respectively. The NiAl(110) slab exhibited a negligibly small net magnetic moment. Figure 5.14a and b show site- and angular momentum-projected partial density of states combining up-spin and down-spin components, for Ni and Al atoms in the bulk NiAl structure and at the interface, respectively. For the interface plane where 2 Ni atoms have been replaced by 2 Cr atoms and 1 Cr atom replaces 1 Ni atom below the interface plane, the ideal work of adhesion for the interface has been calculated as 3523.57 mJ/m^2 that is slightly lower than that with pure Ni substrate as shown in Table 5.2. The relaxed structure also shows that Cr atoms at the interface tend to relax by slightly moving inward away from the interface plane and it is shown in Figure 5.15.

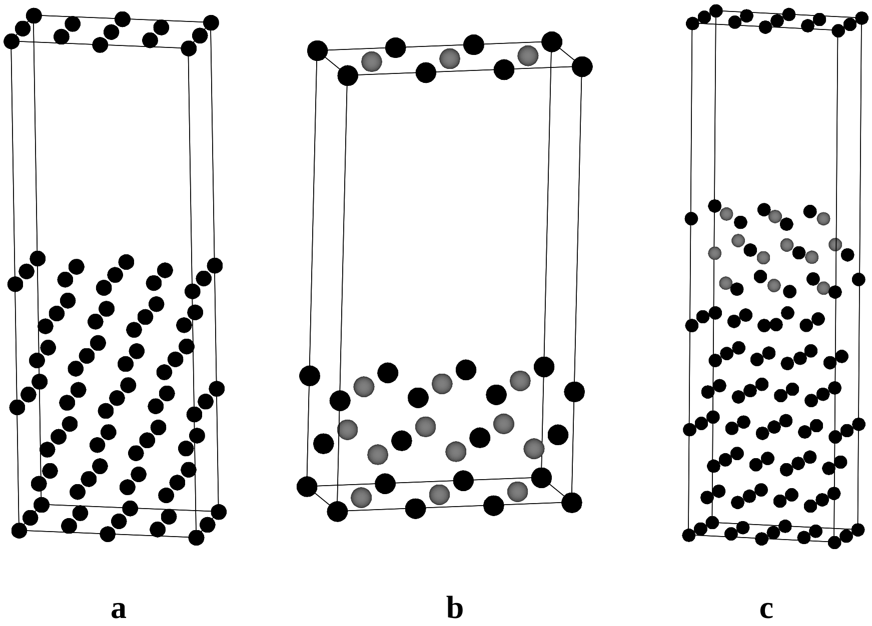

Figure 5.13 (a) Unrelaxed isolated Ni(111) substrate slab, (b) unrelaxed isolated NiAl(110) coating slab and (c) relaxed Ni(111)/NiAl(110) interface slab. The black spheres represent Ni atoms and gray spheres represent Al atoms.

Table 5.2: Calculated surface and interface energies and ideal work of adhesion for unrelaxed and fully relaxed slabs.

Slab	Unrelaxed slab		Relaxed slab	
	Energy, eV	W^{ad}(ideal), mJ/m^2	Energy, eV	W^{ad}(ideal), mJ/m^2
Ni(111)	-292.441	-	-292.443	-
NiAl(110)	-87.464	-	-87.80	-
Ni(111)/NiAl(110)	-382.867	1106.77	-390.092	3683.58

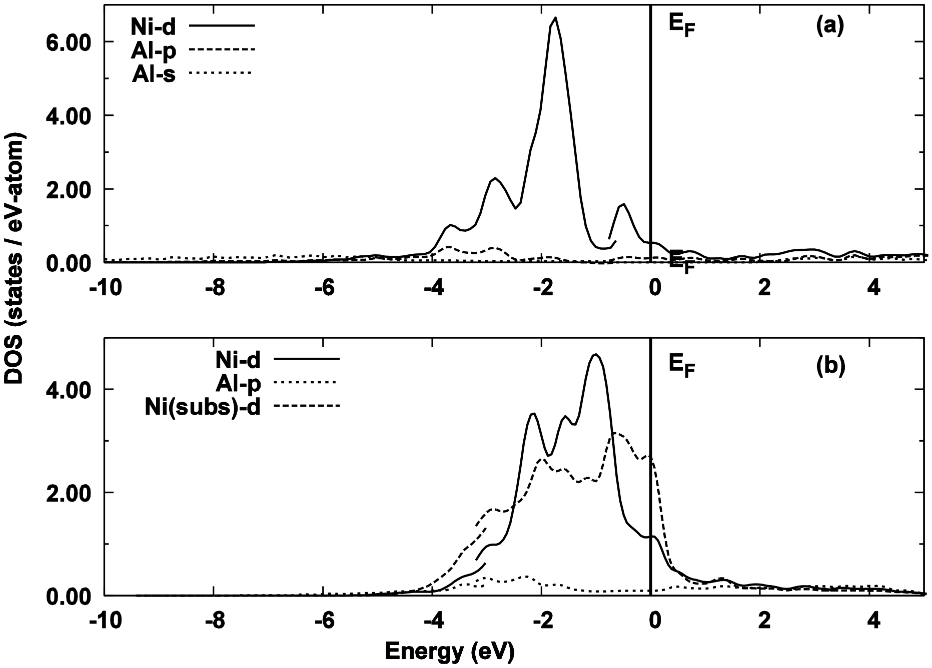

Figure 5.14 The site- and angular momentum-projected partial density of states for (a) bulk NiAl and (b) Ni(111)/NiAl(110) interface. In (b) the 'Ni' atom belongs to the one in the coating and the 'Ni(subs)' atom belongs to the one in the substrate at the interface. The density of states for up-spin and down-spin contributions has been combined.

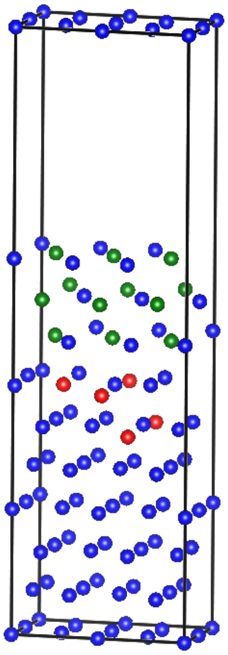

Figure 5.15 Cr-doped relaxed Ni(111)/NiAl(110) interface slab where 2 Ni atoms at the interface plane replaced by 2 Cr atoms and 1 Cr atom replaces 1 Ni atom below the interface plane. The blue spheres represent Ni atoms, green spheres represent Al atoms and red spheres represent Cr atoms.

5.3 Discussion

In the present study on aluminized (10 wt.% Al) superalloy 690 substrate, microhardness tests along the cross-section indicated a variation of KHN in the range of 225 to 1142 indicating aluminide layer formation as revealed by SEM and EPMA. Since aluminides are very hard, substantially high microhardness has been noticed at the edges of the cross-section, consisting of aluminide layers, as compared to substrate. The results appear to be consistent with the microstructure of aluminized alloy substrate. For aluminized (10 wt.% Al) superalloy 800 substrate, a variation of microhardness value in the range from 213 to 1098 KHN has been obtained for the alloy substrate along the cross-section. Substantially high microhardness values for the aluminide layers as compared to substrate have been recorded. Moderate hardness values in the region between these two indicate a decrease in microhardness value with the decrease in Al-content of the aluminide. These results are quite consistent with microstructures of multilayer. In case of superalloy 690 substrate aluminized with 2 wt.% Al, similar consistent behaviour has been noticed. Sensitivity of Knoop microhardness measurements has been observed by Maupin et al. [89] who have made Knoop and Vickers microhardness measurements of wear surface for ordered Fe_3Al alloys before and after abrasive wear testing. The authors [89] have reported that in each case, there has been a trend towards increased hardness with distance traveled over the abrasive and the effect has been found to be more pronounced in the case of low load Knoop microhardness measurements. This near wear surface region phenomenon has been explained by them in terms of dynamic recrystallization.

Wear tests on aluminized (10 wt.% Al) superalloy 690 specimen with WC ball at a load level of 15 N with frequencies at 10, 15, 20 Hz have indicated that for ball, the wear rate has been 1.9×10^{-6}, 1.2×10^{-5} and 1.5×10^{-5} mm^3/Nm, whereas the same has been 5.8×10^{-5}, 3.8×10^{-4} and 4.6×10^{-4} mm^3/Nm respectively for the aluminized specimen indicating good adherent surface coating. The coefficient of friction, the static ones have been obtained in the vicinity of 0.2, 0.3 and 0.5, while dynamic ones have been 0.3, 0.4 and 0.4 respectively. Sierra and Vázquez [90] have used a pin-on-disk tribometer and NiAl coatings have been tested against Al_2O_3 and WC-Co balls. The friction coefficients of NiAl/Al_2O_3 and NiAl/WC couples have been obtained as 0.36 and 0.37. It is indicated from their [90] results that NiAl coatings or coatings composed mainly of NiAl possess high wear resistance. According to the investigators [90], NiAl undergoes a third-body abrasion on dry sliding against Al_2O_3 or WC-Co balls. The third-body particles are NiAl particles detached from the surface and get oxidized because of heat generation due to friction. It is further proposed that the oxidized particles those remain between the ball and the coating result in wearing of the coating [90]. Similar role of third-body particles on wear of Ni/Cu multilayer has also been discussed by Ghosh et al. [91]. Sliding wear behaviour of hot pressed nickel aluminides has been reported by some researchers [92]. NiAl base intermetallics containing 55 at.% Ni or greater have been found to exhibit wear rates those are lower than the 440C martensitic stainless steel (reference material). According to the authors [92], although sub-surface deformation has been minimal for the near-stoichiometric NiAl intermetallics, the wear proceeds by the formation of voids and cracks beneath the wear scar and the generation of plate-like wear debris. It is, therefore, indicated that the wear and friction tests results obtained for aluminized superalloy 690 specimen in the present investigation are in accordance with the results of other investigators [90,92] and are consistent with microhardness measurements, microstructures and microanalyses of aluminides. The third-body particles appear to have played some role in wear of aluminized superalloy 690 specimen and WC ball. An increase in coefficient of friction as well as wear rate of specimen and ball with the frequency is related to their wear volumes as seen in the present study.

In the present investigation, the scratch test of aluminized (10 wt.% Al) superalloy 800 specimen along the cross-section has indicated good adherence of aluminide layers in the load level between 0.9 and 10 N showing a maximum penetration in the vicinity of only 12 μm and absence of peeling off either at aluminide layers or at layer/substrate interfaces. A maximum value of coefficient of friction for the substrate has been obtained as 0.22, whereas the same has been found to be much lower for the aluminide layers. For aluminized (10 wt.% Al) superalloy 690 specimen, an average penetration of 45 micron was obtained along the top surface for the load value varying between 0.9 to 20 N over a length of 3 mm indicating very good adherence of aluminide coating. A maximum value of friction coefficient in the vicinity 0.4 has been obtained.

In case of scratch test of aluminized (2 wt.% Al) superalloy 690 substrate along the cross-section, a comparatively lower friction coefficient as well as penetration depth of multilayer as compared to that of alloy substrate has been noticed. In addition, no peeling off either at the multilayer or at layer/substrate interface has been observed, which is indicative of good adherence of multilayer. Xia et al. [93] have performed nano-scratch tests at room temperature on Fe-40 at.%Al in as-received condition. Five different loads those were 5, 10, 20, 30 and 100 mN were chosen for scratching with a speed of 300 nm/s for a total length of 200 μm. The authors have noticed that the scratch depth has increased with load. A maximum scratch depth in the vicinity of 350 nm has been obtained with the maximum load value of 100 mN for as-received alloy. Kumar et al. [94] have carried out scratch tests on ball-milled and plasma-processed Fe-Al thermal spray coatings at load levels of 30 N and 90 N with a scratch velocity of 0.1 mm/s over a scratch length of 12 mm. Coefficient of friction measured by scratch tester has been obtained [94] in the range of 0.19 to 0.28. It is, therefore, indicated that the scratch test results obtained for aluminized alloy specimens in the present study are in accordance with the results of other investigators [93,94].

The results of ab-initio simulations on Ni(111)/NiAl(110) interface are given in Table 5.2. Comparison of unrelaxed and relaxed slab energies shows that the substrate and coating slabs do not exhibit much relaxations. The interface slab, where the atoms in the coating and only top 3 mono-layers of Ni substrate are relaxed, exhibit much larger relaxations at the interface. The interface gap of 0.0745 Å is found to be minimum between an Al atom in the coating and a Ni atom in the substrate. The Al atoms in the interface layer exhibit a relative net vertical displacement of 0.0021 Å towards the substrate as compared to the Ni atoms in the coating. The ideal work of adhesion (W^{ad} (ideal)), which can be defined [95,96] as the energy needed (per unit area) to reversibly separate an interface into two free surfaces, ignoring plastic and diffusional degrees of freedom, calculated as

$$W^{\mathrm{ad}}\ (\mathrm{ideal}) = (E^{substrate} + E^{coating} - E^{interface}) / A$$

where $E^{substrate}$, $E^{coating}$ and $E^{interface}$ are the energies of the isolated substrate, coating and interface slabs, respectively and '*A*' is the area of the interface. The W^{ad} (ideal) for the fully relaxed interface is calculated to be 3683.58 mJ/m^2 (Table 5.2), which is quite high [95,96] and is thus indicative of very good adhesion at the interface. Almost equivalent work of adhesion (3523.57 mJ/m^2) shows that Cr atoms at the interface do not affect much the interfacial adhesion. This is along the line of the experimental results of scratch test that indicates good adherence of multilayer and interface as discussed above. As mentioned earlier, this value is the lowest bound to the W^{ad} (ideal), as the interface is formed between two most stable surfaces. It can be seen from Figure 5.14a that in the bulk NiAl, the covalent mixing of Ni *d* and Al *p* states in the lower energy part of the valence band is responsible for its stability; while at the interface (Figure 5.14b), one can observe a covalent bonding component arising from mixing of Ni *d* and Al *p* states in the lower energy part of the valence band and a strong metallic bonding component arising from Ni *d* Ni *d* interactions imparting high adhesion strength at the interface.

5.4 Summary

Properties of aluminides formed on substrates of superalloys 690 and 800 by using pack aluminization process with high Al-containing (10 wt.% Al) pack at 1273 K in argon atmosphere have been discussed in detail in the present work that has focused on development of materials related to high temperature applications. For aluminized superalloy 690 substrates, the properties those have been evaluated are microhardness along the cross-section while friction coefficient, wear rate and adherence along the topmost surface. In case of superalloy 800 specimens, those have been microhardness, friction coefficient and adherence along the cross-section. Besides this, similar measurements have been done on aluminides that formed on superalloy 690 substrates with low Al-containing pack (2 wt.% Al). All these findings of the present work have been tried to justify from the viewpoint of existing microstructure and compared with the results of other researchers. Based on experimentation and understanding as well as ab-initio modeling of Ni(Cr)/NiAl interface structure, a few salient points of this investigation can be summarized as follows

(a) Superalloy 690 substrates pack aluminized at 1273 K with high Al-containing pack (10 wt.% Al) indicates a variation of microhardness along the cross section showing high hardness values of the aluminides. Wear tests of aluminized alloy sample at load level of 15 N with different frequencies show good adherence of surface coating.

(b) For superalloy 690 specimens pack aluminized with low-Al containing pack (2 wt.% Al), an increase in microhardness with Al-content has been noticed for multilayer (mainly aluminides). Scratch test (adherence test) at a constant load level of 2 N along the cross-section of aluminized sample indicates good adherence of multilayer.

(c) In case of superalloy 800 substrates pack aluminized with 10 wt.% Al, microhardness of aluminide has been found to increase with Al-content. Scratch test along the cross-section of aluminized specimen at load levels ranging from 0.9 to 10 N shows good adherence of aluminide coatings.

(d) Based on the computational results and understanding, a few interesting points of ab-initio modeling can be stated as

(i) First-principle calculations on Ni(111)/NiAl(110) interface has indicated strong adhesion.

(ii) Ideal work of adhesion, W^{ad} (ideal) = 3684 mJ/m^2 ; lowest bound value.

(iii) Strong metallic Ni *d* Ni *d* interaction and covalent Ni *d* Al *p* mixing of states give rise to strong adhesion at the Ni(111)/NiAl(110) interface.

(iv) For Cr-doped interface, Ideal work of adhesion, W^{ad} (ideal) = 3524 mJ/m^2 that is slightly lower as compared to that with pure Ni substrate.

CHAPTER 6: OXIDATION BEHAVIOUR OF ALUMINIZED SUPERALLOYS AND EVALUATION OF STABILITY OF ALUMINIZED AND OXIDIZED SUPERALLOY 690

6.1 Background

The choice of Ni-Cr based alloys for vitrification furnaces was due to their ability to form a continuous, thick Cr_2O_3 layer under favourable condition that passivates the alloys leading to low corrosion rate in molten glass [97-102]. However, due to formation of thick, continuous Cr_2O_3 layer at the interface, the alloy near the said region has been reported to be depleted in Cr [8,9,103,104]. Besides this, flaking off continuous Cr-oxide layer can occur due to development of compressive stress because of its high thickness and convective motion within borosilicate melt pool adjacent to the region. These phenomena can lead to leaching out of Cr from the alloys ultimately leading to premature failure of metallic melter pot furnaces. Therefore, it is of prime importance to develop effective diffusion barrier coatings on the alloys so that the life of the components can be extended. Aluminides are found to be very effective in functioning as diffusion barrier coatings as they form a protective layer of Al_2O_3 when exposed to high temperature [65-67,105,106]. At temperatures above 1273 K and in many aggressive environments with low oxygen partial pressures, $\alpha-Al_2O_3$ is reported to be more protective than Cr_2O_3 scale [107]. Interaction between alumina substrate and borosilicate melt at temperatures from 1123 K to 1223 K indicates formation of nonporous interdiffusion layer at alumina/glass interface [108]. For high nickel moderate chromium containing Fe-based superalloy 800, a few studies [10-12] have focused on development of diffusion barrier coatings. Miller et al. [10] have used different Cr-Al masteralloys and alkali halide vapours to form an interdiffusion zone enriched in Cr and Al for Incoloy 800 but have not succeeded to achieve the desired one.

Investigation by Haanappel et al. [11] has indicated that aluminide coatings formed on Incoloy 800H can provide resistance to sulphidation up to 823 K. Vokál et al. [12] have reported the formation of (Ni,Fe)Al and Fe_2Al_5 phases on top surface of Alloy 800 after pack cementation and have noticed degradation of (Ni,Fe)Al coating after the exposure of coated specimens in 50 mol% KCl + 50 mol% K_2SO_4 at 923 K. In view of development of diffusion barrier coatings on superalloys 690 and 800 substrates for high temperature applications, a study on evaluation of thermal oxidation resistance of aluminides formed on these superalloys has been undertaken. This is followed by evaluation of stability of thermally oxidized aluminides in sodium borosilicate melt at 1248 K. As the said environment is relevant to application related issues of superalloy 690, no exposure was performed with aluminized and thermally oxidized superalloy 800 substrates.

6.2 Results

6.2.1 Thermal oxidation resistance of aluminides in air at 1273K

Aluminized (10 wt.% Al) superalloys 690 and 800 substrates subjected to thermal oxidation in air at 1273 K for a total period of 4 hours have indicated good thermal oxidation resistance. For aluminized superalloy 690 substrates, an average weight gain of 0.7 mg has been noticed for the specimens in the first two hours of thermal oxidation treatment, while no change has been observed for the later period. In case of aluminized superalloy 800 substrates, an average weight gain of 0.45 mg has been noticed for the samples for the first two hours of thermal oxidation treatment, whereas no change has been recorded for the later period. In case of aluminized (2 wt.% Al) superalloy 690, the results of thermal oxidation are shown in Figure 6.1 in which average weight gain (mg/cm^2) of the specimens is plotted against oxidation period. The weight gains have been found to increase up to 6 hours, while no gain was recorded for the last 2 hours indicating good oxidation resistance of aluminized specimens with the formation of thin layer. It is to be mentioned that the average (of weight gain) has been taken on atleast 2-3 specimens and the precision of the balance used has been up to 5th decimal place. Figure 6.2a-b demonstrates the oxidation behaviour of bare superalloy substrate 690 and 800 respectively. It is evident from these results that the thermal oxidation resistance of aluminides formed on either superalloy 690 substrate or superalloy 800 substrate is superior to their respective bare alloy substrate.

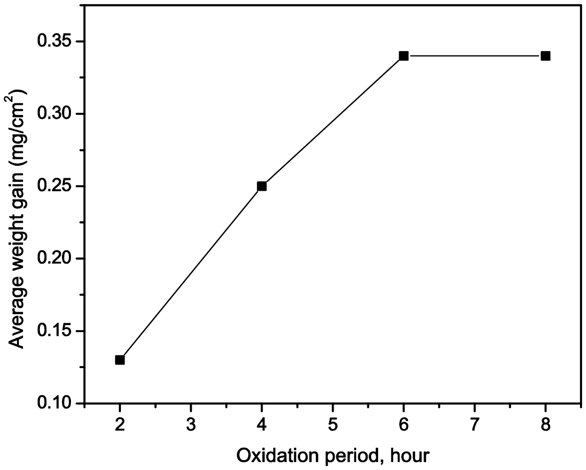

Figure 6.1 Variation of weight gain with oxidation period for aluminized (2 wt.% Al) superalloy 690.

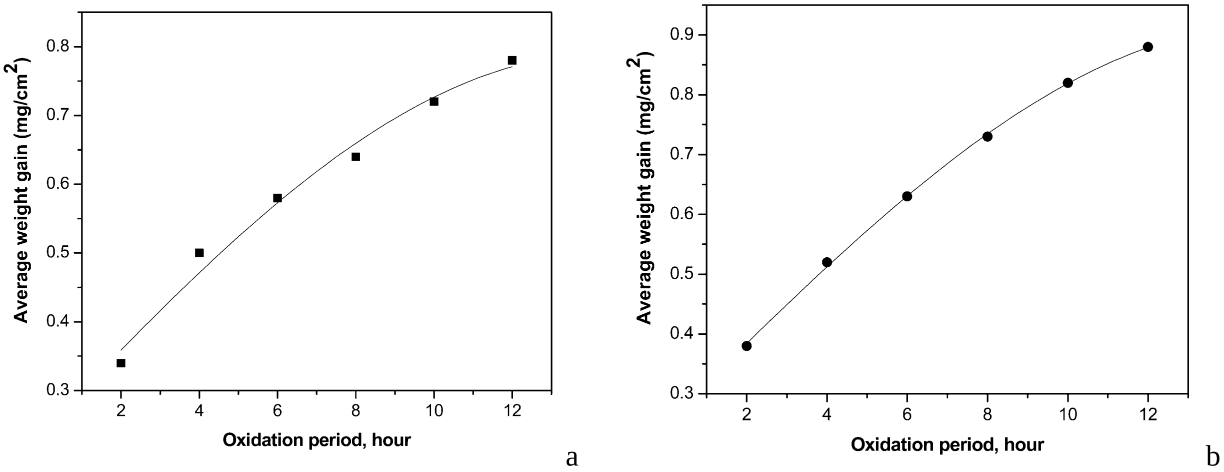

Figure 6.2 Variation of weight gain with oxidation period for bare (a) superalloy 690 and (b) superalloy 800 substrates.

6.2.2 Type of oxide layer formed on nickel aluminides

SEM examination with EDXS analysis along the cross-section of aluminized (10 wt.% Al) and thermally oxidized superalloy 690 substrate indicated presence of continuous, interdiffusion layer of almost uniform thickness adjacent to substrate followed by (NiCr)Al type layer, (NiCr)Al + Cr_5Al_8 type layers and Al_2O_3 layer. As compared to the initial microstructure, there is conversion of Ni_2Al_3 type phase into (NiCr)Al type phase during oxidation that appears to have taken place by inward diffusion of Al and slight composition change. Figure 6.2 clearly reveals substrate and different aluminides, whereas Figure 6.3 demonstrates their corresponding compositions. The formation of about 2 μm thick Al_2O_3 layer on uppermost surface along with its EDXS analysis is shown separately and clearly in Figure 6.4.

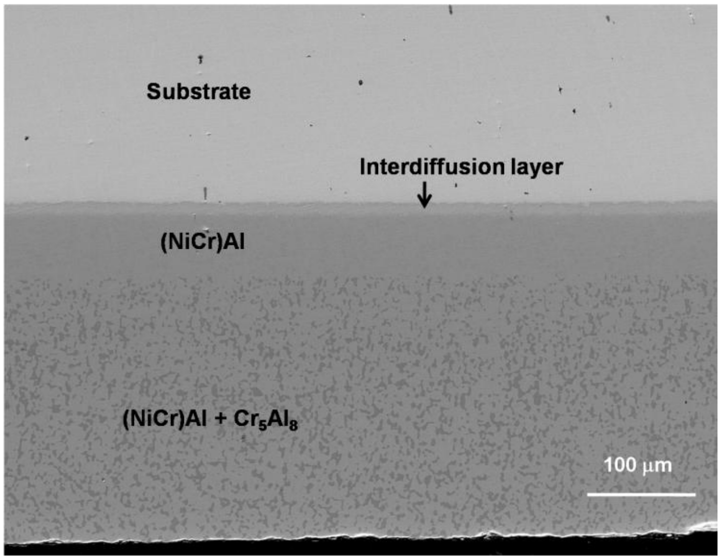

Figure 6.3 Aluminized (10 wt.% Al) and thermally oxidized (1273 K for 4 hours in air) superalloy 690 sample revealing different layers along the cross-section.

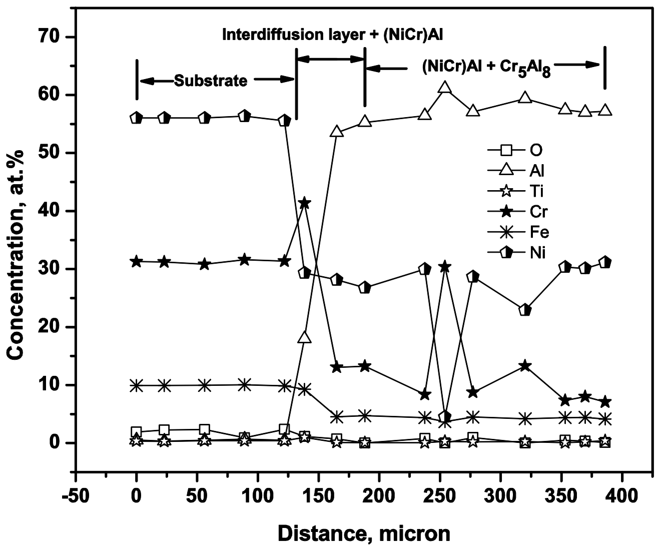

Figure 6.4 EDXS analysis of aluminized and thermally oxidized superalloy 690 specimen along the cross-section as shown in Figure 6.3. Different layers are marked.

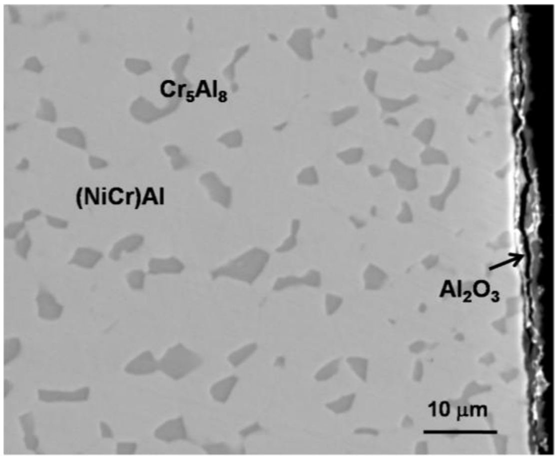

EDXS point analysis of thermally grown oxide

Elements in at.%				
O	Al	Cr	Fe	Ni
59.86	35.30	1.57	0.89	2.38
59.56	37.18	0.94	0.51	1.80

Figure 6.5 SEM micrograph revealing formation of Al_2O_3 type layer on aluminides for the aluminized (10 wt.% Al) and thermally oxidized (1273 K for 4 hours in air) superalloy 690 specimen. EDXS point analyses of oxide are also shown.

For aluminized (2 wt.% Al) and thermally oxidized (1273 K for 8 hours in air) superalloy 690 specimen, XRD analysis has revealed the presence of α-Al_2O_3 phase along with predominantly NiAl type phase as demonstrated in Figure 6.5.

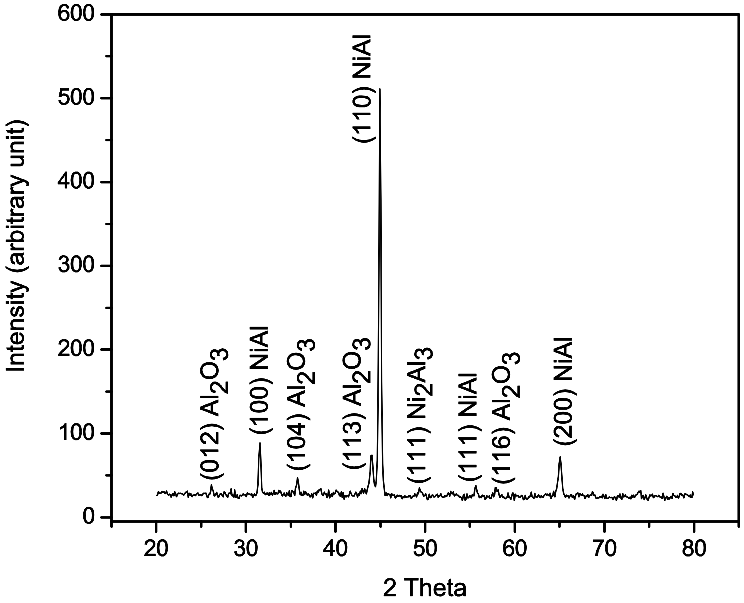

Figure 6.6 X-ray diffractogram of aluminized (2 wt.% Al) superalloy 690 after thermal oxidation of 1273 K for 8 hours in air revealing presence of Al_2O_3 phase along with predominantly NiAl type phase.

6.2.3 Stability of pre-oxidized nickel aluminides in sodium borosilicate melt

Bare alloy substrate exposed in sodium borosilicate melt at 1248 K for 192 hours indicated oxidation and formation of a continuous, thick Cr_2O_3 layer at the substrate/glass interface. Figure 6.6 shows SEM micrograph along the cross-section of bare substrate with adhered glass and Figure 6.7 illustrates its corresponding EDXS analysis.

For aluminized (10 wt.% Al) and thermally oxidized (1273 K for 4 hours in air) specimen of superalloy 690, a good stability of aluminides with Al_2O_3 layer was noticed after the exposure of 192 hours in sodium borosilicate melt at 1248 K without any phase formation at the coating/glass interface as revealed by SEM with EDXS analysis along the cross-section of aluminide coated sample with adhered glass phase. However, some Al enrichment in glass phase adjacent to interface was noticed. There was no significant enrichment of Ni or Cr in glass phase near the interface region. Due to exclusion of B in glass phase for both the cases during quantitative EDXS analysis, some overestimation of elements was noticed. These elements are primarily Si, Al and O. Some changes of compositions of aluminides have been observed after prolonged exposure in borosilicate melt. These are illustrated in Figures 6.8 and 6.9 respectively marking various layers. Interdiffusion zone, (NiCr)Al type layer and (NiCr)Al + Cr_5Al_8 type layers those were present in aluminized and thermally oxidized specimen (Figures 6.2 and 6.3) have been found to have modified to Ni-rich NiAl type layer and Al-rich NiAl + CrAl type layers with an enrichment of Ni and reduction of Cr and Al after prolonged exposure in borosilicate melt as is evident from Figures 6.8 and 6.9. Figure 6.10 demonstrates X-ray diffractogram of aluminized, thermally oxidized and exposed (in borosilicate melt at 1248 K for 192 hours) specimen indicating existence of Al_2O_3 type phase along with NiAl and Cr_5Al_8 type phases. These XRD results on aluminides are found to be consistent with SEM-EDXS analysis.

For aluminized (2 wt.% Al) superalloy 690 substrates thermally oxidized at 1273 K for 8 hours in air and exposed in sodium borosilicate melt at 1248 K for a total period of 192 hours, the results are also encouraging. Existence of aluminide coating with the formation of some phases comprising Al, Ni, O and Cr at the glass/coating interface was noticed for thermally oxidized NiAl type layer after exposure in borosilicate melt as shown in Figure 6.11.

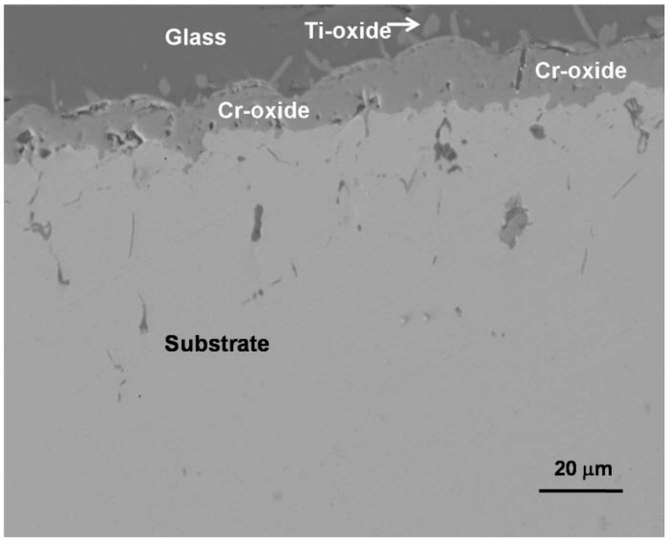

Figure 6.7 SEM micrograph along the cross-section of bare superalloy 690 substrate with adhered glass (exposed in sodium borosilicate melt) revealing formation of a continuous, thick Cr-oxide (Cr_2O_3 type) layer at the glass/alloy interface. Ti-oxide in glass phase is also noticed.

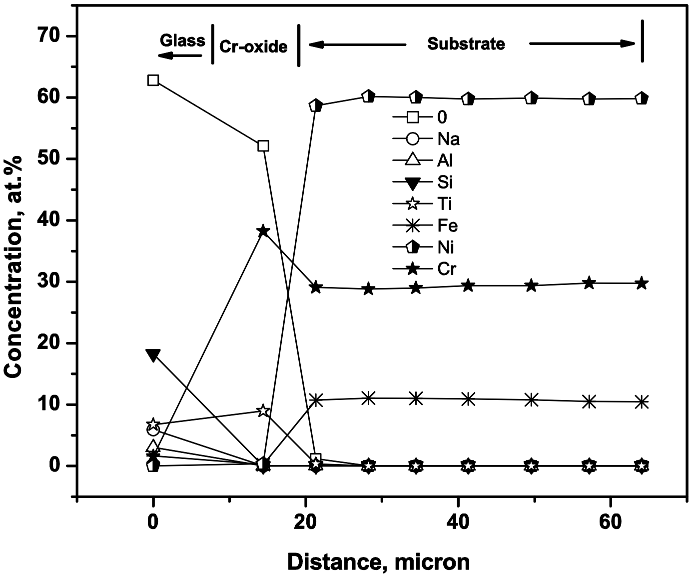

Figure 6.8 EDXS analysis of bare alloy substrate with adhered glass along the cross-section as shown in Figure 6.7. Different phases are marked.

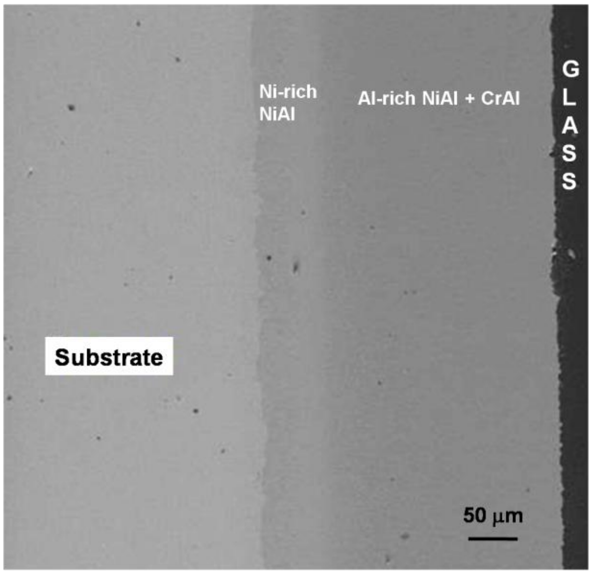

Figure 6.9 SEM micrograph along the cross-section of aluminized (10 wt.% Al), thermally oxidized superalloy 690 substrate with adhered glass (exposed in sodium borosilicate melt) revealing aluminides along with good stability of coating without any phase formation at the coating/glass interface.

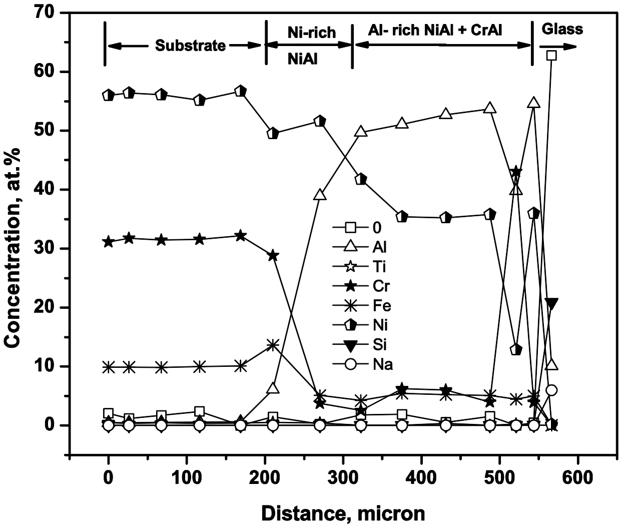

Figure 6.10 EDXS analysis of the specimen along the cross-section as shown in Figure 6.9. Various layers are marked along with the glass phase.

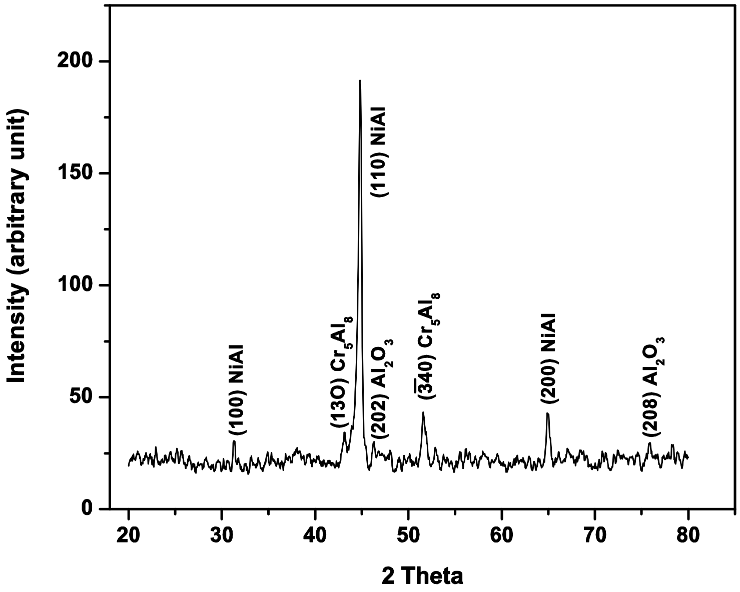

Figure 6.11 X-ray diffractogram of aluminized (10 wt.% Al), thermally oxidized and exposed (in borosilicate melt) sample of superalloy 690 indicating existence of Al_2O_3 type phase along with NiAl and Cr_5Al_8 type phases.

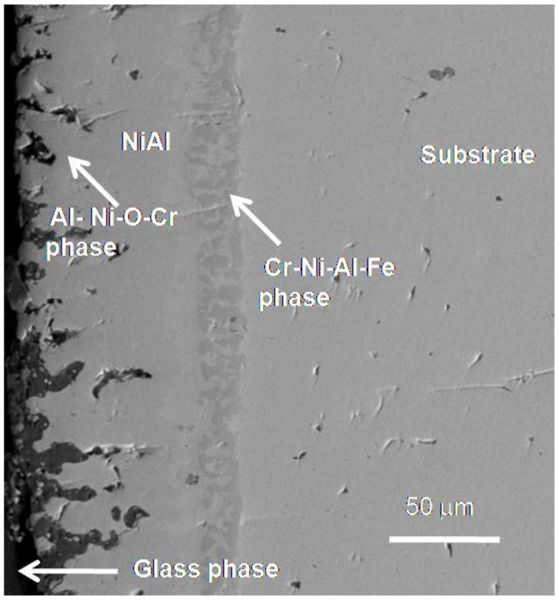

Figure 6.12 Existence of NiAl type layer along with formation of some phases comprising Al, Ni, O and Cr at the glass/coating interface for aluminized (2 wt.% Al) superalloy 690 sample thermally oxidized and exposed in borosilicate melt.

6.3 Discussion

Superalloys 690 and 800 substrates aluminized with 10 wt.% Al have shown very little weight gain after thermal oxidation at 1273 K indicating their good oxidation resistance. SEM with EDXS analysis on superalloy 690 specimens has revealed that the surface oxide layer formed at 1273 K is of Al_2O_3 type known as diffusion barrier coating. Superalloy 690 substrates aluminized with 2 wt.% Al have exhibited good oxidation resistance with the formation of a thin oxide layer. Bare superalloy substrates have also shown good oxidation resistance in air at 1273 K. It is worth mentioning in this context that the bare substrates of the superalloys reported to possess good cyclic oxidation resistance at 1368 K in air [4]. Although the oxidation behaviour of the aluminized samples resembles to some extent logarithmic behaviour that is very much desirable for high temperature applications, the behaviour cannot be emphasized as it is generally observed with thin oxides at low temperatures [109]. The oxide that formed on aluminized (2 wt.% Al) superalloy 690 substrate is of α-Al_2O_3 type as is evident from XRD analysis that reveals the presence of predominantly NiAl type phase along with α-Al_2O_3 phase. An $\alpha-Al_2O_3$ type layer has been reported to have formed on NiAl and NiAl-Cr alloys after an exposure of about 300 hours in oxygen + helium atmosphere at 1273 K [110]. During oxidation of $\beta-$NiAl coating prepared on Ni-based superalloy at 1223 K in air, most of $\theta-Al_2O_3$ grains have been found to have transformed into $\alpha-Al_2O_3$ after 3 hours of oxidation [111]. Choi et al. [41] have studied phase transformation of thermally grown oxide layer on $\beta-$NiAl by performing oxidation at 1373 K for 6 hours in air. They have observed that the oxide layer is primarily composed of $\alpha-Al_2O_3$ containing very little trace of θ-Al_2O_3. It is, therefore, evident that the formation of Al_2O_3 type layer on nickel aluminides as noticed in the present study is in agreement with the findings of other investigators [41,110,111].

For superalloy 690 substrates aluminized with 10 wt. % Al, a good stability of thermally oxidized aluminide coating was observed in the present study after the exposure of 192 hours in sodium borosilicate melt at 1248 K. No phase formation was noticed at the coating/glass interface. However, some Al enrichment in glass phase adjacent to interface was noticed without any significant Ni or Cr enrichment. In case of aluminized (2 wt.% Al) superalloy 690 substrates thermally oxidized and exposed in sodium borosilicate melt, the results are also encouraging. The stability of aluminide coating with the formation of some phases comprising Al, Ni, O and Cr at the glass/coating interface was observed after exposure in borosilicate melt. SEM-EDXS analysis of bare substrate exposed under similar experimental condition indicated oxidation of alloy and formation of a continuous, thick Cr_2O_3 layer at the bare substrate/glass interface. Reaction between borosilicate melt and Alloy 690 tube at 1223 K for 24 hours in air has been examined by some investigators [8]. The authors [8] have reported depletion of Cr in alloy specimen near the reacting interface and formation of Cr-rich products on the glass side of the interface that has been found to be depleted in Si and enriched in Na. Sengupta et al. [9,103,112] have also noticed formation of Cr_2O_3 type layer, needle-shaped Ni_2CrO_4 type phase and cube-shaped $NiCr_2O_4$ type phase at Alloy 690/glass interface. In case of Alloy 625, material/glass interface has indicated the presence of $(Fe,Ni)CrO_4$ and $(Fe,Ni)Cr_2O_4$ type phases after interaction with borosilicate melt loaded with waste oxides at 1223 K [104]. Solubility of Cr_2O_3 in soda-silicate melts has been extensively investigated by Khedim et al. [100,101]. Carton et al. [102] have reported formation of a continuous Cr_2O_3 layer at the chromium/glass interface in the passive state. According to the investigators [102], it is maintained up to a temperature called depassivation temperature that is close to 1433 K in a borosilicate melt and is shifted to the higher values when the melt is enriched into oxidizing species. Vidensky et al. [113] have reported modification and degradation of microstructure of Alloy 690 due to attack by the molten salts (sulfate and chloride) and salt vapours. According to them [113], presence of an oxide layer on Alloy 693 (containing about 3 wt.% Al) composed primarily of Al_2O_3 type has resulted in superior corrosion resistance of the alloy as compared to Alloy 690. Zhu et al. [114] have also noticed superior corrosion resistance of Alloy 693 as compared to Alloy 690 in an iron phosphate melt containing 30 wt.% of simulated low activity waste at 1323 K. In addition, the investigators [114] have noticed an altered surface layer depleted in Ni and composed of $(Fe, Cr)_2O_3$ type phase for both the alloys exposed in iron phosphate melt. Studies [114] on reaction kinetics between borosilicate melt and sapphire (alumina substrate) at 1123 K to 1223 K have revealed that nonporous interdiffusion layer is formed with Al^{+3} ion dissolving from sapphire and K^+ ion diffusing from borosilicate glass at the interface and both the ions are coupled together in the reaction layer. According to the authors [108], the interdiffusion layer moves toward borosilicate glass with time and the reaction commences immediately at the selected temperatures without any incubation period. The thickness of the interdiffusion layer has been reported to follow a parabolic rate equation and the parabolic growth rate constant has been found to increase with temperature. It is, therefore, indicated that the finding of oxidation of superalloy 690 in borosilicate melt and formation of a continuous, thick Cr_2O_3 layer at the glass/ alloy interface due to low solubility of Cr_2O_3 in borosilicate melt as obtained in the present study is in accordance with the findings of other researchers [8,9,97-104,112]. Good stability of thermally oxidized aluminide coating on superalloy 690 substrates that was observed even after the exposure of 192 hours in sodium borosilicate melt at 1248 K is attributed to modification of glass composition at the coating/glass interface [108]. The enrichment of Al that has been noticed in glass phase in close vicinity of coating/glass interface appears to be from interdiffusion layer that is a modified glass. The existence of Al_2O_3 phase along with NiAl and Cr_5Al_8 type phases that revealed in XRD results of the specimen exposed in borosilicate melt is indicative of the fact that preexisting alumina layer is partially dissolved to form a modified glass phase at the interface region. Partial dissolution of Al_2O_3 appears to have resulted in increase in viscosity of glass and thus severely restricting the diffusion of ions and slowing down the growth of the reaction layer [108]. The existence of Al_2O_3 and its role as observed in the present study appears to be in agreement with the results of other investigators [108,113,114]. It is, therefore, indicative of the fact that diffusion barrier coating on superalloy 690 substrate can be a useful option to extend the life of the component.

6.4 Summary

Oxidation resistance of aluminides formed on substrates of superalloys 690 and 800 by using aluminization process at 1273 K in argon atmosphere has been evaluated in the present study that is relevant to work related to development of diffusion barrier coatings for high temperature applications. For specimens of superalloys 690 and 800 pack aluminized with high Al-containing pack (10 wt.% Al), thermal oxidation at 1273 K in air has been carried out up to a period of 4 hours (2 hours each) followed by air cooling. In case of superalloy 690 substrates pack aluminized with low Al-containing pack (2 wt.% Al), the total period of oxidation has been 8 hours. In each case, the average weight gain of the specimens has been recorded. In case of superalloy 800 specimens, the evaluation of thermal oxidation resistance has been confined by recording weight gain of the specimens with oxidation period and examining the data For aluminized superalloy 690 specimens, additional experiments have been conducted as it has been intended to evaluate the stability of aluminide coatings in environment pertaining to the application of the alloy. In doing so, the type of oxide that formed on aluminized and thermally oxidized specimens of superalloy 690 has been characterized by using either SEM with EDXS or XRD followed by exposure in sodium borosilicate melt at 1248 K for a total period of 192 hours and finally evaluation of the stability of the coating by SEM with EDXS and XRD. It is to be mentioned that the sodium borosilcate environment is relevant to application related issues of superalloy 690 but not of superalloy 800 during high level nuclear waste immobilization process as mentioned earlier. All the results of the present investigation have been discussed and compared with the findings of other investigators to evaluate the stability of aluminide coatings. Based on experimental evidences and understanding, a few important points of the present work can be summarized as follows

(a) Good oxidation resistance has been noticed for pack aluminized superalloy 690 substrates at 1273 K in air, which is attributable to formation of a thin Al_2O_3 layer. A fairly good oxidation resistance has also been exhibited by pack aluminized superalloy 800 specimens under similar experimental conditions.

(b) In borosilicate melt, superalloy 690 is oxidized and a thick, continuous Cr_2O_3 layer forms at the glass/alloy interface because of low solubility of Cr_2O_3 in borosilicate melt.

(c) A good stability of aluminide coatings with Al_2O_3 layer for superalloy 690 substrates in borosilicate melt at 1248 K is attributed to modification of glass composition at the coating/glass interface that is believed to have induced by partial dissolution of alumina from preexisting Al_2O_3 layer.

CHAPTER 7: CONCLUSIONS

The present study has concentrated on aluminizing of Alloy 690 and Alloy 800, their microstructural characterization and property evaluation. It has dealt with primarily pack aluminization of high chromium and low iron containing Ni-based superalloy 690 and high nickel and moderate chromium Fe-based superalloy 800 substrates followed by microstructural characterization and microanalysis of aluminides. The properties of aluminized substrates of superalloys have been evaluated by performing microhardness, friction, wear and adherence tests. Besides this, the stability of NiAl phase and adhesion strength of Ni(Cr)/NiAl interface has been determined by employing first-principle computational approach. The bonding across the interface and its structure has also been determined. Oxidation resistance of the aluminized superalloys has been evaluated at 1273 K. In addition, the stability of thermally oxidized nickel aluminides has been determined by conducting experiments in sodium borosilicate melt at 1248 K along with the bare substrates. Based on the studies carried out on superalloys 690 and 800 substrates, the following conclusions can be drawn.

1. In high Al-containing pack, multilayer in superalloys 690 and 800 forms by inward diffusion of Al and outward diffusion of alloying elements like Ni, Cr, Fe. In case of low Al-containing pack, multilayer in superalloy 690 forms by outward diffusion of Ni.
2. Aluminides have exhibited much higher microhardness as compared to substrates of superalloys. Aluminides have also shown increase in microhardness with Al content.
3. Scratch test and wear test have indicated good adherence of aluminide coatings.
4. First-principle calculations on Ni/NiAl interface have indicated strong adhesion arising from metallic Ni *d* Ni *d* interaction and covalent Ni *d* and Al *p* mixing of states. Cr-doping in Ni has been found to have slight adverse effect on adhesion strength.

5. Aluminides have exhibited good oxidation resistance at 1273 K in air that could be attributed to formation of thin Al_2O_3 layer.
6. Aluminized superalloy 690 containing either mixture of Ni- and Cr-aluminides or Ni-aluminide on the topmost surface and aluminized superalloy 800 containing Fe-aluminides on the topmost surface could be promising materials for applications up to 1273 K where tensile strength at higher temperatures is not of primary consideration.
7. Aluminized and thermally oxidized superalloy 690 substrates containing Al_2O_3 layer exposed in borosilicate melt at 1248 K for 192 hours have exhibited good stability in molten glass. Good stability of aluminide coatings in molten glass is attributed to existence of Al_2O_3 layer. In this regard, the performance of high Al-containing mixed Ni- and Cr-aluminides is superior to low Al-containing Ni-aluminide that could be related to coverage of Al_2O_3 layer on the surface.
8. The findings on good stability of aluminide coatings in borosilicate melt at 1248 K look to be quite encouraging as it simulates service conditions of superalloy 690 as melter pot in nuclear waste immobilization process. The proposed coatings could be a remedial measure for enhancing the service life of metallic melter pot.

Scope for future research

There is ample scope to pursue the work in future to evaluate the stability of nickel-aluminides/(nickel + chromium)-aluminides/iron-aluminides coatings for high temperature applications in oxidizing/non-oxidizing and aggressive environments and to optimize the compositions of aluminides accordingly. This can be exemplified as follows:

(1) The performances of different nickel-aluminides/different volume fractions of nickel-aluminides + chromium-aluminides/different volume fractions of iron-aluminides in oxidizing and aggressive environments at elevated temperatures can be evaluated followed by optimization of their compositions to achieve desirable properties of coatings.

(2) In case of high temperature applications of aluminides in non-oxidizing and aggressive environments, oxidation treatments prior to exposures in high temperature aggressive environments can be employed to evaluate the stability of the coatings.

(3) Detailed surface studies of aluminides after the exposures in environments can be taken up to understand the interaction between the elements and the environments.

(4) Similar studies can be extended to other superalloys (other than superalloys 690 and 800) belonging to the family of Ni-Cr-Fe based alloys.

References:

[1] C. Sims, N. Stoloff, W. Hagel (Eds.), Superalloys II: High Temperature Materials for Aerospace and Industrial Power, John Wiley and Sons, 1987.

[2] R.F. Decker, C.T. Sims in: C.T. Sims, W.C. Hagel (Eds.), The Superalloys, John Wiley and Sons, N.Y., 1972, p 33.

[3] R.W. Fowley in : C.T. Sims, W.C. Hagel (Eds.), The Superalloys, John Wiley and Sons, N.Y., 1972, p 3.

[4] Special Metals, web: www.specialmetals.com.

[5] Superalloys: A Technical Guide 2002, ASM International, www.asminternational.org.

[6] R.S. Dutta, in: I.S. Wang (Ed.), Corrosion Research Trends, Nova Science Publishers, Inc., NY, 2007, pp 349-365.

[7] R.S. Dutta, 'Corrosion aspects of Ni–Cr–Fe based and Ni–Cu based steam generator tube materials', J. Nucl. Mater. 393 (2009) 343-349.

[8] V. Kain, P. Sengupta, P.K. De, S. Banerjee, 'Case Reviews on the Effect of Microstructure on the Corrosion Behavior of Austenitic Alloys for Processing and Storage of Nuclear Waste', Metall. Mater. Trans. A 36 A (2005) 1075-1084.

[9] P. Sengupta, C.P. Kaushik, G.B. Kale, D. Das, K. Raj, B.P. Sharma, 'Evaluation of alloy 690 process pot at the contact with borosilicate melt pool during vitrification of high-level nuclear waste', J. Nucl. Mater. 392 (2009) 379-385.

[10] D. M. Miller, S. C. Kung, S. D. Scarberry, R. A. Rapp, 'Simultaneous Chromizing-Aluminizing Coating of Austenitic Stainless Steels', Oxidation of Metals 29 (1988) 239-254.

[11] V. A. C. Haanappel, B. Geerdink, T. Fransen, P. J. Gellings, 'The corrosion and mechanical behaviours of aluminide, FeCrA1Y and CoCrA1Y coatings in aggressive environments', Mater. Sci. and Engg. A 148 (1991) 131-139.

[12] V. Vokál, V. Rohr, M. J. Pomeroy, M. Schütze, 'Corrosion of alloys and their diffusion aluminide coatings by KCl: K_2SO_4 deposits at 650° C in air', Mater. and Corr. 59 (2008) 374-379.

[13] S.C. Deevi and V.K. Sikka, 'Nickel and iron aluminides: an overview on properties, processing and applications', Intermetallics 4 (1996) 357-375.

[14] V. Paidar, 'Mechanical properties of iron- and nickel-base aluminides', Mater. Sci. and Eng. A234-236 (1997) 15-21.

[15] SGTE database for Al-Ni alloy, www.crct.polymtl.ca.

[16] SGTE database for Al-Fe alloy, www.crct.polymtl.ca.

[17] T. N. Rhys-Jones, 'Coatings for blade and vane applications in gas turbines', Corr. Sci. 29 (1989) 623-446.

[18] G.W. Goward, 'Progress in coatings for gas turbine airfoils', Surf. and Coatings Tech. 108–109 (1998) 73–79.

[19] G.W. Goward, D.H. Boone, 'Mechanism of formation of diffusion aluminide coatings on Nickel-base superalloys', Oxid. Met. 3 (1971) 475–495.

[20] S. Shankar, L.L. Seigle, 'Interdiffusion and Intrinsic Diffusion in the NiAl (δ) Phase of the Al-Ni System', Met. Trans. A 9A (1978) 1467–1476.

[21] F.S. Pettit, 'Oxidation mechanisms for nickel-aluminium alloys at temperatures between 900°C and 1300°C', Trans. Met. Soc. AIME 239 (1967) 1296–1305.

[22] C.S. Giggins, F.S. Pettit, 'Oxidation of Ni-Cr-Al Alloys Between 1000° and 1200°C',

J. Electrochem Soc. 118 (1971) 1782–1790.

[23] E. Godlewska, K. Godlewski, ‘Chromaluminizing of Nickel and Its Alloys’, Oxid. Met. 22 (1984) 117–131.

[24] W.T. Wu, A. Rahmel, M. Schorr, ‘Role of platinum in the Na_2SO_4-Induced hot corrosion resistance of aluminum duffusion coatings’, Oxid. Met. 22 (1984) 59–81.

[25] W.Y. Lee,Y. Zhang, I.G.Wright, B.A. Pint, P.K. Liaw, ‘Effects of Sulfur Impurity on the Scale Adhesion Behavior of a Desulfurized Ni-Based Superalloy Aluminized by Chemical Vapor Deposition’, Met. Trans. A 29 (1998) 833-841.

[26] S. J. Hong, G.H. Hwang, W.K. Han, S.G. Kang, ‘Cyclic oxidation behavior of Pt-modified aluminide coating treated with ultrasonic nanocrystal surface modification (UNSM) on Ni-based superalloy’, Surf. and Coatings Tech. 205 (2011) 2714-2723.

[27] V.K. Tolpygo, D.R. Clarke, K.S. Murphy, ‘Evaluation of interface degradation during cyclic oxidation of EB-PVD thermal barrier coatings and correlation with TGO luminescence’, Surf. and Coatings Tech. 188-189 (2004) 62-70.

[28] R.T. Wu, K. Kawagishi, H. Harada, R.C. Reed, ‘The retention of thermal barrier coating systems on single-crystal superalloys: Effects of substrate composition’, Acta Mat. 56 (2008) 3622-3629.

[29] S. Dryepondt, J.R. Porter, D.R. Clarke, ‘On the initiation of cyclic oxidation-induced rumpling of platinum-modified nickel aluminide coatings’, Acta Mat. 57 (2009) 1717-1723.

[30] M.F. del Grosso, H.O. Mosca, G. Bozzolo, ‘Atomistic modeling of Pt additions to NiAl’, Intermetallics 16 (2008) 1305-1309.

[31] S. Dryepondt, D.R. Clarke, ‘Effect of superimposed uniaxial stress on rumpling of platinum-modified nickel aluminide coatings’, Acta Mat. 57 (2009) 2321-2327.

[32] J. Tien, F.S. Pettit, ‘Mechanism of oxide adherence on Fe-25Cr-4Al(Y or Sc) alloys’, Met. Trans. 3 (1972) 1587–1599.

[33] A.W. Funkenbusch, J.G. Smeggil, N.S. Bornstein, ‘Reactive element-sulfur interaction and oxide scale adherence’, Met. Trans. 16A (1985) 1164-1166.

[34] B.A. Pint, ‘Experimental Observations in Support of the Dynamic-Segregation Theory to Explain the Reactive-Element Effect’, Oxid. Met. 45 (1996) 1–37.

[35] R. Erikson, H. Brodin, S. Johansson, L. Östergren, Xin-Hai Li, ‘Influence of isothermal and cyclic heat-treatments on the adhesion of plasma sprayed thermal barrier coatings’, Surf. and Coatings Tech. 205 (2011) 5422-5429.

[36] T. Patterson, A. Leon, B. Jayaraj, J. Liu, Y.H. Sohn, ‘Thermal cyclic lifetime and oxidation behavior of air plasma sprayed CoNiCrAlY bond coats for thermal barrier coatings’, Surf. and Coatings Tech. 203 (2008) 437-441.

[37] Y.H. Sohn, E.Y. Lee, B.A. Nagaraj, R.R. Biederman, R.D. Sisson Jr., ‘Microstructural characterization of thermal barrier coatings on high pressure turbine blades’, Surf. and Coatings Tech. 146-147 (2001) 132-139.

[38] E.P. Busso, Z.Q. Qian, M.P. Taylor, H.E. Evans, ‘The influence of bondcoat and topcoat mechanical properties on stress development in thermal barrier coating systems’, Acta Mat. 57 (2009) 2349-2361.

[39] T.R. Kakuda, A. M. Limarga, T.D. Bennett, D.R. Clarke, ‘Evolution of thermal properties of EB-PVD 7YSZ thermal barrier coatings with thermal cycling’, Acta Mat. 57 (2009) 2583-2591.

[40] T.S. Hille, T.J. Nijdam, A.S.J Suiker, S. Turteltaub, W.G. Sloof, 'Damage growth triggered by interface irregularities in thermal barrier coatings', Acta Mat. 57 (2009) 2624-2630.

[41] H.J. Choi, J. Jedlinski, B. Rao, Y.H. Sohn, 'Transmission electron microscopy observations on the phase composition and microstructure of the oxidation scale grown on as-polished and yttrium-implanted β-NiAl', Surf. and Coatings Tech. 205 (2010) 1206-1210.

[42] R. Bianco, R.A. Rapp, 'Pack Cementation Aluminide Coatings on Superalloys: Codeposition of Cr and Reactive Elements', J. Electrochem. Soc., 140 (1993) 1181-1190.

[43] C.J. Wang, C.C. Li, Surf. Coat. Technol. 177–178 (2003) 37.

[44] C.J. Wang, S.M. Chen, 'Microstructure and cyclic oxidation behavior of hot dip aluminized coating on Ni-base superalloy Inconel 718', Surf. and Coatings Tech. 201 (2006) 3862–3866.

[45] A. Eslami, H. Arabi, S. Rastegari, 'Gas phase aluminizing of a nickel base superalloy by a single step HTHA aluminizing process', Canadian Metallurgical Quarterly, 48 (2009) 91-98.

[46] T. N. Rhys-Jones, 'Thermally sprayed coating systems for surface protection and clearance control applications in aero engines', Surf. and Coatings Tech. 43/44 (1990) 402-415.

[47] E.G. Ivanov, 'Thermodynamic analysis of phase transformations during aluminizing', Translated from Metallovedenie i Termicheskaya Obrabotka Metallov, No.6, pp 33-35, June, 1979.

[48] G. Kresse, J. Furthmueller, 'Efficient iterative schemes for ab initio total-energy calculations using a plane-wave basis set', Phys. Rev. B 54 (1996) 11169-11186.

[49] G. Kresse, J. Furthmueller, 'Efficiency of ab-initio total energy calculations for metals and semiconductors using a plane-wave basis set', Comput. Mater. Sci. 6 (1996) 15-50.

[50] J. P. Perdew, K. Burke, M. Enzerhof, 'Generalized Gradient Approximation Made Simple', Phys. Rev. Let. 77 (1996) 3865-3868.

[51] P. E. Blöchl, 'Projector augmented-wave method', Phys. Rev. B 50 (1994) 17953-17979.

[52] H. J. Monkhorst, J. D. Pack, 'Special points for Brillouin-zone integrations', Phys. Rev. B 13 (1979) 5188-5192.

[53] M. Methfessel, A. T. Paxton, 'High-precision sampling for Brillouin-zone integration in metals', Phys. Rev. B 40 (1989) 3616-3621.

[54] R. S. Sundar, R. G. Baligidad, Y. V. R. K Prasad, D. H. Sastry, 'Processing of iron aluminides', Mater. Sci. Eng. A 258 (1998) 219-228.

[55] N. S. Stoloff, 'Iron aluminides: present status and future prospects', Mater. Sci. Eng. A 258 (1998) 1-14.

[56] R. Checchetto, C. Tosello, A. Miotello, G. Principi, 'Structural evolution of Fe–Al multilayer thin films for different annealing temperatures', J. Physics: Condensed Matter. 13 (2001) 811-821.

[57] G. Sharma, M. Sundararaman, N. Prabhu, G. L. Goswami, 'Sliding wear resistance of iron aluminides', Bull. Mater. Sci. 26 (2003) 311-314.

[58] C. Houngniou, S. Chevalier, J. P. Larpin, 'Synthesis and characterisation of pack cemented aluminide coatings on metals', Applied Surf. Sci. 236 (2004) 256-269.

[59] J. Xia , C. X. Li, H. Dong, ‘Thermal oxidation treatment of B2 iron aluminide for improved wear resistance’, Wear 258 (2005) 1804-1812.

[60] Y. Chen, H. M. Wang, ‘Microstructure and wear resistance of laser-melted TiC reinforced nickel aluminide dual-phase matrix in situ composite’, Intermetallics 14 (2006) 325-331.

[61] R. A. Mahesh, R. Jayaganthan, S. Prakash, ‘Evaluation of hot corrosion behaviour of HVOF sprayed Ni–5Al and NiCrAl coatings in coal fired boiler environment’ Surf. Eng. 26 (2010) 413-421.

[62] D. Li , Y. Xu, D. Lin, ‘Oxidation behavior of FeAl alloys with and without titanium’, J. Mater. Sci. 36 (2001) 979-983.

[63] Z. D. Xiang, S. R. Rose, P. K. Datta, ‘Low-temperature formation and oxidation resistance of nickel aluminide/nickel hybrid coatings on alloy steels’, Scripta Mater. 59 (2008) 99-102.

[64] H. Guoxin, X. Zhengxia, L. Jianju, L. Yanhong, ‘Microstructure and corrosion resistance of simultaneous Al–Fe coating on copper by pack cementation’, Surf. Coatings Tech. 203 (2009) 3392-3397.

[65] J.M. Guilemany, N. Cinca, S. Dosta, C. R. C. Lima, ‘High-temperature oxidation of Fe40Al coatings obtained by HVOF thermal spray’, Intermetallics 15 (2007) 1384-1394.

[66] M. Tacikowski, R. Sitek, K. Sikorski, T. Wierzchoń, ‘Structure of Al–Ni intermetallic composite layers produced on the Inconel 600 by the glow discharge enhanced-PACVD method’, Intermetallics 17 (2009) 1098-1104.

[67] M. A. Espinosa-Medina, G. Carbajal-Dela Torre, H. B. Liu, A. Martińez-Villafañe, J. G. González-Rodriguez, Corr. Sci. 51 (2009) 1420-1427.

[68] S. Kamal, R. Jayaganthan, S. Prakash, ‘Hot corrosion behaviour of D-gun sprayed NiCoCrAlYTa coated superalloys at 900°C in molten salt environment’, Surf. Eng. 26 (2010) 453-462.

[69] M. Yamaguchi, H. Inui, K. Ito, ‘High-temperature structural intermetallics’, Acta Mater. 48 (2000) 307-322.

[70] R. Prescott, M. J. Graham, ‘The Oxidation of Iron-Aluminium Alloys’, Oxidation of Metals 38 (1992) 73-87.

[71] C. Christoglou, N. Voudouris, G. N. Angelopoulos, ‘Formation and modelling of aluminide coatings on iron by a fluidised bed CVD process’, Surf. Coatings Tech. 155 (2002) 51-58

[72] L. Levin, A. Ginzburg, L. Klinger, T. Werber, A. Katsman, P. Schaaf, ‘Controlled formation of surface layers by pack aluminization’, Surf. Coatings Tech. 106 (1998) 209-213.

[73] Z. D. Xiang, J. S. Burnell-Gray, P. K. Datta, ‘Aluminide coating formation on nickel-base superalloys by pack cementation process’, J. Mater. Sci. 36 (2001) 5673-5682.

[74] Smithells Metals Reference Book, in: W.F.Gale and T.C. Totemeier (Eds.), Butterworth-Heinmann, Oxford, 2004.

[75] H. Okamoto, J. Phase Equilibria, 14 (2), 257-259 (1993).

[76] S.R. Levine, R.M. Caves, ‘Thermodynamics and Kinetics of Pack Aluminide Coating Formation on IN-100’, J. of Elec. Soc. 121 (1974) 1051-1064.

[77] A. Thevand, S. Poize, J.P. Crousier, R. Streiff, ‘Aluminization of nickel-formation of intermetallic phases and Ni_2Al_3 coatings’, J. Mater. Sci. 16 (1981) 2467-2479.

[78] D.K. Das, V. Singh, S.V. Joshi, ‘Evolution of Aluminide Coating Microstructure on Nickel-Base Cast Superalloy CM-247 in a Single-Step High-Activity Aluminizing Process’, Metall. and Mater. Trans. A 29A (1998) 2173-2188.

[79] W. Da Costa, B. Gleeson, D.J. Young, ‘Co-deposited chromium-aluminide coatings. III. Origins of nonequilibrium effects’, Surf. and Coating Tech. 88 (1996) 165-171.

[80] H.L. Huang, Y.Z. Chen, D. Gan, ‘Microstructure of first-stage aluminized coating on a Ni–Cr alloy’, Mater. Sci. and Engg. A 328 (2002) 238-244.

[81] J.L. Murray, J of Phase Equilibria, 19(4) (1998) 368.

[82] U.R. Kattner, B.P. Burton, Phase Diagrams of Binary Iron Alloys, H. Okamoto, ed., ASM International, Materials Park, OH, 12-28 (1993).

[83] M. Palm, ‘Concepts derived from phase diagram studies for the strengthening of Fe–Al-based alloys’, Intermetallics 13 (2005) 1286-1295.

[84] B. L. Bates, Y. Q. Wang, Y. Zhang, B. A. Pint, ‘Formation and oxidation performance of low-temperature pack aluminide coatings on ferritic–martensitic steels’, Surf. Coatings Tech. 204 (2009) 766-770.

[85] M.A. Chowdhury, D.M. Nuruzzaman, B.K. Roy, A. Islam, Z. Hossain, M.R. Hasan, ‘Experimental Investigation of Friction Coefficient and Wear Rate of Stainless Steel 202 Sliding against Smooth and Rough Stainless Steel 304 Counter-faces’, Friction and Wear Research 1 (2013) 34-41.

[86] K. Singh, P.K. Limaye, N.L. Soni, A.K. Grover, R.G. Agarwal, A.K. Suri, ‘Wear studies of (Ti–Al)N coatings deposited by reactive magnetron sputtering’, Wear, 258 (2005) 1813-1824.

[87] Smithell Metals Reference Book, in: E.A. Brandes, G.B. Brook (Eds.), Butterworth-Heinemann, Oxford, 1992.

[88] A. Ernst, G. Van deer Laan, W.M. Temmerman, S. S. Dhesi, Z. Szotek, 'Contesting results for magnetic moments in nickel thin films', Phys. Rev. B, 62 (2000) 9543-9547.

[89] H.E. Maupin, R.D. Wilson, J.A. Hawk, 'Wear deformation of ordered Fe-Al intermetallic alloys', Wear 162-164 (1993) 432-440.

[90] C. Sierra, A.J. Vázquez, 'Dry sliding wear behaviour of nickel aluminides coatings produced by self-propagating high-temperature synthesis', Intermetallics 14 (2006) 848.

[91] S.K. Ghosh, P.K. Limaye, B.P. Swain, N.L. Soni, R.G. Agarwal, R.O. Dusane, A.K. Grover, 'Tribological behaviour and residual stress of electrodeposited Ni/Cu multilayer films on stainless steel substrate', Surf. and Coatings Tech. 201 (2007) 4609-4618.

[92] J-H Jin, D.J. Stephenson, 'The sliding wear behaviour of reactively hot pressed nickel aluminides', Wear 217 (1998) 200-207.

[93] J. Xia, C. X. Li, H. Dong, 'Hot-stage nano-characterisations of an iron aluminide', Mater. Sci. and Eng. A 354 (2003) 112-120.

[94] S. Kumar, V. Selvarajan, P. V. A. Padmanabhan, K. P. Sreekumar, 'Characterization and comparison between ball milled and plasma processed iron-aluminium thermal spray coatings', Surf. Coatings Tech. 201 (2006) 1267-1275.

[95] S. Majumdar, A. Arya, I.G. Sharma, A.K. Suri, S. Banerjee, 'Deposition of aluminide and silicide based protective coatings on niobium', Applied Surf. Sci. 257 (2010) 635-640.

[96] A. Arya, E.A. Carter, 'Structure, bonding, and adhesion at the TiC(100)/Fe(110) interface from first principles', J. Chem. Phy. 118 (2003) 8982-8996.

[97] S. Abdelouhab, C. Rapin, R. Podor, P. Berthod, M. Vilasi, ‘Electrochemical Study of Chromium Corrosion in Na_2O-xSiO_2 Melts’, J. Electrochem. Soc. 154 (2007) 500-507.

[98] H. Khedim, S. Abdelouhab, R. Podor, C. Rapin, M. Vilasi, ‘Relationship between chromia solubility and superalloy corrosion in silicate melts-a first attempt’, Mater. Sci. Forum 595-598 (2008) 621-627.

[99] C. Rapin, R. Podor, J. Gassert, M. Vilasi, ‘Impedance spectroscopy applied to metal corrosion study’, Mater. Sci. Forum 595-598 (2008) 1119-1126.

[100] H. Khedim, R. Podor, P.J. Panteix, C. Rapin, M. Vilasi, ‘Solubility of chromium oxide in binary soda silicate melts’, J. Non-Cryst. Solids 356 (2010) 2734-2741.

[101] H. Khedim, S. Abdelouhab, R. Podor, C. Rapin, M. Vilasi, P.J. Panteix, M. Toplis, F. Faure, ‘Kinetic study of the chromium solubility in soda-silicate melts’, J. Non-Cryst. Solids 357 (2011) 31-42.

[102] A. Carton, C. Rapin, R. Podor, P. Berthod, ‘Corrosion of Chromium in Glass Melts’, J. Electrochem. Soc. 153 (2006) 121-127.

[103] P. Sengupta, J. Nucl. Mater. ‘Interaction study between nuclear waste-glass melt and ceramic melter bellow liner materials’, 411 (2011) 181-184.

[104] P. Sengupta, J. Mittra, G.B. Kale, ‘Interaction between borosilicate melt and Inconel’, J. Nucl. Mater. 350 (2006) 66-73.

[105] Z.D. Xiang, S.R. Rose, P.K. Datta, ‘Low-temperature formation and oxidation resistance of nickel aluminide/nickel hybrid coatings on alloy’, Scripta Mater. 59 (2008) 99-102.

[106] J. Xia, C.X. Li, H. Dong, ‘Thermal oxidation treatment of B2 iron aluminide for improved wear resistance’, Wear 258 (2005) 1804-1812.

[107] J. Klöwer, U. Brill, U. Heubner, 'High temperature corrosion behaviour of nickel aluminides : effects of chromium and zirconium', Intermetallics 7 (1999) 1183-1194.

[108] J.H. Jean, T.K. Gupta, 'Kinetics of interfacial reaction between borosilicate glass and sapphire substrate', Mater. Res. Soc. 7 (1992) 2514-2520.

[109] M.G. Fontana, Corrosion Engineering, third ed., McGraw-Hill, New York, 1987.

[110] M.W. Brumm, H.J. Grabke, 'The oxidation behavior of NiAl I. Phase-transformations in the alumina scale during oxidation of NiAl and NiAl-Cr Alloys', Corr. Sci. 33 (1992) 1677-1690.

[111] G. Liu, M. Li, M. Zhu, Y. Zhou, 'Transient of alumina oxide scale on β-NiAl coated on M38G alloy at 950°C', Intermetallics 15 (2007) 1285-1290.

[112] P. Sengupta, C.P. Kaushik, R.K. Mishra, G.B. Kale, 'Microstructural Characterization and Role of Glassy Layer Developed on Inconel 690 During a Nuclear High-Level Waste Vitrification Process', J. Am. Ceram. Soc. 90 (2007) 3057-3062.

[113] I. Vidensky, H. Gan, L. Pegg, in: G.L. Smith, S.K. Sundaram, D.R. Spearing (Eds.), Environmental Issues and Waste Management Technologies VII, American Ceramic Society, Ohio, 2002, pp. 141-150.

[114] D. Zhu, C.W. Kim, D.E. Day, 'Corrosion behavior of Inconel 690 and 693 in an iron phosphate melt', J. Nucl. Mater. 336 (2005) 47-53.

List of publications:

a. Published

1. ‘Characterization of aluminides formed on superalloy 690 substrate’

   R. S. Dutta, S. Majumdar, P. K. Limaye, U. D. Kulkarni and G. K. Dey, Trans. IIM, vol. 64, Issues 1 & 2, February-April 2011, pp 31-36.

2. ‘Formation and characterization of aluminide coatings on Alloy 800 substrate’

   R. S. Dutta, S. Majumdar, A. Laik, K. Singh, U. D. Kulkarni, I. G. Sharma and G. K. Dey, Surface & Coatings Technology, vol. 205, 2011, p 4720-4725.

3. ‘Thermally grown oxide layer on aluminized superalloy 690 substrate and its stability in nitrate-based environment’

   Rabi Sankar Dutta, Chelakkattu Yusufali, Sanjib Majumdar, Raman Kumar Mishra, Chetan Parkash Kaushik, Rohidas Jagannath Kshirsagar, Ulhas Digambar Kulkarni and Gautam Kumar Dey, Materials Science Forum, vol. 710, 2012, pp 733-738.

4. ‘Formation of diffusion barrier coating on superalloy 690 substrate and its stability in borosilicate melt at elevated temperature’

   R.S. Dutta, C. Yusufali, B. Paul, S. Majumdar, P. Sengupta, R.K. Mishra, C.P. Kaushik, R.J. Kshirsagar, U.D. Kulkarni and G.K. Dey, Journal of Nuclear Materials, vol. 432, 2013, pp 72-77.

5. ‘Formation of aluminides on Ni-based superalloy 690 substrate, their characterization and first-principle Ni(111)/NiAl(110) interface simulations’

   R.S. Dutta, A. Arya, C. Yusufali, B. Vishwanadh, R. Tewari, G.K. Dey, Surface & Coatings Technology, vol. 235, 2013, pp 741-747.